Wayne State University
DigitalCommons@WayneState

Wayne State University Dissertations

1-1-2012

Single molecule studies of rna-target interactions

Sharla Leann Wood
Wayne State University,

Follow this and additional works at: http://digitalcommons.wayne.edu/oa_dissertations

Recommended Citation
Wood, Sharla Leann, "Single molecule studies of rna-target interactions" (2012). *Wayne State University Dissertations.* Paper 522.

This Open Access Dissertation is brought to you for free and open access by DigitalCommons@WayneState. It has been accepted for inclusion in Wayne State University Dissertations by an authorized administrator of DigitalCommons@WayneState.

SINGLE MOLECULE STUDIES OF RNA-TARGET INTERACTIONS

by

SHARLA WOOD

DISSERTATION

Submitted to the Graduate School

of Wayne State University,

Detroit, Michigan

in partial fulfillment of the requirements for

DOCTOR OF PHILOSOPHY

2012

MAJOR: CHEMISTRY (Analytical)

Approved by:

_____

Advisor Date

_____

_____

_____

DEDICATION

Dedicated to my family

ACKNOWELEDGEMENTS

First and foremost, I would like to thank God for all of the blessings and strength that He has given me. *"Blessed be the God and Father of our Lord Jesus Christ, who hath blessed us with all spiritual blessings in heavenly places in Christ* (Ephesians 1:3). Without Him, nothing would be possible. *"I can do all things through Christ which strengtheneth me* (Philippians 4:13). I especially want to thank my family for their love, support, inspiration, and understanding. I would never have come this far or achieved this much without them.

I want to express my sincerest gratitude and utmost respect to my advisor, Dr. David Rueda, for putting up with me when I challenged him and for never giving up. I can only hope to be as good of a mentor and scientist as he is. I also must thank Dr. David Coleman who offered me the wonderful opportunity to work in the CIF. I learned more from him, as well as the experience, than I ever could have imagined. I also thank him for graciously accepting to join my committee at the last minute. I thank my commiittee members, Dr. Ashok Bhagwat, Dr. Athar Ansari, and Dr. Tiffany Mathews, for their constructive criticism and guidance throughout my time in graduate school. I also had the privilege of having Dr. Adrian Ferré-d'Amaré as a collaborator on the c-di-GMP riboswitch project. I must thank him for his immense helpfulness and cooperation in publishing my first paper.

I would like to thank and acknowledge my fellow lab members, Elvin, Amanda, Alfonso, Rajan, Rui, Zhuojun, May, Gayan, Chandani, Hansini, Bishnu, Eric, Marcus, Imali, Pramodha, and Holly for their never-ending kindness, support, and friendship. Each and every one of them helped to make the

experience of graduate school a bearable one and I am a better person for knowing them.

Finally, I thank everyone else in the chemistry department for their help, guidance, and friendship along the way.

Thank you all!

TABLE OF CONTENTS

LIST OF TABLES

LIST OF FIGURES

Chapter 1

INTRODUCTION

1.1 Roles of RNA in biology

According to the central dogma of biology, DNA is transcribed into RNA, which is then translated into proteins (Figure 1.1). For a long time, RNA was thought to act only as an intermediate for translation of the genetic code into proteins. However, many important biological roles of RNA have since been discovered. For instance, RNA also can convey genetic information and plays important roles in splicing, editing, and regulation and silencing of gene expression. The structure of RNA plays an important part in facilitating these multiple functions. RNA can fold into a wide range of structures from a simple hairpin to structures of enormous complexity(*2, 3*).

1.1.1 Natural aptamers and riboswitches

One way that RNA uses structure to perform a function is as a riboswitch. Riboswitches are gene-regulatory mRNA domains that directly recognize small molecule metabolites and second messengers(*4-13*). A riboswitch consists of an aptamer domain that specifically recognizes a ligand by folding into a specific structure that allows for specific binding of the ligand to the RNA. This aptamer domain is followed downstream by an expression platform, which upon binding of the ligand to the aptamer, regulates gene expression by acting as a switch turning on or off transcription or translation (Figure 1.2). Riboswitch-mediated gene regulation employs a conformational change, either global or local, upon binding of the ligand. A riboswitch has recently been discovered that recognizes cyclic

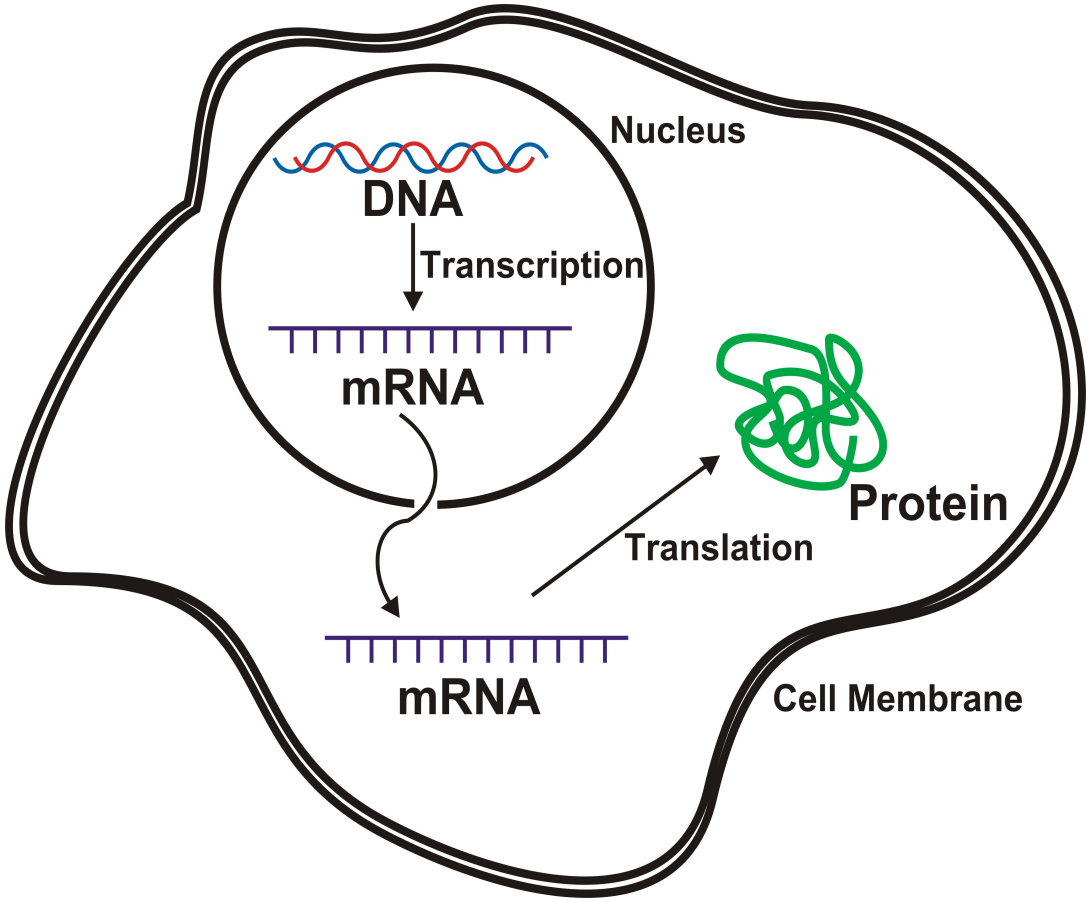

Figure 1.1 The central dogma of biology.

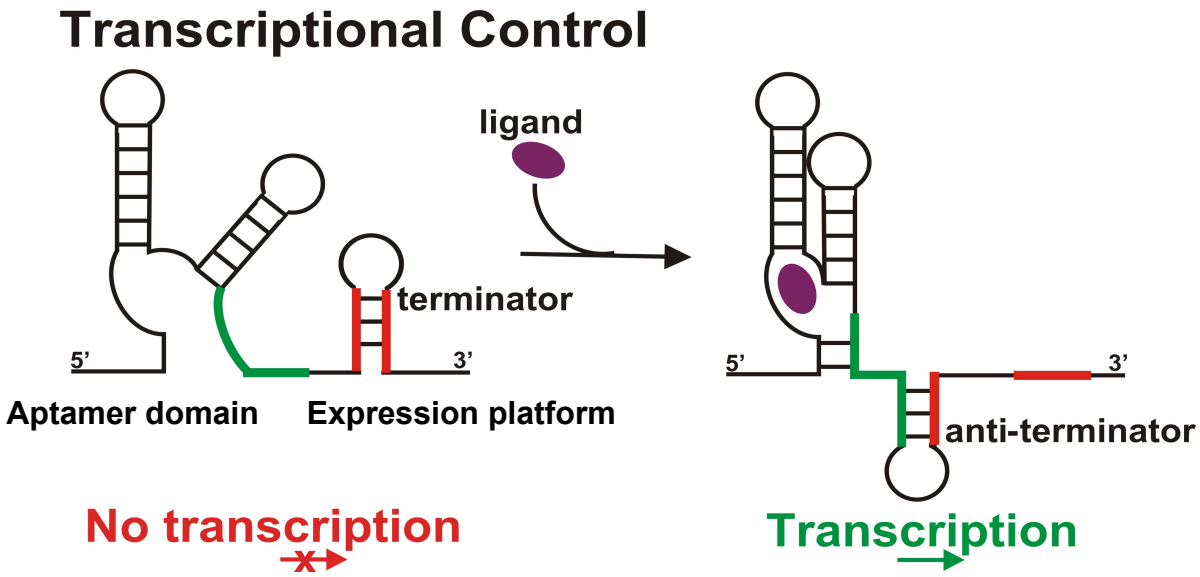

Figure 1.2 A transcriptional-on riboswitch. In the absence of ligand, the terminator stem is formed in the downstream expression platform and transcription is prevented from occurring. When the aptamer domain binds the ligand (purple), there is some type of conformational change in which formation of the terminator stem is prevented and the anti-terminator is formed, thus turning on transcription.

diguanylate (c-di-GMP)(*14*). c-di-GMP is a bacterial second messenger that regulates a host of vital cellular functions such as virulence, motility, and biofilm formation(*15-17*). Here, we have used single molecule FRET to investigate how the c-di-GMP riboswitch uses conformational change to regulate the gene expression.

1.2 RNA as a tool

1.2.1 Artificial aptamers

Artificial aptamers have also been shown to be an effective analytical tool to detect a specific analyte of interest, which in this study is tetramethylrhodamine (TAMRA), an organic fluorophore(*18-21*). It has been proposed that this method could be a useful tool to label endogenous RNA *in vivo*. To do this, several of these aptamers could be placed in the 5' untranslated region of an RNA, and upon binding of the fluorophore to the aptamer, the RNA would be fluorescently labeled. Here, we used several biophysical techniques to characterize how binding to the aptamer affects the fluorescent properties of TAMRA.

1.2.2 Molecular beacons

RNA can be used as an analytical tool to detect an assortment of analytes. For example, molecular beacons (MB) are hairpin probes that fluoresce upon hybridization to their target sequence (Figure 1.3) (*22*). This is accomplished with the use of a fluorophore conjugated to one end and a quencher on the other. The MB consists of a loop sequence, generally 15 to 20 nucleotides, specific for the target of interest and a self-complementary stem sequence ranging from five to seven base pairs. When the MB encounters the

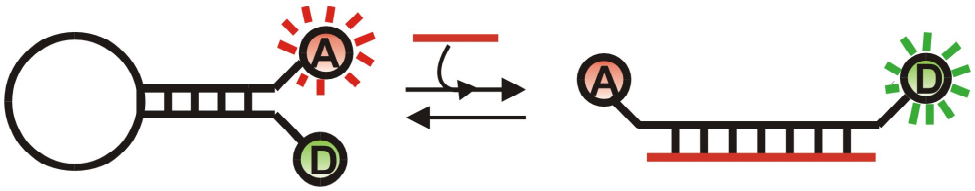

Figure 1.3 The molecular beacon is a hairpin probe that fluoresces upon binding to the target sequence. The probe consists of a loop sequence that is specific for the target and a self-complementary stem sequence. A fluorophore is conjugated to one end of the stem, while a quencher is on the other. The probe is in the hairpin, nonfluorescent, form in the absence of target. Binding to the target unfolds the MB resulting in a fluorescent signal.

target sequence, it binds to the target to form a hybrid that is more stable than the stem duplex of the hairpin. As a result of optimized design, the MB has been shown to possess the ability to discern single base mismatches. The MB can be designed such that a hybrid with a target sequence containing a single mismatch is no longer more stable than the hairpin. In the absence of target, the hairpin is folded bringing the fluorophore into close proximity to the quencher, thus quenching the fluorescence. However with target present, the hairpin unfolds and hybridizes to the target sequence increasing the distance between the fluorophore and the quencher resulting in a fluorescent signal. A drawback of using these probes *in vivo* is that RNA is readily degraded by RNases in the cell(*23-25*). The 2'-OH moiety is often modified to prevent this degradation(*26-32*). Here, we used FRET and single molecule FRET to determine the effects that these commonly used 2' modifications have on the ability of molecular beacons to fold and to recognize their target.

1.3 RNA Tracking

1.3.1 Techniques

Current techniques to monitor mRNA expression include fluoresence *in situ* hybridization (FISH), transfection of full-length fluorescent mRNA, transgenic models, and molecular beacons (MB). FISH involves the use of labeled oligonucleotide probes to localize a target sequence in a tissue section. However, FISH requires fixed tissues, and any unhybridized probes must be washed away to limit background signals(*33*). Another approach is to modify the gene encoding the mRNA with a sequence with an affinity towards the bacteriophage MS2 coat

protein. The cells are then transfected with a fusion protein of green fluorescent protein (GFP) and MS2 coat protein. The GFP fusion protein then binds to the modified mRNA resulting in a fluorescent signal. This method, however, cannot be used to monitor endogenous mRNA and transgenes often do not have the same functionality as the endogenous gene(*33, 34*).

Molecular beacons have also been used to track RNA inside cells. This fluorescence will identify the location of the target mRNA. Since the fluorescence is quenched when the MB is unbound to the target, there is no need to wash away any unbound probes to decrease background, as was the case with FISH, adding to the MBs appropriateness for use in living cells and single molecule detection(*22, 30, 34-36*).

1.3.2 Delivery

Numerous nucleic acid delivery methods have been demonstrated including microinjection, cell-penetrating peptides, and biolistic delivery by gene gun(*34, 37*). Microinjection involves the use of a fine needle to directly inject the MB into the cell. The method is, however, ineffective for MB delivery into a large number of cells, and the probes have a tendency to accumulate in the nucleus(*23, 34*). The gene gun has proven effective in the delivery of molecular beacons. In this method, MBs are delivered to the cells along with a cytoplasmic dye, to ensure delivery, via small gold particles that penetrate the plasma membrane, which then reseals (Figure 1.4) (*37*). However, the gene gun shoots a random subset of cells. Delivery by means of cell-penetrating peptides, for example HIV-1 Tat peptide, has also shown great promise. These peptides are

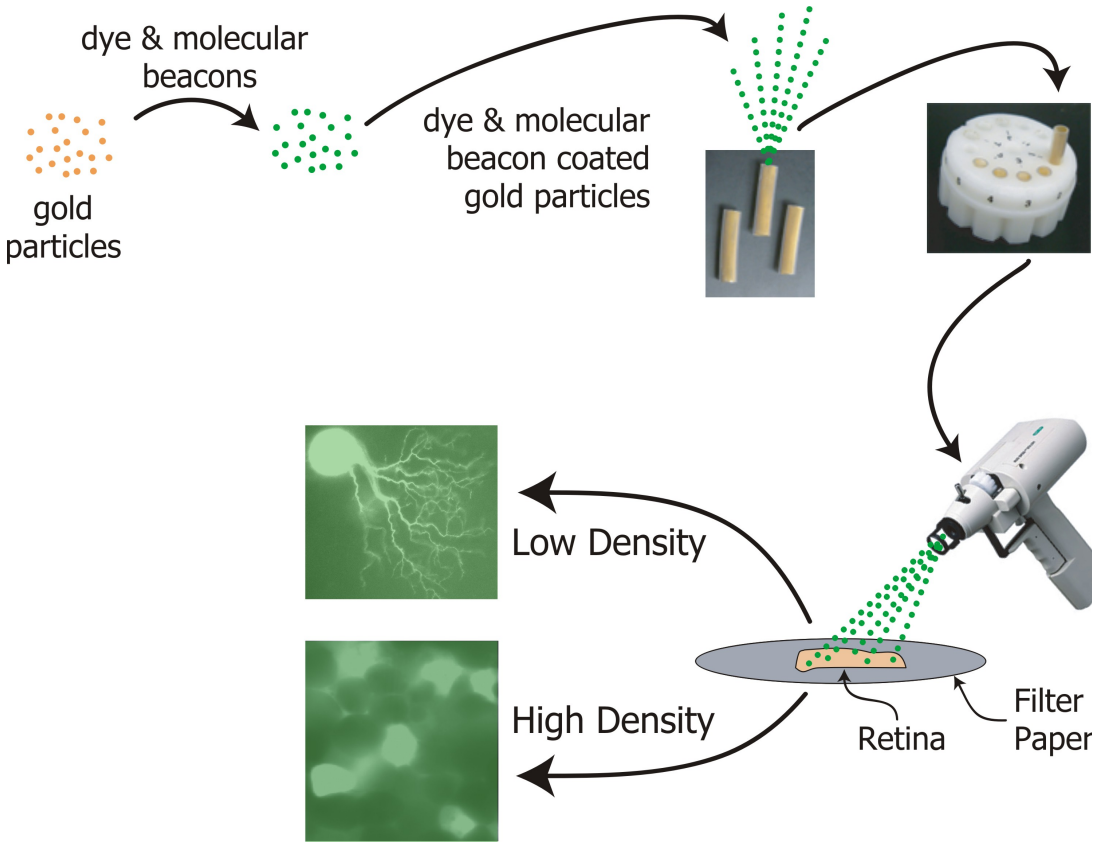

Figure 1.4 The biolistic delivery of molecular beacons. Small gold particles are coated with molecular beacons and a cytoplasmic dye and injected via a gene gun into cells. *Figure courtesy of Dr. Karen Myhr.*

generally short and rich in cationic amino acids and are most likely transported into the cell via endocytosis. Molecular beacons may be conjugated to the peptide by a biotin/streptavidin interaction, a thiol/maleimide linkage, or a disulfide bridge that is cleavable by the reducing environment of the cytoplasm(*24, 34, 38*).

1.4 Single molecule and FRET

Single molecule spectroscopy reveals structural dynamics and functions of a system that would otherwise be concealed in ensemble-averaged techniques. Fluorescence resonance energy transfer (FRET) is a method often used in conjunction with single molecule techniques. FRET involves the energy transfer between two fluorophores, a donor and acceptor. The fluorophore pair is chosen so that the emission peak of the donor overlaps the excitation peak of the acceptor (Figure 1.5). The emission energy of the donor is transferred and excites the acceptor, which then emits. FRET is a distance-dependent phenomenon whose efficiency is expressed in the following equation,

$$E_{FRET}(R) = \frac{1}{1 + \left(\frac{R}{R_0}\right)^6}$$

where R is the distance between the two fluorophores and R_0 is the distance at which FRET efficiency is 50% (Figure 1.6).

Total internal reflection (TIR) was chosen as a means to reduce background signals. This is accomplished by

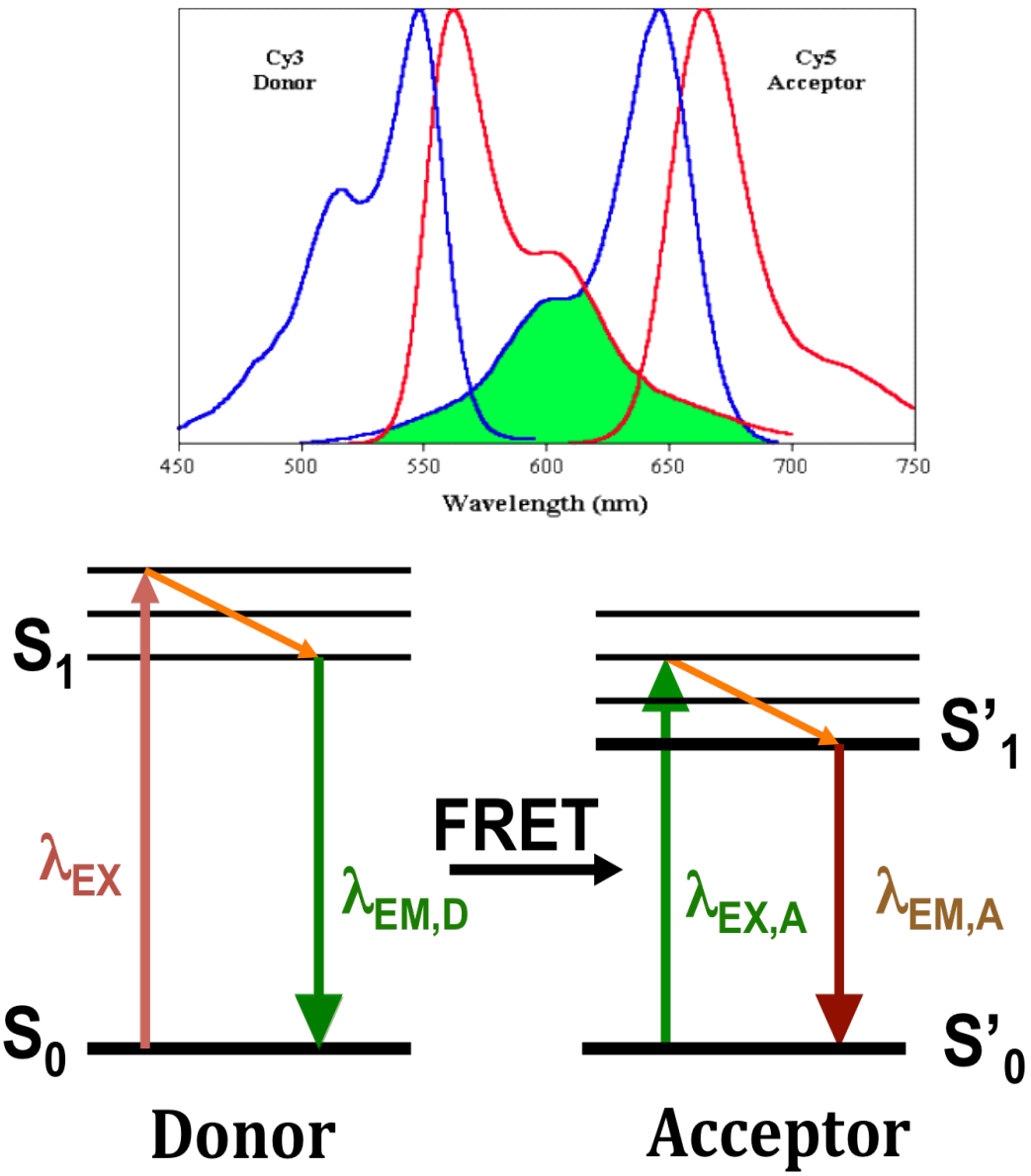

Figure 1.5 Principle of fluorescence resonance energy transfer (FRET).

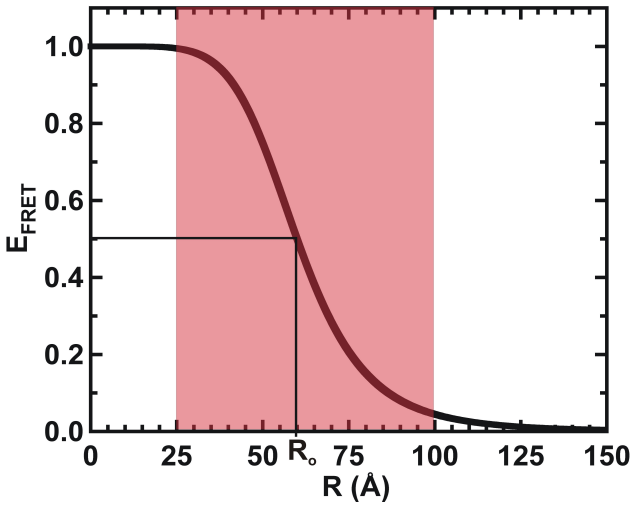

Figure 1.6 Distance dependence of FRET.

reducing the detection volume to a small area at the interface between the quartz slide and solution. A 532 nm laser beam was directed towards the interface through a prism at an incidence angle greater than the critical angle leading to total reflection of the laser beam at the interface. Although totally reflected, the wave properties of the incident light create an evanescent field at the interface. The intensity of this evanescent field decreases exponentially as the distance from the interface increases. This field penetrates a distance of a few hundred nanometers into the solution exciting those fluorophores that are close to the slide/solution interface. This results in those molecules far away from the interface not being excited by the laser, decreasing any background emission signal that would otherwise be produced by those molecules (Figure 2.4).

1.5 Fluorescent labeling of nucleic acids

Fluorescence-based assays have become increasingly important in biophysical studies of the structure, function and dynamics of nucleic acids. The advent of single molecule fluorescence spectroscopy has offered insight into many kinetic and mechanistic details previously hidden by ensemble techniques. These studies require the site-specific and stable incorporation of fluorescent tags into the system of interest. Ribonucleic acid (RNA) and deoxyribonucleic acid (DNA) do not contain naturally occurring fluorophores, therefore, to perform fluorescence assays, it is necessary to introduce these groups. For short nucleic acid constructs, a fluorophore may be conjugated to a nucleotide at the 5’ end, 3’ end or internally. For longer nucleic acid constructs, a fluorophore label may be added by ligation or hybridization of short fluorescently labeled oligonucleotides.

1.5.1 Short Nucleic Acids

Short nucleic acids (less than 60 nucleotides) can be fluorophore labeled by conjugating to the 5' end, the 3' end or an internal nucleotide. The label may be added during oligonucleotide synthesis through the incorporation of fluorescently nucleotide analogs or by post-synthetic covalent attachment of the fluorophore to a modified base.

1.5.1.1 Labeling during synthesis

Fluorophores may be incorporated directly to an oligonucleotide during solid-phase synthesis by use of fluorescent phosphoramidites. Drawbacks of fluorescent labeling during synthesis include the limited availability of fluorescent phosphoramidites and many fluorophores are not stable enough to withstand multiple rounds of synthesis.

1.5.1.2 Post-synthetic labeling

Post-synthetic fluorescence labeling is the most common method for labeling nucleic acids. To post-synthetically add a fluorescent label to the 5' end or 3' end of an oligonucleotide, an amino ($-NH_2$) or thiol (-SH) group is added via an aliphatic carbon linker that is linked to the terminal phosphate group. Succinimidyl ester, isothiocyanate or sulfonyl chloride derivitized fluorophores may be then covalently linked to those nucleotides with amino functionalities (Figure 1.7a). Maleimide or iodoacetamide derivitized fluorophores may be covalently linked to those nucleotides with thiol functionalities (Figure 1.7b).

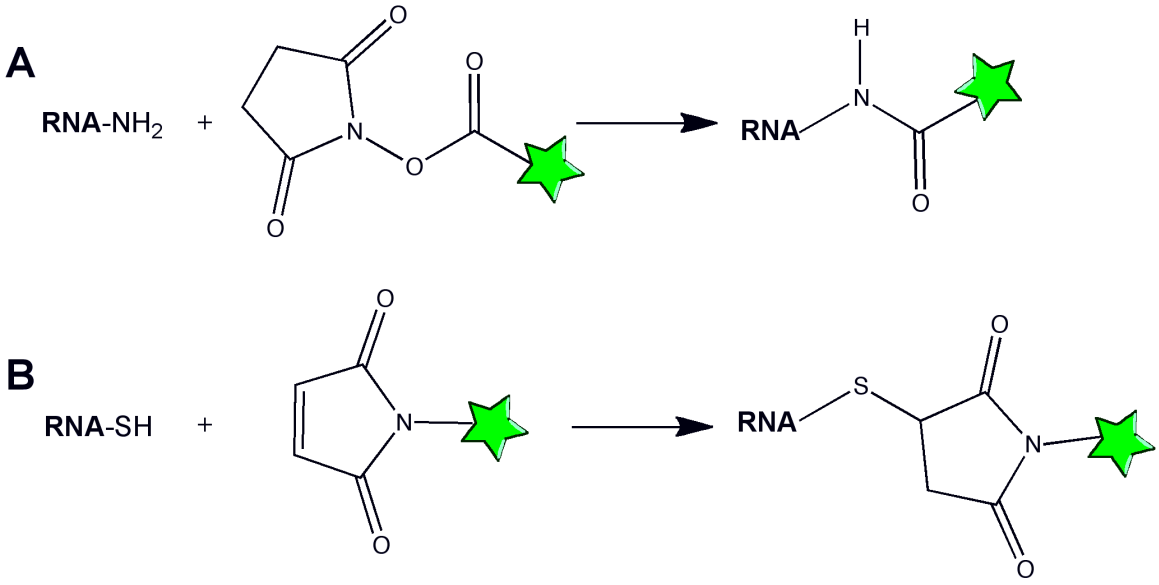

Figure 1.7 Post-synthetic fluorophore labeling via covalent reaction. A) Amino group on oligonucleotide reacts with succinimidyl ester conjugated to a fluorophore. B) Thiol group on oligonucleotide reacts with maleimide conjugated to a fluorophore.

Labeling protocols have previously been published and are provided along with the dye from the manufacturer(*39-41*). Labeling reactions can typically be carried out at room temperature under mild conditions. To post-synthetically add a fluorescent label to an internal nucleotide, an aliphatic carbon linker with an amino or thiol group may be linked to the C5 of a modified thymine or cytosine. The amino or thiol moieties may be reacted with the derivitized fluorophores mentioned above. Other less common labeling strategies have been described, including conjugation via click chemistry, biotin/avidin, antibody/antigen, crosslinking, and caging(*39-41*).

1.5.1.3 Labeling during transcription

The 5' end of an oligonucleotide may be labeled during transcription by introduction of fluorescently labeled nucleotide analogs or by functionalizing the 5' terminus with a thiophosphate, which is then reacted with a derivatized fluorescent dye. In the latter, an excess of guanosine 5'-monothiosphosphate (GMPS) over guanosine triphosphate (GTP) is added to the transcription reaction. As the excess GMPS can only be incorporated at the 5' end, the majority of RNA transcripts will be primed with 5' GMPS. The thiol group at the 5' end can then be conjugated to a maleimide or iodoacetamide derivitized fluorophore. This method has been successfully used to site-specifically label the 5' end of precursor $tRNA^{Asp}$ (*42*).

1.5.2 Long Nucleic Acids

Longer nucleic acids (greater that 60 nucleotides) present more of a challenge for fluorescent labeling, as such RNAs cannot be efficiently synthesized by solid phase synthesis and RNA polymerase cannot incorporate dyes site specifically during transcription. Two main strategies, hybridization of short fluorescently labeled oligonucleotides and ligation, have been developed to introduce a fluorescent label onto these longer nucleic acids.

1.5.2.1 Labeling via hybridization

A fluorescent label may be introduced to a longer oligonucleotide via hybridization, in which a short fluorescently labeled oligonucleotide is designed to selectively hybridize to an appropriate single-stranded stretch of the RNA or DNA. A specific loop sequence may be engineered to afford hybridization of the labeled oligonucleotide. A group II intron was fluorescently labeled via hybridization (Figure 1.8a) in order to investigate the conformational changes of this large, catalytic RNA(*43*). The ribosome was also site-specifically labeled (Figure 1.8b) by hybridizing fluorescently labeled oligonucleotides to extensions in ribosomal RNA hairpins(*44*). Thirdly, a long RNA derived from the catalytic domain of RNase P was fluorescently labeled (Figure 1.8c) by replacing a functionally unimportant hairpin loop with one complementary to a short fluorescently labeled oligonucleotide(*45*).

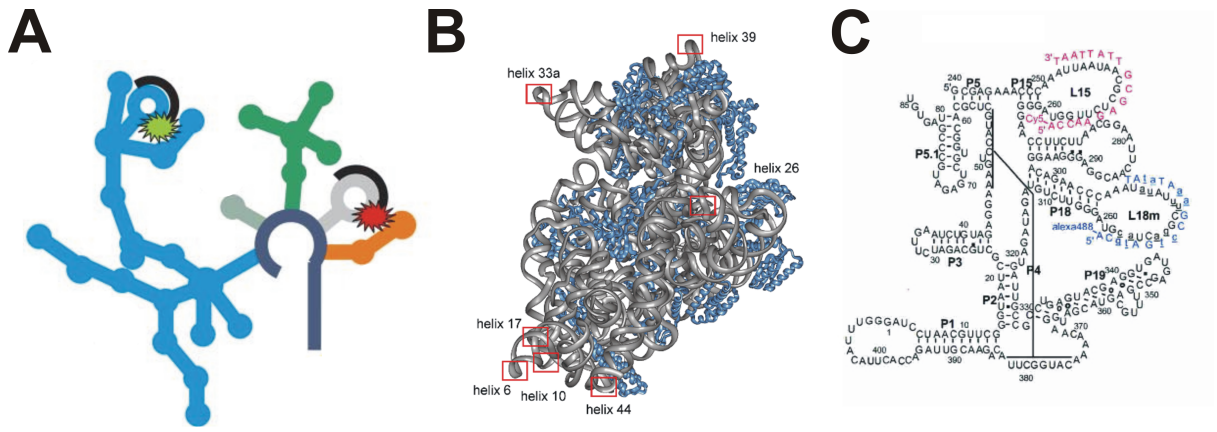

Figure 1.8 Fluorophore labeling via hybridization with fluorescently labeled oligonucleotide. A) Fluorescence labeling of a group II intron from *Saccharomyces cerevisiae* (Steiner 2008). B) Site-specific fluorescence labeling of the ribosomal 30S subunit from *Thermus thermophilus* by introducing helix extensions for hybridization with fluorescently labeled oligonucleotides (Dorywalska 2005). Red boxes indicate helices that were extended for labeling. C) Fluorescence labeling of the catalytic domain of RNase P from *Bacillus subtilis* (Smith 2005). Labeled oligonucleotides (red and blue) hybridized to the extended loops L15 and L18m. All figures were reproduced with permission.

1.5.2.2 Labeling via ligation

A fluorescent label may also be introduced to a longer oligonucleotide via ligation of a fluorescently labeled oligonucleotide. In short, a fluorescently labeled oligonucleotide is ligated to the long unlabeled RNA strand via a short DNA splint oligonucleotide that is complementary to the ends of the two oligonucleotides to be connected. T4 DNA ligase is then added to connect the two oligonucleotides and DNase may be added to degrade the splint (Figure 1.9). T4 DNA ligase has been shown to be effective at ligation as long as either the splint or the oligonucleotides to be ligated is DNA. T4 RNA ligase has been shown to be more efficient at ligating two RNA oligonucleotides. pre-mRNA was fluorescently labeled via ligation in order to monitor splicing by single molecule spectroscopy (*46*).

Labeling via hybridization and ligation both offer advantages and disadvantages. Labeling via ligation allows site-specific labeling anywhere in the RNA but the structure of the RNA competes with hybridization of the DNA splint leading to a large variation in labeling efficiency. Labeling via hybridization of fluorescently labeled oligonucleotides offers a more efficient labeling reaction as well as high specificity; however, the complimentary oligonucleotide may dissociate limiting the duration of experiments as well it may be difficult to find a loop in the native sequence that is sufficient for hybridization so it is often necessary to introduce a non-native sequence for successful hybridization of the

labeled oligonucleotide.

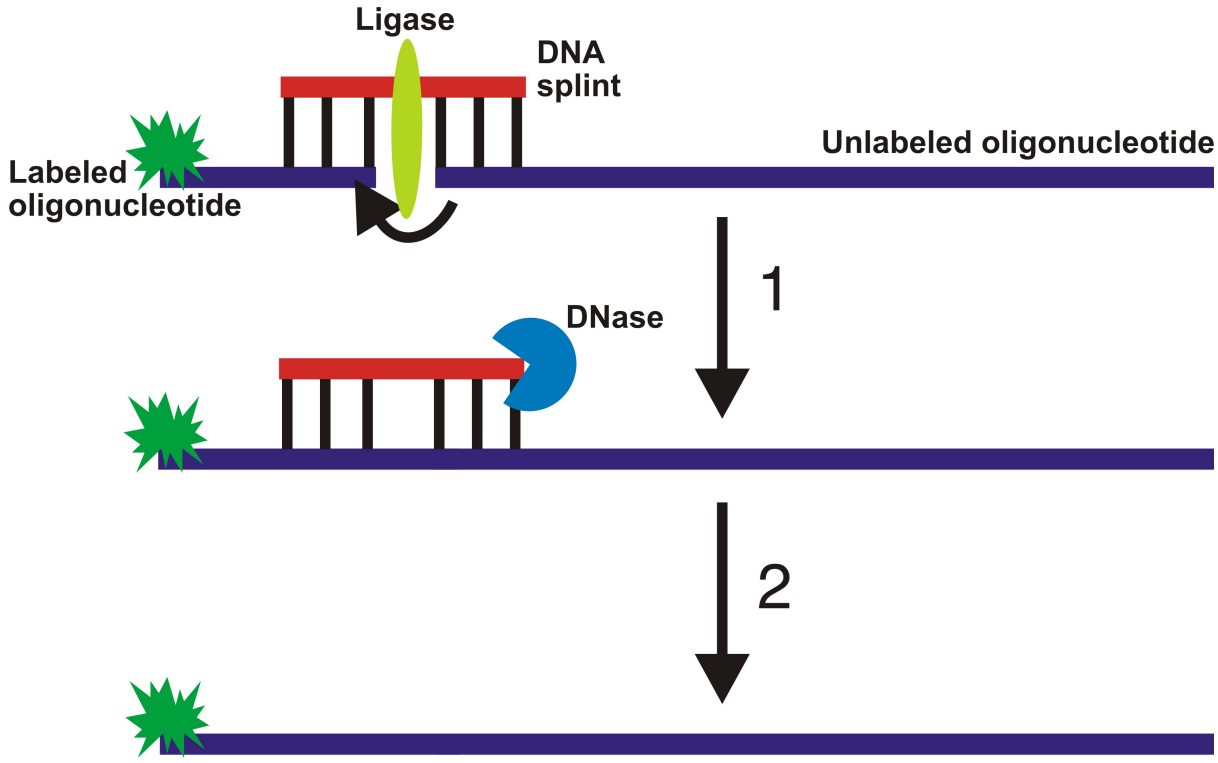

Figure 1.9 Fluorophore labeling via ligation with fluorescently labeled oligonucleotide. Step 1: T4 DNA ligase or T4 RNA ligase II ligates unlabeled oligonucleotide with labeled oligonucleotide. Step 2: DNase degrades DNA splint.

Chapter 2

Allosteric tertiary interactions pre-organize the c-di-GMP riboswitch and accelerate ligand binding (*47*)

Adapted from Wood S., Ferre-d'Amare A., and Rueda D. Allosteric Tertiary Interactions Preorganize the c-di-GMP Riboswitch and Accelerate Ligand Binding. *ACS Chemical Biology,* **2012**, 7(5): 920-927.

2.1 Introduction

Riboswitches are gene-regulatory mRNA domains that directly recognize small molecule metabolites and second messengers(*4, 8-10, 12, 13, 48, 49*). With the exception of the catalytic *glmS* ribozyme-riboswitch(*50, 51*), these genetic regulators function by adopting ligand occupancy-dependent conformations that modulate transcription, translation or alternative splicing. The substructure of a riboswitch that suffices for specific ligand binding *in vitro* is known as its "aptamer" domain. Biophysical characterization of the aptamer domains of different riboswitch classes shows that their global structural response to ligand binding is idiosyncratic(*52*). For instance, the aptamer domain of the flavin-mononucleotide (FMN) riboswitch from *Bacillus subtilis* is largely pre-organized in the absence of FMN at physiologic Mg^{2+} concentrations, while that of the class I S-adenosylmethionine (SAM) riboswitch from the same organism is only partly ordered in the absence of its cognate metabolite, and adopts its most compact form upon SAM binding(*52*). Moreover, the degree of compaction induced by ligand binding or by a particular Mg^{2+} concentration varies even between the aptamer domains of members of the same class of riboswitch [*e.g.* the thiamine-pyrophosphate (TPP) riboswitches from *Escherichia*

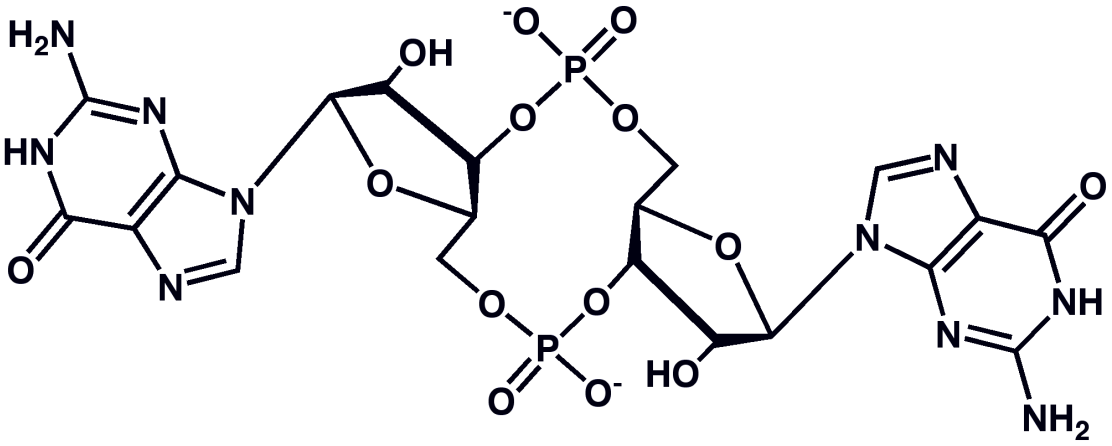

Figure 2.1 Structure of cyclic diguanylate (c-di-GMP).

coli and *Arabidopsis thaliana*](*53*). Although it has been suggested that this variation may reflect the distinct regulatory requirements of each genetic locus(*53*), the functional significance of ligand binding-induced global folding of riboswitch aptamer domains remains to be established.

Cyclic diguanylate (c-di-GMP) is a bacterial second messenger involved in the regulation of a variety of complex physiological adaptations including motility, virulence, biofilm formation, and cell cycle progression (Figure 2.1) (*15-17, 54, 55*). Two structurally distinct classes of riboswitches that recognize c-di-GMP have been described(*14, 56*). Of these, the class-I riboswitches (c-di-GMP-I) are the most widespread. Over 500 different c-di-GMP-I riboswitches have been identified in a wide range of bacterial species. This riboswitch is often found in multiple copies in bacterial genomes. For instance, as many as 30 different genetic loci in *Geobacter uraniumreducens* appear to be under c-di-GMP-I riboswitch regulation(*57*). Crystallographic structure determinations of the aptamer domain of the c-di-GMP-I riboswitch associated with the *tfoX* gene of *Vibrio cholerae* bound to the second messenger revealed that the RNA consists of three helices, paired regions P1a, P1b, and P2, joined in a three-way junction by joining regions J1a/b, J1b/2, and J2/1a (Figure 2.2) (*1, 58*). c-di-GMP binds at the junction, participating in a network of interactions between P1a, P1b, and the three joining regions. The conserved A47 from J1b/2 intercalates between the two guanine bases of the second messenger (Figure 2.2, purple). The bound c-di-GMP and A47 mediate continuous coaxial stacking between P1b and P1a. P2 docks side-by-side with P1b. This arrangement appears to be stabilized by two

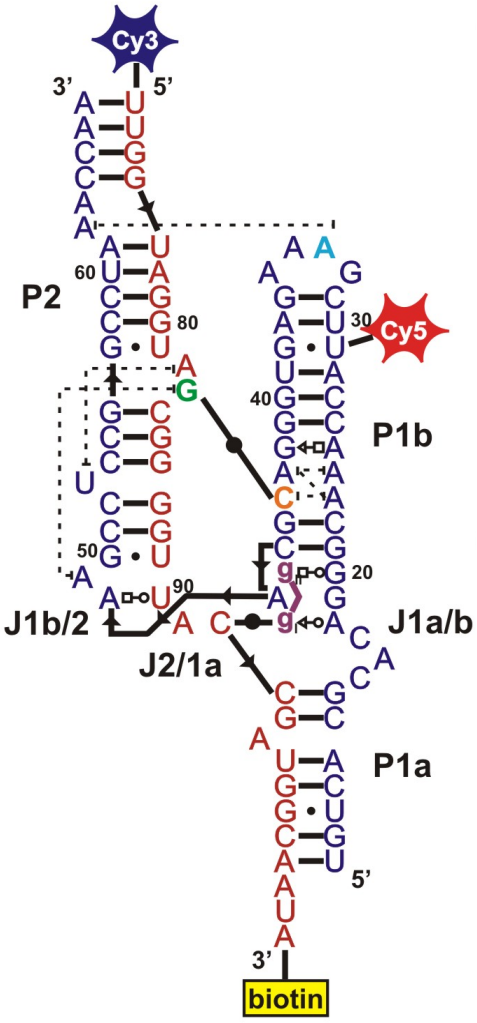

Figure 2.2 Secondary structure of the c-di-GMP-I riboswitch aptamer domain from *Vibrio cholerae* with c-di-GMP bound. For smFRET, a two-piece construct was used with the strands highlighted in red and blue. The red strand was covalently labeled with a Cy3 fluorophore on the 5' end and a biotin on the 3' end for immobilization to the quartz slide for smFRET experiments. The blue strand was internally labeled with a Cy5 fluorophore. Bound c-di-GMP is highlighted in purple and G83C, C44A, and A33U mutations are highlighted in green, orange, and cyan, respectively.

sets of phylogenetically conserved tertiary interactions distal to the junction, in addition to the c-di-GMP-bound junction itself. First, the GNRA tetraloop (GT) that caps P1b docks against a tetraloop receptor (TR) in P2(*59*). Second, an interhelical Watson-Crick pair is formed between C44 of P1b and G83 of P2 (Figure 2.2, green and orange) (*1, 58*).

Small-angle X-ray scattering (SAXS) experiments revealed a dramatic compaction of the class-I riboswitch aptamer domain induced by c-di-GMP binding in the presence of physiologic concentrations of Mg^{2+} ion(*1, 53*). Low-resolution molecular envelopes calculated from the SAXS data suggest that in the absence of the second messenger, the RNA adopts an extended conformation in which P1b and P2 are splayed apart, and neither the GT/TR interaction nor the C44•G83 base pairing takes place. Nuclease protection and in-line probing experiments are consistent with disruption of both sets of tertiary interactions in the absence of c-di-GMP, and also suggest that P1a becomes disordered under these conditions(*1, 14*). Previous studies of large catalytic RNAs have shown that tertiary interactions promote RNA folding within compact intermediates resulting from an early divalent-cation induced collapse, in which the helices interact but are not yet stably docked (reviewed in (*60*)). For instance, in the case of the *Azoarcus* group I ribozyme, a GT/TR interaction has been shown cooperatively to promote tertiary structure throughout the RNA, increasing the speed and accuracy of its folding(*61*). Unlike these catalytic RNAs, which require only divalent cations to achieve their native state, riboswitch

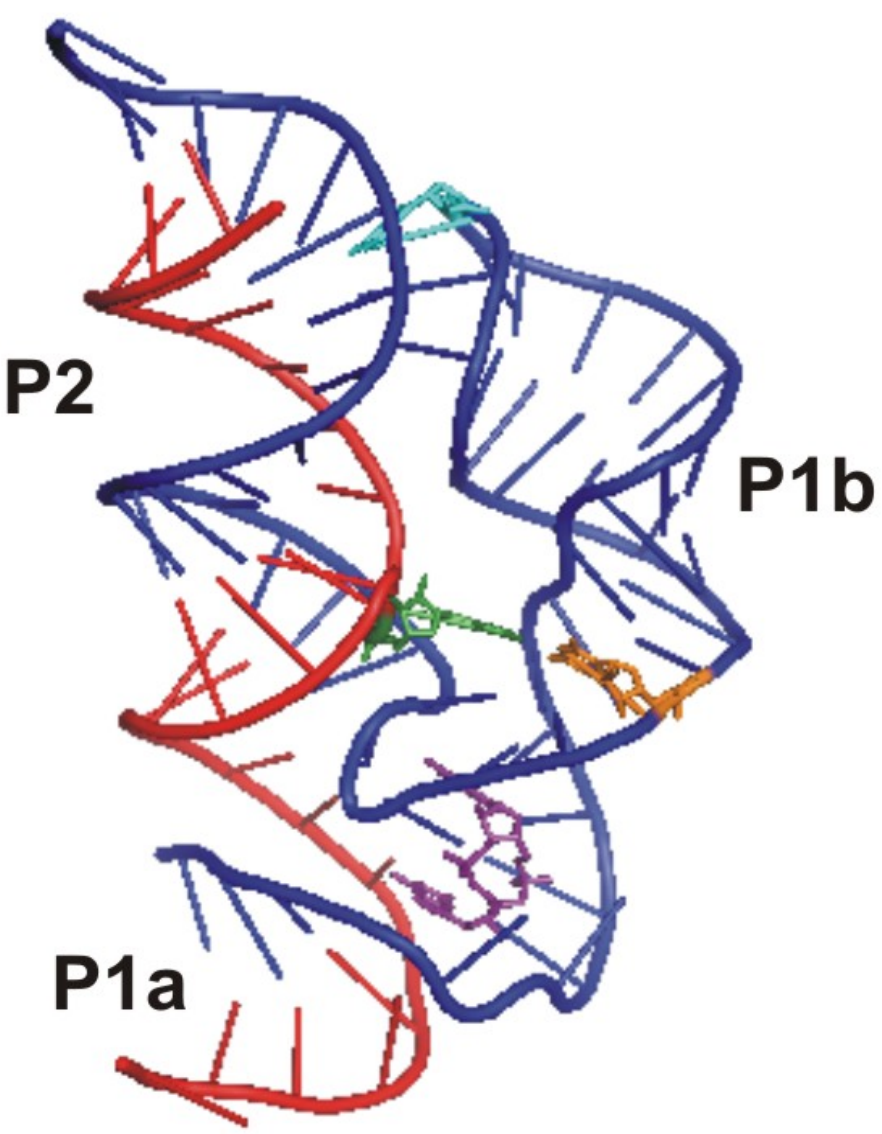

Figure 2.3 Three-dimensional structure of the c-di-GMP-I riboswitch aptamer domain(*1*), color-coded as in Figure 2.2.

aptamer domains have evolved to recognize small molecules concomitant with folding.

In order to dissect the interplay of cations, second-messenger ligand and tertiary interactions in riboswitch folding, we have now analyzed the c-di-GMP-I aptamer domain using single molecule fluorescence resonance energy transfer (smFRET)(*39, 62-68*). These studies confirm that this RNA samples extended and compact conformations. However, the smFRET analysis, which can uncover structural dynamics of individual molecules that would otherwise be hidden in ensemble-averaged experiments, reveal that the aptamer domain is kinetically partitioned into four distinct populations: two that in the timeframe of the experiment remain statically docked or undocked (compact or extended, respectively), one that fluctuates between docked and undocked but is preferentially in the docked state, and another that fluctuates but is preferentially undocked. The population structure shifts in response to Mg^{2+} and c-di-GMP concentration, such that at saturating second messenger and physiologic Mg^{2+} concentration, the majority of the molecules are statically docked. smFRET analysis of site-directed mutants that disrupt the GT/TR or C44•G83 tertiary interactions indicates that these are required not only for binding of c-di-GMP, but also profoundly impact the population structure of the RNA in the absence of ligand. Thus, we find that these tertiary interactions, which are distant from the c-di-GMP binding site, serve to pre-organize the aptamer domain. *In vivo*, this would allow the nascent riboswitch transcript to fold and recognize its ligand

rapidly and thus respond effectively to varying intracellular levels of the second messenger.

2.2 Results

2.2.1 Single molecule FRET reveals four distinct populations

We incorporated a Cy3 (donor) and a Cy5 (acceptor) fluorophores near the distal tips of P2 and P1b, respectively, of an RNA construct based on the *Vibrio cholerae tfoX* c-di-GMP riboswitch (Figure 2.2) (*39*). With this labeling scheme, the extended conformation is expected to result in a low FRET ratio, while the compact conformation is expected to result in a high FRET ratio(*1*). Characteristic smFRET time trajectories in standard conditions (which contain 2.5 mM Mg^{2+}) are shown in Figure 2.5. The aptamer domain RNA exhibits FRET ratios of 0.2 and 0.8, which may correspond to the extended and docked conformations, respectively, deduced from the SAXS reconstructions(*1*). States with intermediate FRET efficiencies were not observed with a time resolution of 33 ms. In the absence of c-di-GMP, most molecules (49 ± 4% of 282, Table 2.1) remain in a low FRET state over the time of the experiment (a few minutes). We refer to this population as static undocked. A smaller population (27 ± 5%) resides primarily in the high FRET state with brief excursions into the low FRET state. We refer to this population as dynamic docked. Two other minor populations are also observed: one in which molecules exhibit high FRET for the duration of the experiment (7 ± 2%), and another in which molecules display primarily low FRET with brief excursions into a high FRET state (17 ± 8%). We refer to these populations as static docked and dynamic undocked, respectively.

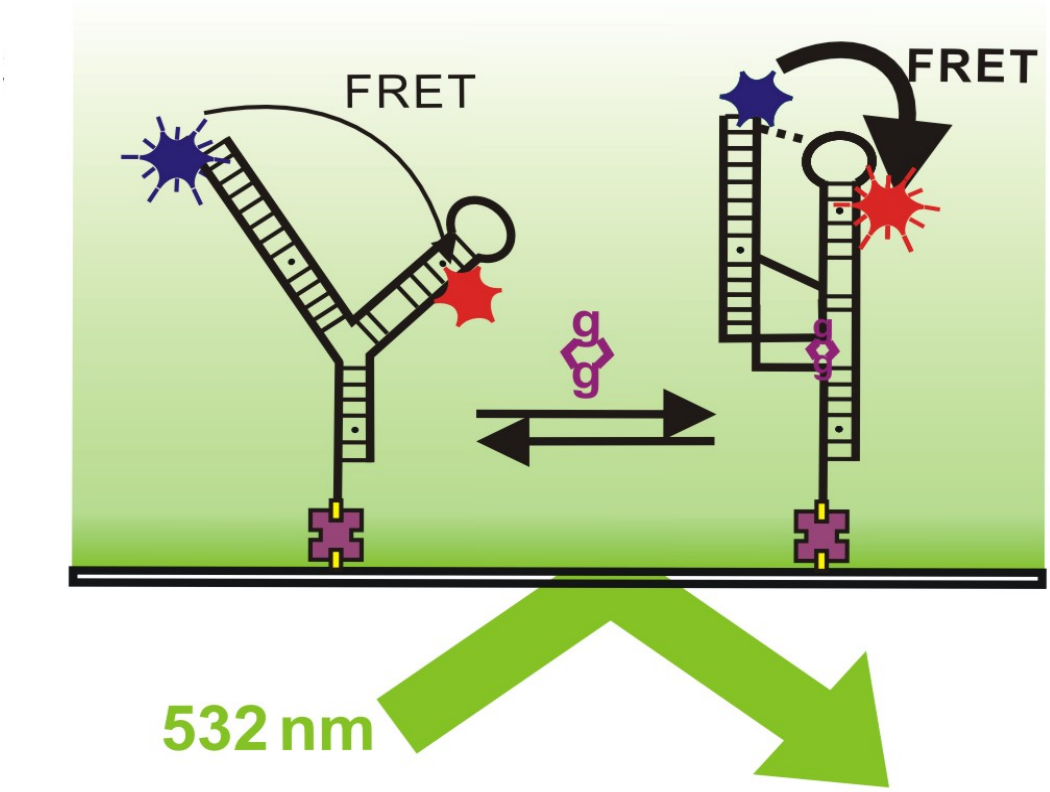

Figure 2.4 Single molecule FRET reveals four populations. Schematic diagram of single molecule experiments. The RNA complex is immobilized to the quartz slide surface through a biotin-streptavidin bridge. The fluorophores are excited in a prism-based total internal reflection microscope. Fluorescence is collected through the objective and monitored with a CCD camera.

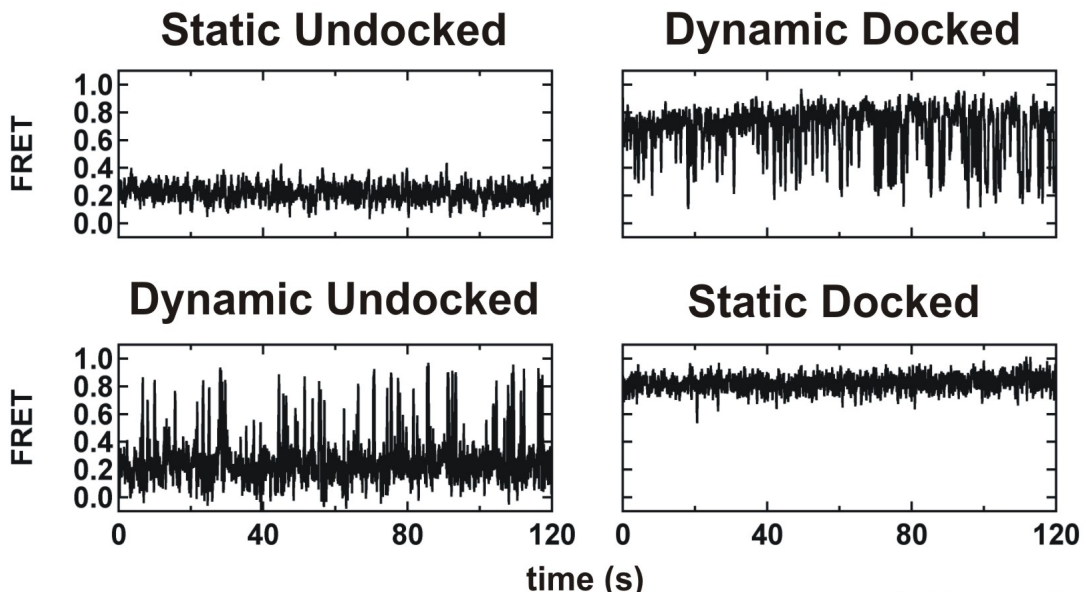

Figure 2.5 Single molecule FRET reveals four populations. smFRET time trajectories. The static undocked population is identified by a static 0.2 FRET ratio. The dynamic docked population is identified by a mostly 0.8 FRET ratio with brief excursions to low FRET. The dynamic undocked population is identified by a mostly 0.2 FRET ratio with brief excursion to high FRET. The static docked population is identified by a static 0.8 FRET ratio.

	c-di-GMP	[Mg^{2+}] (mM)	N	Static Undocked (%)	Dynamic Undocked (%)	Dynamic Docked (%)	Static Docked (%)
WT	-	0	75	96 ± 6	4 ± 4	0	0
	+	0	98	95 ± 4	4 ± 4	0	1 ± 1
	-	0*	107	100 ± 0	0	0	0
	+	0*	144	100 ± 0	0	0	0
	-	2.5	282	49 ± 4	17 ± 8	27 ± 5	7 ± 2
	+	2.5	250	29 ± 6	8 ± 6	2 ± 2	61 ± 4
	c-di-AMP	2.5	149	54 ± 8	14 ± 2	29 ± 13	3 ± 2
	-	50	118	29 ± 1	27 ± 7	34 ± 1	10 ± 5
	+	50	97	19 ± 10	7 ± 7	4 ± 4	70 ± 10
G83C	-	2.5	108	95 ± 9	5 ± 1	0	0
	+	2.5	164	80 ± 6	17 ± 1	1 ± 1	2 ± 2
C44A	-	2.5	99	93 ± 3	7 ± 4	0	0
	+	2.5	166	68 ± 5	7 ± 4	0	25 ± 7
A33U	-	2.5	99	68 ± 6	29 ± 8	4 ± 2	1 ± 1
	+	2.5	101	49 ± 5	12 ± 1	2 ± 1	37 ± 3
	-	20	102	60 ± 9	23 ± 9	17 ± 9	1 ± 1

Table 2.1 Percentage of molecules residing in the static undocked, dynamic docked, dynamic undocked, and static docked populations for wild-type (WT) and mutant c-di-GMP-I riboswitch aptamers as a function of [Mg^{2+}] and the presence of 1 μM c-di-GMP or c-di-AMP, as indicated. N is the number of molecules. Percentages were calculated as the number of molecules residing in each population out of the total number of molecules analyzed. Confidence intervals stem from the standard deviation between at least two replicate experiments.

*Conditions with no Mg^{2+} and high monovalent (150 mM K^+ and 30 mM Na^+).

	[Mg^{2+}] (mM)	K_D (nM)	ΔH (kcal/mol)	$-T\Delta S$ (kcal/mol)	ΔG (kcal/mol)	*n*
WT	0.5	12000	-56.3	49.4	-6.9	0.9
	2.5	13.8 ± 1.6	-42.2 ± 1	31.2 ± 1	-10.9 ± 0.2	1.0 ± 0.1
	10	5.9 ± 1.4	-38.4 ± 1.5	27.1 ± 1.8	-11.3 ± 0.3	0.9 ± 0.1
G83C	10	7250 ± 353	-37.8 ± 4.6	30.7 ± 4.5	-7.1 ± 0.1	1.0 ± 0.1
C44A	10	496 ± 53	-41.7 ± 2.1	32.9 ± 1.9	-8.8 ± 0.1	0.9 ± 0.1
G83U	10	1500	-41.6	33.6	-8.0	0.8
A33U	10	12.5 ± 3.5	-37.7 ± 0.1	26.8 ± 0.2	-10.9 ± 0.1	1.1 ± 0.1
A34U	10	23 ± 2.8	-45.8 ± 1.3	35.1 ± 1.3	-10.6 ± 0.1	0.9 ± 0.1
A34G	10	16.5 ± 2.1	-35.2 ± 0	24.2 ± 0	-10.9 ± 0	1.1 ± 0.1
A34C	10	26 ± 7	-47.3 ± 0.3	36.7 ± 0	-10.6 ± 0.3	1.0 ± 0.1

Table 2.2 Isothermal titration calorimetry analysis of c-di-GMP binding by wild-type (WT) and mutant c-di-GMP-I riboswitch aptamers. *n* denotes the stoichiometry indicated by the non-linear least-squares fit. Results are reported as the mean ± standard deviation. WT titrations at 2.5 mM and 10 mM Mg^{2+} were carried out in triplicate and a single titration at 0.5 mM Mg^{2+}. Mutant titrations were carried out in duplicate, except for the G83U titration, which was carried out once. T = 303.15 K for all experiments. For $-T\Delta S$ values, error was propagated by multiplying the error of ΔS by T.

We used dwell time analysis to determine the rate constants of docking and undocking for the two dynamic populations (Figures 2.6 and 2.7) (*39*). In the absence of c-di-GMP, k_{dock} and k_{undock} for the dynamic docked population are 6.6 ± 0.2 s^{-1} and 1.0 ± 0.1 s^{-1}, respectively, while k_{dock} and k_{undock} for the dynamic undocked population are 1.6 ± 0.1 s^{-1} and 6.7 ± 0.1 s^{-1}, respectively. Thus, the dynamic docked molecules spend most of the time in the docked conformation and the dynamic undocked molecules spend most of the time in the undocked conformation. The distinct kinetic properties of these two populations become readily apparent by scatter analysis (Figure 2.7b).

In the presence of saturating c-di-GMP (1 μM, standard conditions containing 2.5 mM Mg^{2+}), the static docked population becomes predominant (61 ± 4% of 250 molecules, Table 2.1), suggesting that this population is ligand-bound. Both the static undocked and dynamic docked populations decrease significantly in the presence of ligand (to 29 ± 6% and 2 ± 2%, respectively). The rate constants for docking and undocking for the dynamic populations in the presence of 100 nM c-di-GMP were similar to those in the absence of c-di-GMP (Figures 2.6 and 2.7), suggesting that these dynamic populations do not have c-di-GMP bound. Upon inspection of >100 single molecule time trajectories, we found that the static docked population can form from any of the other three populations, static undocked, dynamic undocked, and dynamic docked (Figure 2.8), providing further evidence that the static docked population is ligand-bound and indicating that any of these populations are able to bind c-di-GMP and form the stable docked conformation. Experiments with lower laser power and longer

exposure showed the static docked conformation has a lifetime longer than 30 min (Figure 2.8b), consistent with a previously reported slow bulk k_{off}(*58*).

To determine the second messenger binding affinity, we measured the fraction of c-di-GMP bound-riboswitch (static docked population) as a function of c-di-GMP concentration under standard conditions. In the absence of c-di-GMP, 7 ± 2% of riboswitches fold into the static docked conformation. The fraction of static docked RNA molecules increases with the concentration of c-di-GMP and saturates at 68 ± 9% total bound with the remaining molecules persisting in the undocked conformation. A fit to the Langmuir equation results in a K_D = 90 ± 20 nM (Figure 2.9), comparable with that determined by bulk isothermal titration calorimetry (ITC) experiments (Table 2.2). This demonstrates the surface immobilization of the RNA construct does not adversely affect the folding and ligand binding of the aptamer. However, the affinity determined by smFRET and ITC is several orders of magnitude weaker than those based on electrophoretic gel mobility-shift analyses reported previously(*58*), suggesting that the aptamer domain behaves differently in the polyacrylamide gel matrix.

To test the selectivity of the c-di-GMP-I riboswitch, we performed similar experiments using c-di-AMP, a structural analog of c-di-GMP and recently discovered putative bacterial second messenger(*1, 58, 69*). In bulk experiments, c-di-AMP does not bind to the c-di-GMP-I riboswitch(*1, 58*). Consistent with this, in our smFRET experiments, the aptamer displays similar behavior in the presence of 1 μM c-di-AMP as in the absence of c-di-GMP, with comparable

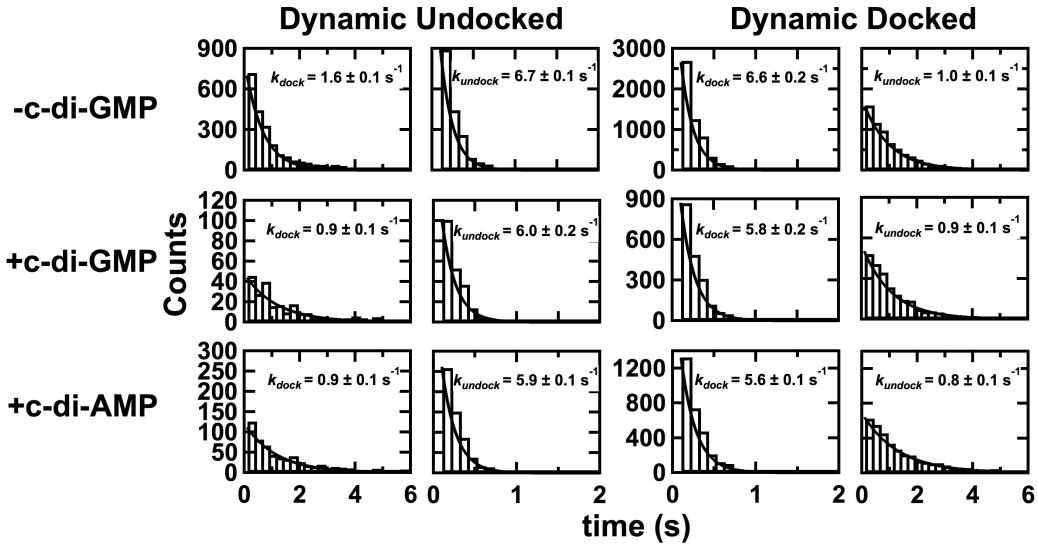

Figure 2.6 The dynamic populations are not bound to c-di-GMP. Dwell time distributions were plotted for the dynamic undocked and dynamic docked populations (left and right, respectively) in the absence of and presence of 100 nM c-di-GMP and presence of 1 μM c-di-AMP (top to bottom). The distributions were fit to single exponential decays to obtain k_{dock} and k_{undock}.

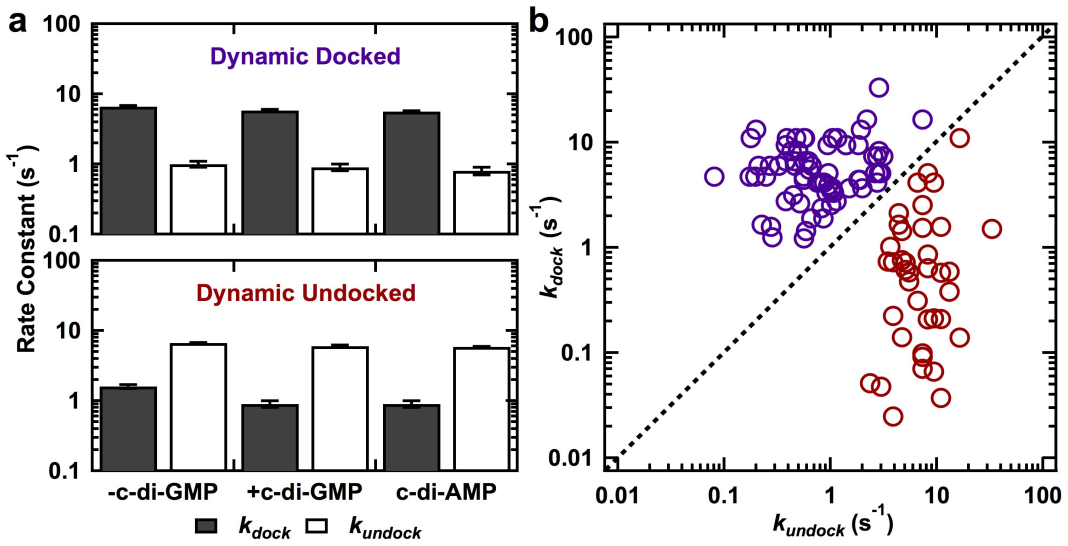

Figure 2.7 The dynamic populations do not have c-di-GMP bound. (**a**) Rate constants k_{dock} (black) and k_{undock} (white) for the dynamic docked and dynamic undocked populations in the absence of and presence of 100 nM c-di-GMP or presence of 1 μM c-di-AMP. The dwell time distributions were fit to single exponential decays to obtain k_{dock} and k_{undock}. (**b**) Scatter plot of the rate constants for both dynamic docked (purple) and dynamic undocked (red) populations in the absence of c-di-GMP demonstrates the existence of two distinct dynamic populations. The dynamic docked molecules lie above the diagonal, while the dynamic undocked lie below.

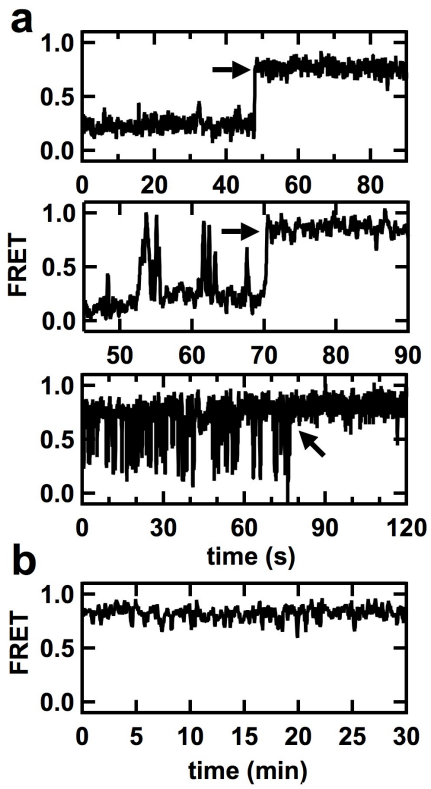

Figure 2.8 All aptamer domain populations can bind c-di-GMP. (**a**) smFRET time trajectories of the c-di-GMP-I riboswitch in the presence of 1 μM c-di-GMP showing formation of the static docked population from static undocked, dynamic undocked, and dynamic docked populations (top to bottom). Arrow indicates transition to the static docked population. (**b**) Single molecule FRET time trajectory showing the long-lived (at least 30 min) static docked population in the presence of 1 μM c-di-GMP.

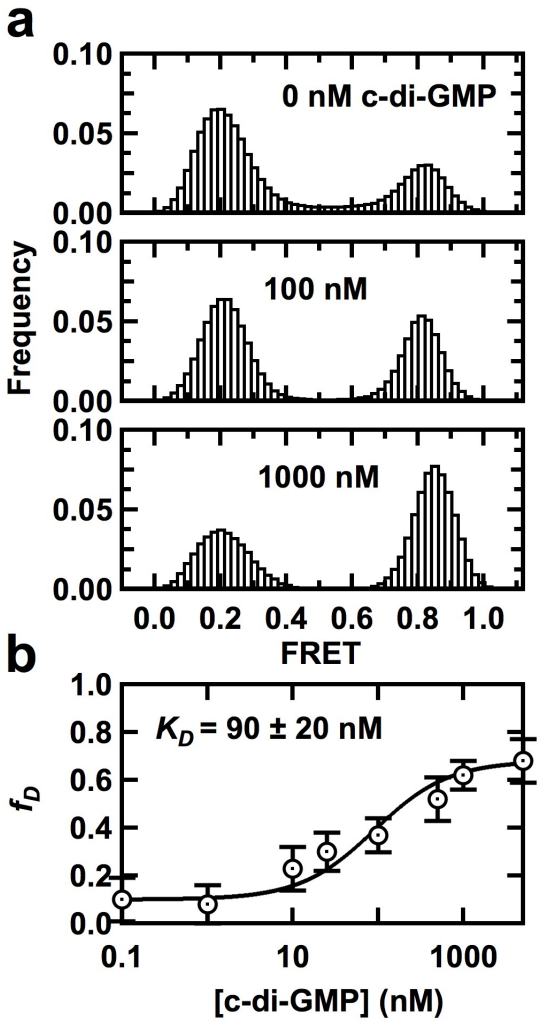

Figure 2.9 Formation of a stable docked conformation requires c-di-GMP. (**a**) smFRET histograms for >100 single molecule trajectories from all four populations combined as a function of the concentration of c-di-GMP, as indicated. In the absence of ligand, the low FRET (0.2) state predominates. As the concentration of c-di-GMP increases, the high FRET (0.8) state becomes more populated. (**b**) The fraction of static docked molecules (f_D) increases as a function of the conentration of c-di-GMP. The line is a fit to a modified Langmuir equation. Error bars are calculated based on the number of molecules.

population distributions (Table 2.1). This similarity extends to the docking and undocking rate constants for the dynamic molecules (Figures 2.6 and 2.7), supporting our interpretation that the dynamic molecules are not bound to the second messenger.

Overall, these data show the c-di-GMP-I riboswitch aptamer domain adopts docked and undocked conformations similar to those deduced from SAXS analysis(*1*). The RNA is kinetically partitioned into four distinct populations that do not readily interconvert in the timeframe of our experiments (several minutes) under steady-state conditions: static undocked and docked as well as dynamic undocked and docked. The RNA binds c-di-GMP tightly and selectively to fold into the stable docked conformation, and this results in a shift in the population structure, since the aptamer domains in the three other populations are competent for second messenger binding.

2.2.2 Stable docked conformation requires both Mg^{2+} and c-di-GMP

Previous SAXS analysis of the *V. cholerae* c-di-GMP-I riboswitch aptamer domain indicates that the RNA undergoes global compaction as the concentration of Mg^{2+} is raised from 2.5 mM to 10 mM (ref (*1*)). This is reminiscent of the behavior of other RNAs with complex structure, such as the group I intron and RNase P, which undergo Mg^{2+} ion-induced folding(*70-72*). Those large ribozymes attain their native conformations upon Mg^{2+} ion-induced folding, as judged by their full catalytic activity(*73, 74*). In contrast, Kratky analysis of the SAXS data on the c-di-GMP-I aptamer domain implies that, unlike the group I intron and RNase P, the riboswitch remains locally disordered even at

high Mg^{2+} concentration until c-di-GMP is bound(*1*). Divalent cations can facilitate RNA folding non-specifically, as part of a diffusely condensed ionic atmosphere, or by making specific, direct interactions with the RNA(*75*). Our smFRET experiments indicate that both modes of action are operative in the c-di-GMP-I riboswitch.

To analyze the role of Mg^{2+} in c-di-GMP riboswitch folding, we measured the fraction of each RNA population as a function of Mg^{2+} concentration. In the absence of both, Mg^{2+} and c-di-GMP, almost all of the molecules (96 ± 6% of 75 molecules) reside in the static undocked population (Table 2.1). In the absence of Mg^{2+} ion, addition of saturating c-di-GMP does not alter the percentage of static undocked molecules. In very high Mg^{2+} ion concentration (50 mM), but in the absence of c-di-GMP, the majority of molecules reside in the dynamic docked and undocked populations, as a consequence of a substantial decrease in the static undocked population. Fitting the fraction of dynamic molecules (including both dynamic docked and undocked) as a function of Mg^{2+} ion concentration to the Langmuir equation yields $K_{1/2}$ = 1.2 ± 0.2 mM (Figure 2.11). Even under these elevated Mg^{2+} concentration conditions, only a small fraction of the molecules (10 ± 5%) are statically docked (Table 2.1). These results indicate that both c-di-GMP and Mg^{2+} are necessary to drive a majority of the molecules into the static docked state, and further supports our assignment of this population to the ligand bound, highly structured conformation characterized crystallographically and by SAXS(*1*).

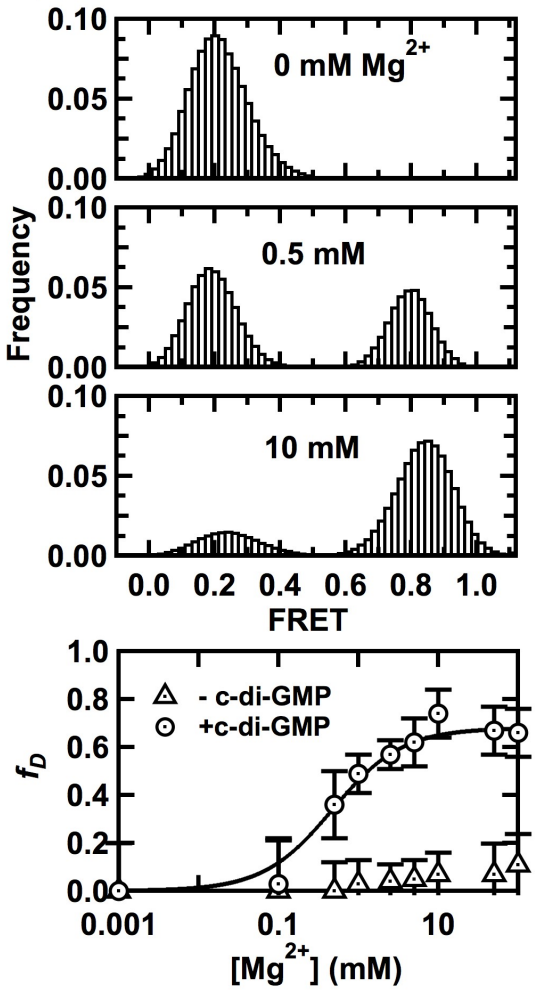

Figure 2.10 Formation of a stable docked conformation requires Mg^{2+}. (**top**) smFRET histograms for >100 single molecule trajectories from all four populations combined in the presence of 1 μM c-di-GMP as a function of the concentration of Mg^{2+}, as indicated. At low Mg^{2+}, the low FRET state predominates. As the concentration of Mg^{2+} increases, the high FRET state becomes more populated. (**bottom**) The fraction of static docked molecules (f_D) increases as a function of the concentration of Mg^{2+} in the presence of 1 μM c-di-GMP (circles). The line is a fit to a modified Langmuir equation resulting in $K_{1/2}$ = 0.5 ± 0.1 mM. However, the fraction of static docked molecules (f_D) does not change significantly as a function of the concentration of Mg^{2+} in the absence of c-di-GMP (triangles). Error bars are calculated based on the number of molecules.

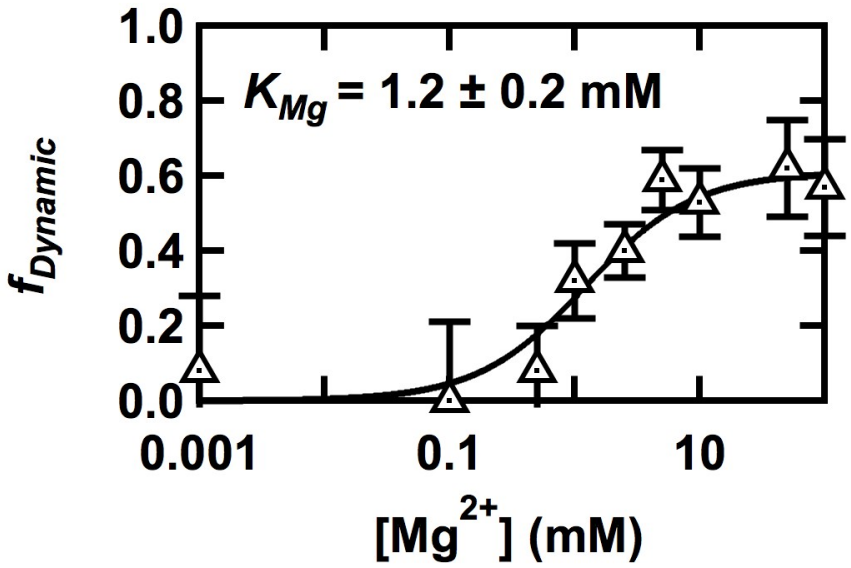

Figure 2.11 The fraction of dynamic molecules ($f_{Dynamic}$) increases as a function of Mg^{2+} concentration in the absence of c-di-GMP. The line is a fit to a modified Langmuir equation. Error bars are calculated based on the number of molecules.

To determine the interplay of Mg^{2+} ion and second messenger binding, we measured the fraction of c-di-GMP bound-riboswitch (the statically docked population) as a function of the concentration of the cation. In the presence of saturating c-di-GMP, the static docked population increases concomitant with increasing Mg^{2+} concentration (Figure 2.10). Fitting the data to the Langmuir equation yields a $K_{1/2}$ = 0.5 ± 0.1 mM (Figure 2.10, circles), a value near the physiological range of concentration for the cation(*76*). In the absence of c-di-GMP, there is no increase in the static docked population (Figure 2.10 triangles), indicating that Mg^{2+} and c-di-GMP binding are strongly cooperative. Experiments in the presence of higher monovalent ion concentrations but no Mg^{2+} (50 mM Tris-HCl, pH 8.0, 150 mM KCl, and 30 mM NaCl) show that the aptamer domain cannot fold into the docked conformation and remains entirely in the static undocked conformation even in the presence of saturating c-di-GMP (Table 2.1). These results suggest that the role of Mg^{2+} ion is not solely electrostatic screening required to fold the riboswitch into an ligand binding-competent conformation, but that it specifically mediates binding to the second messenger. Indeed, crystal structures reveal a hydrated Mg^{2+} ion at the second messenger-binding pocket(*77*) where it bridges a phosphate of c-di-GMP with those of residues G19 and G20 of the RNA, and our smFRET titration may be reporting on this tightly bound cation.

2.2.3 Tertiary interactions are required for the stably docked conformation

To characterize the role of the GT/TR and C44•G83 tertiary interactions (Figure 2.2) (*1*),(*58*) in the formation and stability of the docked structure, we

introduced point mutations to prevent their formation. First, we examined the C44•G83 base pair by mutating G83 to C. smFRET analyses of this G83C mutant show that both in the absence or presence of 1 μM c-di-GMP, most molecules (95 ± 9% and 80 ± 6 %, respectively) reside in the static undocked population (Figure 2.12 and Table 2.1). The G83C mutant RNA is therefore unable to attain neither the dynamic nor static docked state, even with c-di-GMP present. These results are consistent with the results of bulk ITC experiments that show that the G83C mutant RNA is severely disrupted in c-di-GMP binding, and exhibits a 1200-fold increase in the apparent K_D for c-di-GMP even at elevated Mg^{2+} concentration (10 mM) relative to wild-type RNA (Table 2.2). Mutation of G83 to U also severely disrupts affinity for c-di-GMP with a 250-fold increase in K_D at 10 mM Mg^{2+} (Table 2.2).

We also mutated C44 to A, which should prevent its interhelical base pairing with G83. smFRET experiments show that in the absence of c-di-GMP (Figure 2.12), the majority of the molecules (93 ± 3%) reside in the static undocked population. However, in the presence of 1 μM c-di-GMP this mutant exhibits a 25 ± 7% population in the static docked conformation (Figure 2.12 and Table 2.1), indicating that the C44A mutation does not destabilize the docked state as much as the G83C mutation. This result is also consistent with the binding affinity measured by bulk ITC, which shows an 80-fold increase in K_D at 10 mM Mg^{2+} (Table 2.2) relative to wild-type. A possible explanation for this result is that the C44A mutant is capable of forming a non-canonical base pair with G83. Overall, these data show that the tertiary C44•G83 base pair is

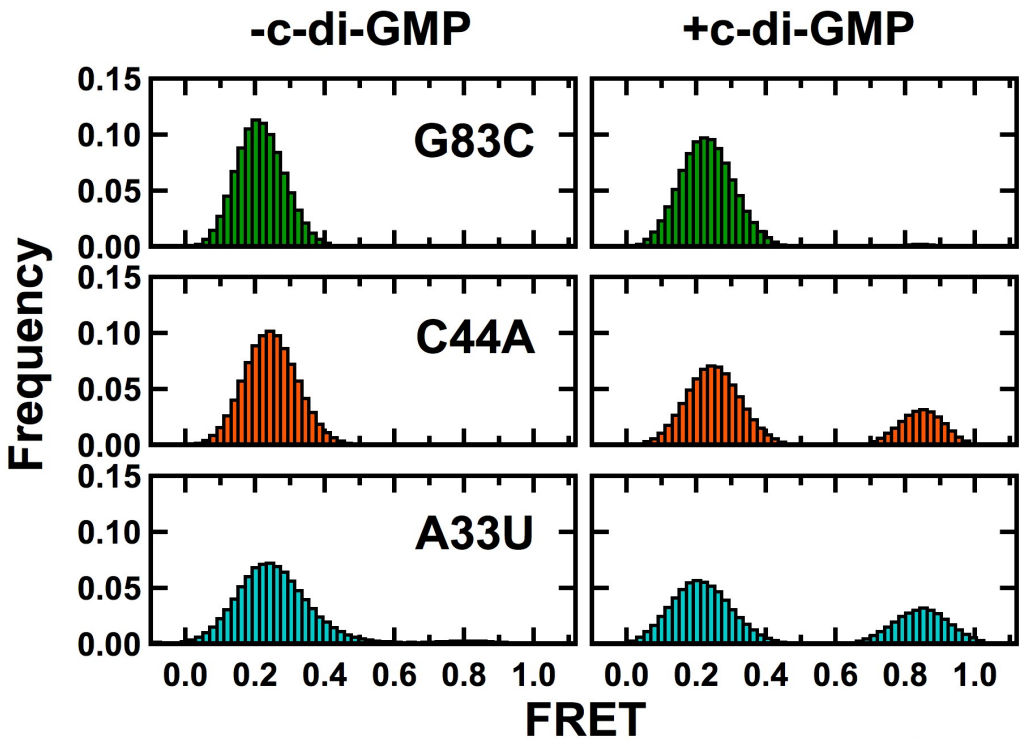

Figure 2.12 Tertiary interactions are necessary for the formation of the docked conformation. Single molecule FRET histograms are shown for >100 single molecule trajectories from riboswitch mutations with and without 1 μM c-di-GMP, as indicated. Colors correspond to the mutations shown in Figure 2.2.

essential for the aptamer domain to attain either the dynamic or static docked states.

Next, we examined the role of the GT/TR interaction between P1b and P2 by mutating A33 to U (Figure 2.2). The crystal structures show that A33 flips out of the GAAA tetraloop to stack with A62 of the TR(*1*). Mutating A33 to U should prevent this stacking, and therefore, impair the GT/TR interaction. smFRET experiments using the A33U mutant in the absence of c-di-GMP show that the majority of molecules (68 ± 6%) reside in the static undocked population but 29 ± 8% of the molecules reside in the dynamic undocked population (Table 2.1). This result shows that, unlike mutations that affect the C44•G83 base pair, mutational destabilization of the GT/TR does not prevent the riboswitch from transiently populating the docked conformation. However, the addition of 20 mM Mg^{2+} was not able to recover the dynamic docked population. In the presence of 1 μM c-di-GMP, the fraction of the molecules in the static undocked population decreases to 49 ± 5% while the static docked population increases to 37 ± 3%, indicating that this mutant can still bind c-di-GMP and form the static docked conformation. This result is in agreement with gel shift experiments, which show a 200-fold increase in apparent K_D for this mutant(*77*). These mutational data indicate that the C44•G83 base pair between P1b and P2 is essential for the formation of the stable docked conformation, while the GT/TR tertiary interaction assists in stabilizing the aptamer in the docked conformation. Overall, our smFRET analyses of riboswitch mutants indicate that docking of P1b and P2

mediated by long-range tertiary interactions is required for formation of a c-di-GMP binding-competent aptamer domain conformation.

2.3 Discussion

Single molecule methods have previously been employed to examine several riboswitches. The adenine and guanine riboswitches are closely related RNAs organized around a three-helix junction, where the purine base binds. In the crystal structures of their ligand-bound aptamer domains(*78, 79*), the loops that close the distal ends of two of the constituent helices of the riboswitch associate through a series of tertiary interactions. smFRET and force spectroscopy experiments imply that some of these long-range interactions can take place in the presence of Mg^{2+} ions alone, prior to purine binding(*63, 64, 67, 80, 81*). smFRET analyses of the class I and II SAM riboswitches suggest that these structurally unrelated RNAs can both transiently sample conformations similar to their respective ligand-bound states in the presence solely of Mg^{2}, and that SAM binding occurs by conformational capture(*65, 66*). The Mg^{2+}-induced, partially folded states of these riboswitches appear to be kinetic intermediates in pathways leading to their ligand-bound (native) states(*64, 66, 67*). This supports the inference that the partially folded states of these RNAs have structural similarity to their native fold.

Like the purine and SAM riboswitches, the c-di-GMP riboswitch can transiently adopt a global fold similar to that of its second messenger-bound form in the presence of Mg^{2+} alone. However, the results of our smFRET analysis reveal that this RNA folds in a complex landscape, populated by four classes of

molecules that interconvert very slowly in the timeframe of the experiment. Such kinetic partitioning has been previously documented in bulk(*82*) and at the single-molecule level(*83-86*) for catalytic RNAs. The shift in the population structure of the RNA upon addition, first of physiologic concentrations of Mg^{2+}, and then c-di-GMP, as well as the cooperativity exhibited by Mg^{2+} and c-di-GMP in formation of the stably docked population suggest that the high FRET state sampled by the dynamic undocked and dynamic docked populations has structural similarity to the native, second-messenger bound conformation. To provide support for this hypothesis, we generated RNAs with site-directed mutations targeting tertiary interactions that are present in the crystal structures of the ligand-bound aptamer domain. We first show calorimetrically that these mutant aptamer domains are impaired, to varying extents, in c-di-GMP binding. smFRET analysis reveals that the mutations perturb the folding landscape of the RNAs, such that decrease in the dynamic populations correlates directly with the deleterious impact of each mutation in ligand binding. This indicates that native-like tertiary interactions are indeed responsible for stabilizing the transiently folded states of the dynamic molecules, thereby demonstrating experimentally that the c-di-GMP riboswitch is pre-organized, rather than simply collapsed. Since the dynamic populations shift to the static docked, ligand-bound conformation in the presence of c-di-GMP, the pre-organization of the riboswitch enables rapid second messenger binding. Our findings parallel those of folding studies on large ribozymes, which have established the importance of forming native-like tertiary interactions early in the

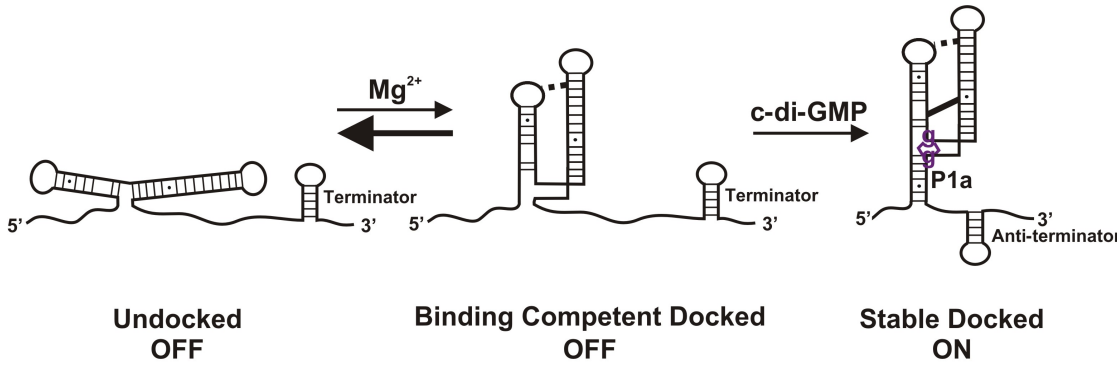

Figure 2.13 Proposed folding pathway of the c-di-GMP-I riboswitch. In the absence of c-di-GMP, the riboswitch adopts a stable undocked conformation, in which P1a is unpaired, allowing formation of the downstream terminator stem-loop and preventing gene expression. In the presence of Mg^{2+}, a population of dynamic riboswitches switch from a docked conformation with brief excursions into the undocked conformation. P1a, however, is not yet formed; therefore, the terminator stem-loop remains, preventing gene expression. This Mg^{2+}-dependent dynamic behavior offers a pre-organized, ligand binding-competent structure that allows efficient cotranscriptional folding and c-di-GMP binding. Binding of c-di-GMP completes the formation of a continuous helical stack between P1a and P1b, which stabilizes the docked conformation, including the P1a helix; the anti-terminator stem forms, preventing formation of the terminator stem-loop, allowing transcription of the downstream gene to proceed.

Mg^{2+} induced collapse of an RNA in order to achieve overall rapid folding (reviewed in (*60*)).

The proposed folding pathway for the c-di-GMP riboswitch is shown in Figure 2.13. In the absence of c-di-GMP, the riboswitch adopts an undocked conformation. In-line and nuclease probing experiments(*1, 14, 58*) indicate that, in the absence of ligand, P1a is unpaired, thus allowing the formation of the downstream terminator stem-loop and preventing gene expression. A Mg^{2+}-dependent population of riboswitches exhibits dynamic switching from this undocked conformation to a docked conformation with brief excursions into the undocked conformation at transcription relevant time scales (~150 ms). This unstable docked conformation is stabilized by the GT/TR and C44•G83 tertiary interactions. The cocrystal structures of the riboswitch(*1, 58*) show that the nucleobase of A49 stacks underneath the C44•G83 base pair. This stacking may help propagate order from the interhelical base pair to the c-di-GMP binding site, in which A47 plays a central role (Figure 2.2). The Mg^{2+}-dependent dynamic population offers a pre-organized structure that allows efficient cotranscriptional folding and ligand binding. Upon binding to the junction region, c-di-GMP completes the formation of a continuous helical stack between P1a and P1b, leading to stabilization of the docked conformation, including the P1a helix. Although we did not directly determine formation of the P1a helix in our experiments, in-line and nuclease probing experiments and crystal structures indicate that this helix is formed in the folded aptamer domain structure(*1, 14, 58, 77*). This helix is the molecular switch controlling gene expression(*14*): the anti-

terminator stem would form, preventing formation of the terminator stem, allowing transcription of the downstream gene to proceed.

The biological significance of the large-scale, ligand-induced folding transition documented by SAXS for the c-di-GMP-I riboswitch has been unclear for two reasons. First, not every riboswitch class examined undergoes such a collapse concomitant with ligand binding(*52, 53*). Second, such large-scale reorganization of the aptamer domain couples the cost of the loss of conformational entropy to ligand recognition, thereby lowering the maximum achievable affinity. Our discovery that the c-di-GMP-I riboswitch aptamer domain transiently folds into a collapsed conformation that has a structure similar to that of the ligand-bound form suggests a role of the global folding transition in a process akin to kinetic proofreading: only molecules in which the P1b and P2 stems have folded correctly (*i.e.* in conformations compatible with making the allosteric GT/TR and C44•G83 tertiary interactions) will present a ligand binding site to the second messenger. It is noteworthy that of the various riboswitches whose Mg^{2+} and ligand induced collapse has been studied by SAXS(*1, 52, 87, 88*), the TPP riboswitch is the RNA that most closely mimics the behavior of the c-di-GMP-I riboswitch. Although their specific sequences are unrelated, the aptamer domains of the c-di-GMP and TPP riboswitches share a similar architecture comprised of a three-helix junction where the ligands bind, and tertiary interactions distal to the ligand binding site stabilizing the side-by-side packing of two helical stems. Biophysical experiments have shown the importance of the allosteric loop-loop interactions in ligand binding by the TPP

riboswitch(*89, 90*). These distal interactions were found to form before the TPP binding site is fully organized(54), paralleling the results of our studies of the c-di-GMP-I riboswitch. Taken together, these studies suggest that large-scale pre-organization coupled to ligand binding may be a strategy to increase structural specificity, and hence accelerate ligand binding, by several riboswitch classes.

2.4 Future Directions

A47 is a conserved residue in junction region J1b/2 of the c-di-GMP riboswitch (Figure 2.14). Upon binding of c-di-GMP, the residue flips out and intercalates between the two guanine bases of the ligand mediating continuous coaxial stacking between helices P1b and P1a. The correct residue is essential for ligand binding and riboswitch activity. Mutation of this residue to C, G, or U severely decreases affinity for c-di-GMP resulting in a decrease of affinity of 770,000-, 380,000-, and 320,000-fold, respectively(*1, 58, 77, 91*). To date, there is no crystal structure of the aptamer in the absence of c-di-GMP and no studies have been done to explore what this residue looks like when the riboswitch is undocked. Does A47 flip out to stack in between the guanine residues upon c-di-GMP binding? Understanding how A47 is involved in ligand binding is important to understand how this riboswitch recognizes its target ligand.

2-aminopurine (Figure 2.15) is a fluorescent purine analog that is a useful tool to probe local changes in nucleic acid conformation(*65, 92-94*). The fluorescence of 2-aminopurine is quenched when the analog is stacked in among other bases and becomes fluorescent when flipped out of the stack or free. A47

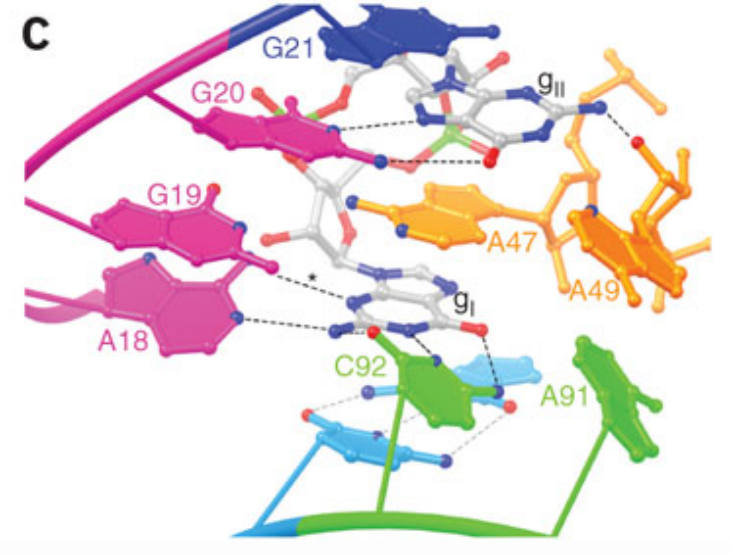

Figure 2.14 In this view from the minor groove, the conserved A47 from J1b/2 intercalates between the two guanine bases (g_I and g_{II}) of c-di-GMP to mediate continuous coaxial stacking between P1b and P1a. Figure from (*1*).

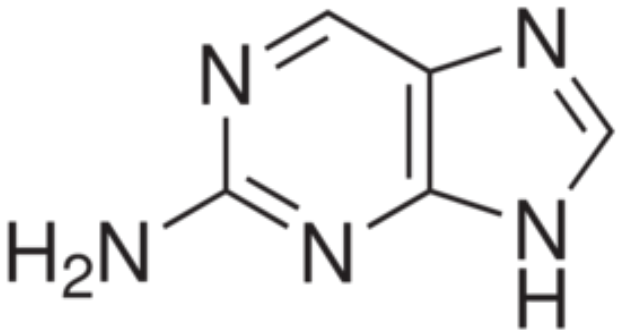

Figure 2.15 Structure of 2-aminopurine.

could be replaced with a 2-aminopurine to investigate the dynamics of this nucleotide both at the bulk and single molecule level. This label could be used in conjunction with the Cy3 and Cy5 labels already present at the distal ends of P2 and P1b that were used to probe the global conformational changes of this riboswitch. Using these three fluorescent labels and single molecule could provide insight into how and at what time point in the folding pathway does this possible conformation change take place.

Further studies into the folding pathway would be interesting to determine the order in which tertiary structures, including the G-C pair and tetraloop/tetraloop receptor interaction, form to ultimately shape the docked structure and what factors, such as Mg^{2+} and c-di-GMP, are required for which structures. Also, are there any transient intermediates? Because the rates of switching between the docked and undocked conformation are so fast, a faster frame rate will be useful in determining if there are any short-lived intermediate structures hidden in the dynamic undocked and dynamic docked populations. Are they in fact switching between a docked and undocked structure or are these populations sampling a variety of intermediate structures?

To date, several studies of various riboswitches, including purine, SAM, and c-di-GMP, have offered a wealth of information concerning the aptamer domain, including both structure and dynamics(*1, 6, 13, 49, 64, 65, 67, 95, 96*). However, there is a lack of data relating the structural

dynamics of the aptamer domain to the way in which it relays information to the downstream expression platform. This could be addressed with the c-di-GMP system by placing FRET labels or a fluorophore-quencher pair at the base of the downstream transcription terminator, which is commonly a hairpin structure. Monitoring how the fluorescence at this expression platform corresponds to the fluorescent dynamics of the aptamer domain could answer various questions such as at what point along the folding pathway of the aptamer domain is the decision made to modulate gene expression downstream.

2.5 Materials and Methods

2.5.1 RNA purification and labeling

The 88-nt c-di-GMP-I aptamer domain previously described(*1*) was used for ITC studies. Mutants were generated using the QuikChange site-directed mutagenesis kit (Stratagene). *In vitro* transcription and purification was as described(*1*). For smFRET experiments, a two-piece construct was used to assemble the aptamer domain of the c-di-GMP riboswitch **(Fig. 1a)**: RED (5'-Cy3-UUG GUA GGU AGC GGG GUU ACC GAU GGC AAU A-Biotin-3') and BLUE (5'-UGU CAC GCA CAG GGC AAA CCA X UCG AAA GAG UGG GAC GCA AAG CCU CCG GCC UAA ACC AA-3', where X is an internal dT with C7 amino linker for Cy5 labeling). RNAs were purchased from the Keck Foundation Resource Laboratory at the Yale University School of Medicine and purified and labeled as described(*41*). The 2'-hydroxyl protection groups were deprotected

according to the manufacturer's protocol. The RNAs were purified by denaturing gel electrophoresis (20% wt/vol polyacrylamide and 8 M urea) and diffusion elution against elution buffer (0.5 M NH_4OAc and 0.1 mM EDTA) overnight at 4°C, followed by chloroform extraction, ethanol precipitation and C8 reverse-phase HPLC. The internal dT C7 amino linker was labeled with Cy5 (GE Healthcare) in labeling buffer (100 mM Na_2CO_3, pH 8.5) overnight at room temperature. The doubly labeled RNA was purified by ethanol precipitation and C8 reverse-phase HPLC. RNA concentrations were measured by UV-Vis absorbance at 260 nm. c-di-GMP was purchased from Axxora LLC, and used without further purification.

2.5.2 Single molecule FRET

Single molecule experiments were performed as described (Figure 2.4) (*39, 68*). We annealed the two RNA strands (Figure 2.2) at 0.5 μM RED and 1 μM BLUE in standard buffer (50 mM Tris-HCl pH 8.0, 30 mM NaCl, 30 mM KCl, and 2.5 mM $MgCl_2$ in saturating trolox). The standard buffer is the same as used in previous SAXS experiments(*1*). We heated a 10 μL solution at 90°C for 45 s before cooling to room temperature over 20 min. We diluted the annealed, biotinylated and fluorophore-labeled complex to 12.5 pM and immobilized the RNA to a streptavidin-coated quartz slide surface via a biotin-streptavidin bridge to generate a surface density of ~0.1 molecules/μm^2. We then excited the donor fluorophore in a home-built total internal reflection microscope with a laser (532 nm, 3 mW, Spectra-Physics Excelsior). We separated the donor and acceptor emission using appropriate dichroic mirrors (610DCXR, Chroma) and detected

them as two side-by-side images on a back-illuminated electron-multiplied CCD camera (Andor I-Xon). We obtained measurements under variable [Mg^{2+}] and [c-di-GMP] (0.001 – 100 mM and 0.1 – 5000 nM, respectively) at room temperature with an oxygen-scavenging system (OSS) consisting of 10% wt/vol dextrose, 750 µg/mL glucose oxidase, and 90 µg/mL catalase to reduce photobleaching. For experiments with c-di-GMP or c-di-AMP (BioLog), a solution of ligand and OSS was injected onto the quartz slide and incubated for 15 min at room temperature before imaging. We then constructed histograms and calculated dwell times for each folding event to determine the folding rate constants, as described. A cutoff of 0.5 FRET was used to distinguish between docked and undocked states. The dwell time histograms were fit to a single exponential to determine k_{dock} and k_{undock}. To determine dissociation constants for c-di-GMP and Mg^{2+}, the fraction of molecules in the static docked population (f_D) was plotted as a function of the concentration of c-di-GMP or Mg^{2+} and fit to a modified Langmuir equation:

$$f_D = f_0 + \left(f_{\max} - f_0\right)\frac{x}{K_D + x}$$

where f_0 is the initial percentage of molecules in the static docked population, f_{max} is the final percentage of molecules in the static docked population, and x is the concentration of c-di-GMP or Mg^{2+}.

2.5.3 Isothermal titration calorimetry

ITC was performed essentially as described(*52*). Briefly, RNA was prepared for ITC by exhaustive dialysis at 298 K against a solution comprised of 50 mM HEPES-KOH (pH 7.5), 100 mM NaCl, 0.5-10 mM MgCl. Concentrated c-

di-GMP stock (5 or 10mM) was diluted in the actual dialysis buffer. The final concentration of c-di-GMP was ~10-15 fold higher than that of the RNA. RNA concentrations were ~5 μM and ~15-25 μM for high affinity and low affinity binders, respectively. ITC was carried out with an ITC_{200} calorimeter (MicroCal) at 303 K, using a reference power of 11 μcal s^{-1}, an initial delay of 60 s, and 24 1.67 μl injections at an injection rate of 0.5 μl s^{-1} with injections spaced 180 s. Data were fit to a single-site binding model using Origin ITC software (MicroCal software Inc.).

2.6 Acknowledgements

We would like to thank Nadia Kulshina for initial characterization of the point mutants and Nathan Baird for help with calorimetry. This work was supported in part by the NIH (R01 GM085116) and an NSF CAREER award (MCB-0747285) to David Rueda, and in part by the intramural program of the National Heart, Lung and Blood Institute, NIH (Adrian R. Ferré-D'Amaré).

Chapter 3

Fluorescence enhancement of TAMRA upon binding to an aptamer

3.1 Introduction

Subcellular localization and trafficking of mRNAs play an important role in essential cellular processes such as memory, morphogenesis, and cell migration. The localization and tracking of endogenous mRNAs inside living cells are necessary tools in studying these various processes. A major hurdle in studying endogenous mRNA in live cells is that no RNA is intrinsically fluorescent, compared to proteins such as green fluorescent protein. Techniques, such as molecular beacons and the MS2 system, in which a fluorescent protein is fused to an RNA binding protein, have been used in the past(*23-25, 33*). Drawbacks of these methods include difficulty in designing molecular beacons that are specific enough for the RNA being studied, while the addition of large proteins to the RNA in the MS2 system adds extra bulk to the RNA, which may affect its movements in the cell. One proposed tool to fluorescently label RNA is through the use of fluorophore-binding aptamers(*18, 19, 21*). An aptamer is an oligonucleotide sequence that specifically binds a ligand, in this case, a fluorophore(*20*). An aptamer (SRB2) was developed by Holeman, *et.al.(21)* to specifically bind sulphorhodamine B (Figure 3.1). From previous work in the Rueda lab, this aptamer was also found to bind tetramethylrhodamine (TAMRA) (Figure 3.2). We sought to characterize how binding to this aptamer would affect the fluorescence properties of TAMRA.

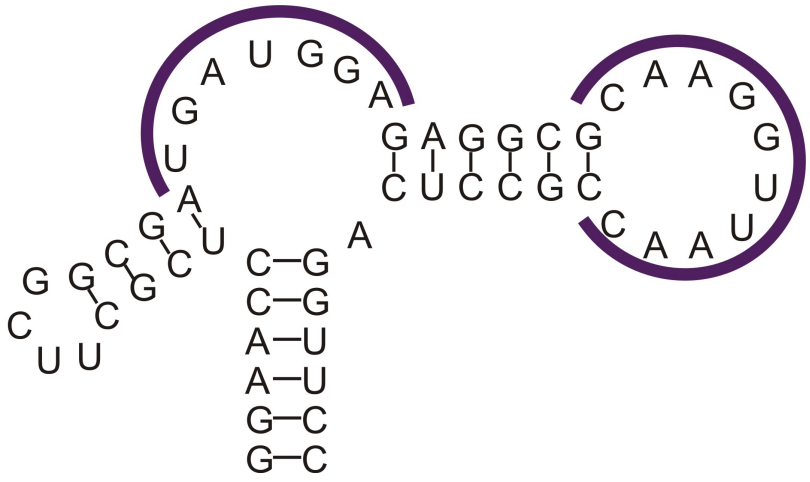

Figure 3.1 Secondary structure of the SRB2 aptamer. Purple indicates the sites of ligand binding.

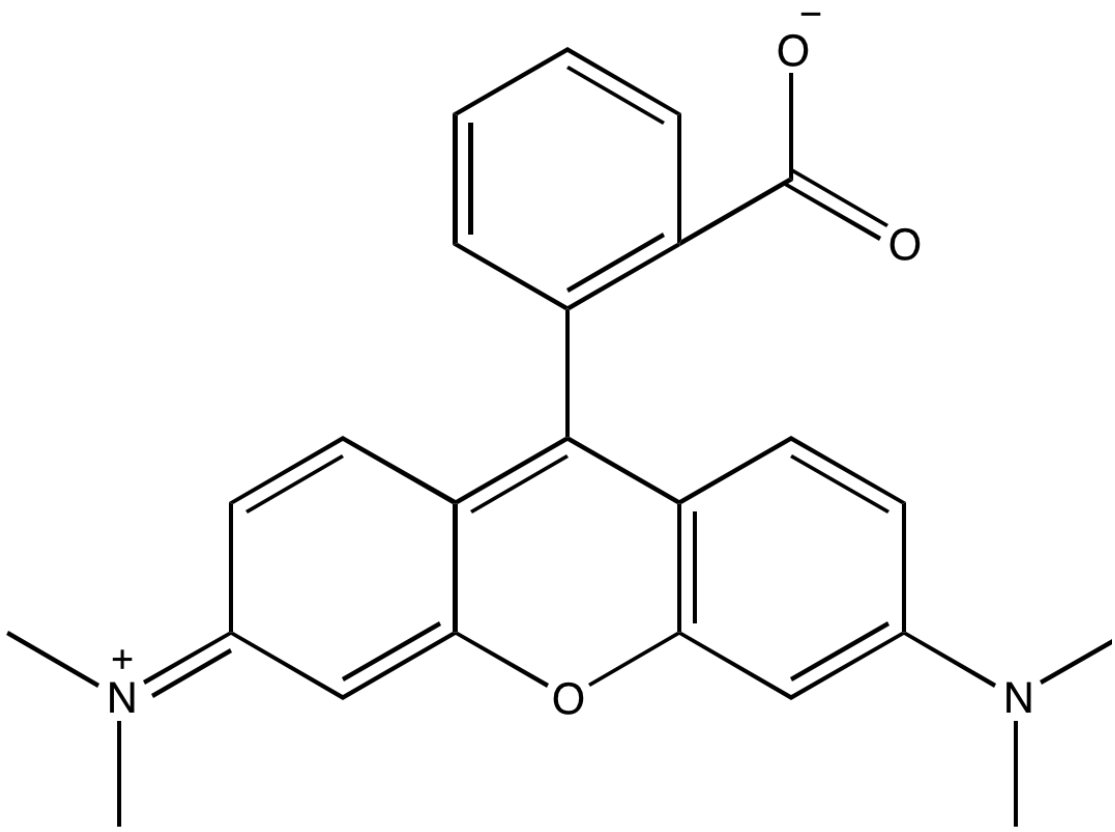

Figure 3.2 Structure of tetramethylrhodamine (TAMRA).

3.2 Results

3.2.1 SRB2 aptamer binds TAMRA

In order to determine if the SRB2 aptamer binds TAMRA and with what affinity, we titrated increasing amounts of aptamer to TAMRA and measured the anisotropy. Anistropy can provide information concerning the size and shape of molecules by measuring the rotational diffusion of a molecule based on fluorescence polarization. As the rotational diffusion changes as the shape and size of a molecule changes, anisotropy is a useful technique to measure the binding interactions of two molecules allowing the determination of binding affinity of said interaction. As the concentration of aptamer increased, the anisotropy of the TAMRA increased indicating binding of TAMRA to the aptamer. When this was fit to the quadratic equation, the resulting binding affinity was 77.1 ± 5.7 nM (Figure 3.3).

3.2.2 Binding to SRB2 increases the quantum yield of TAMRA

Once we confirmed binding of TAMRA to the aptamer, we sought to characterize whether binding to the aptamer changed the quantum yield of TAMRA. The standard quantum yield of TAMRA as measured in methanol is 0.28. Because the studies described here were conducted in buffer (10 mM Tris-HCl, pH 7.5, 100 mM KCl, 5 mM $MgCl_2$), we determined the quantum yield of TAMRA in this buffer using the following equation

$$Q_{unk} = \left(\frac{\eta^2_{unk}}{\eta^2_k}\right)\left(\frac{A_k * I_{unk}}{A_{unk} * I_k}\right) * Q_k$$

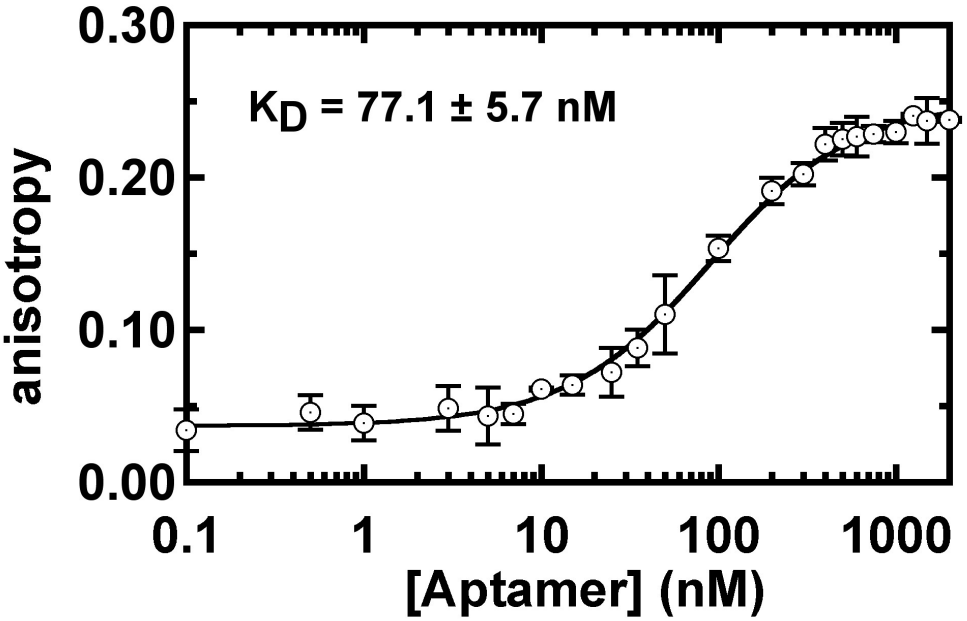

Figure 3.3 Titration curve as increasing amounts of SRB aptamer are added to TAMRA. The curve is fit to the quadratic equation.

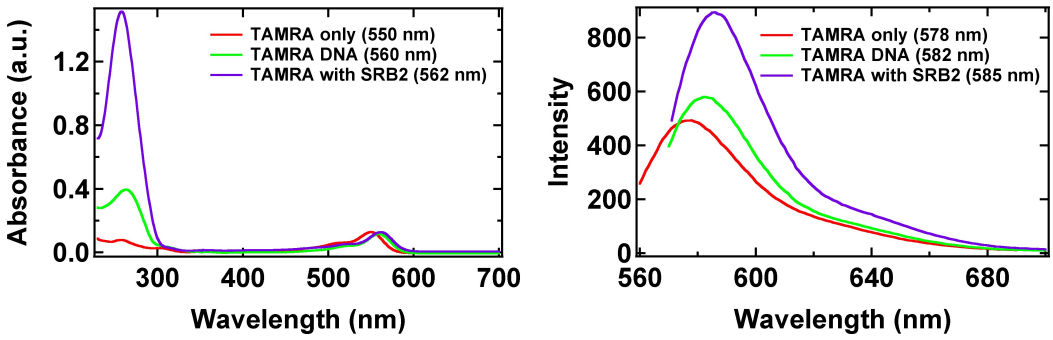

Figure 3.4 (left) Absorbance and **(right)** fluorescence spectra of TAMRA alone (red), TAMRA-DNA (green), and TAMRA-SRB2 (purple).

where Q_{unk} and Q_k are the quantum yields of the unknown and the reference, respectively, n_{unk} and n_k are the refractive indices of the respective solvents, A_{unk} and A_k are the absorbances for the unknown and reference, and I_{unk} and I_k are the fluorescence intensities of the unknown and reference. The quantum yield of TAMRA in buffer is 0.16 and was used as the reference quantum yield in all further calculations. The quantum yield of TAMRA bound to the end of a DNA increased to 0.20 ± 0.02 with a red-shift in absorbance of 10 nm and when bound to SRB2, increased to 0.30 ± 0.03 with a red-shift in absorbance of 12 nm (Figure 3.4).

3.2.3 Binding to SRB2 increases the fluorescence lifetime of TAMRA

To determine the fluorescence lifetime of TAMRA, we used Time Correlated Single Photon Counting. The results are shown in Table 3.1. The fluorescence lifetime of TAMRA increases from 2.1 ns to 2.6 ns when attached to a DNA and to 3.6 ns upon binding to SRB2.

3.2.4 Binding to SRB2 does not affect blinking rates of TAMRA

An intrinsic property of fluorophores that make them problematic to use in assays is blinking in which the molecule enters a dark, non-emissive state. We used single molecule spectroscopy to determine whether binding to the aptamer would change the blinking rate of TAMRA. To do this we immobilized the SRB2 aptamer to a quartz slide via a biotin-streptavidin bridge and excited TAMRA with a 532 nm laser. We then monitored the fluorescence intensity of

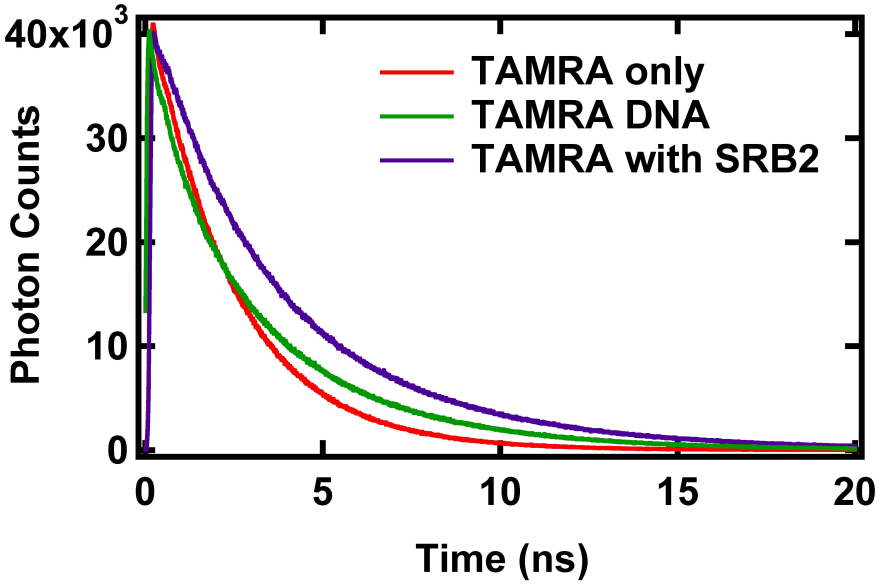

Figure 3.5 Fluorescence lifetime spectra of TAMRA alone (red), TAMRA-DNA (green), and TAMRA-SRB2 (purple).

	TAMRA only		TAMRA DNA		TAMRA with SRB2	
	Lifetime (ns)	**Percentage**	**Lifetime (ns)**	**Percentage**	**Lifetime (ns)**	**Percentage**
Component 1	2.3 ± 0.1	0.9 ± 0.1	3.9 ± 0.1	0.5 ± 0.1	4.6 ± 0.1	0.7 ± 0.1
Component 2	0.9 ± 0.1	0.1 ± 0.1	1.6 ± 0.1	0.3 ± 0.1	2.0 ± 0.1	0.3 ± 0.1
Component 3	0.2 ± 0.1	0.1 ± 0.1	0.4 ± 0.1	0.2 ± 0.1	0.2 ± 0.1	0.1 ± 0.1
Avg Lifetime (ns)	2.1 ± 0.1		2.6 ± 0.1		3.6 ± 0.1	
Fit (χ2)	1.3		1.1		1.1	

Table 3.1 Lifetime measurements of TAMRA, TAMRA-DNA, and TAMRA-SRB2.

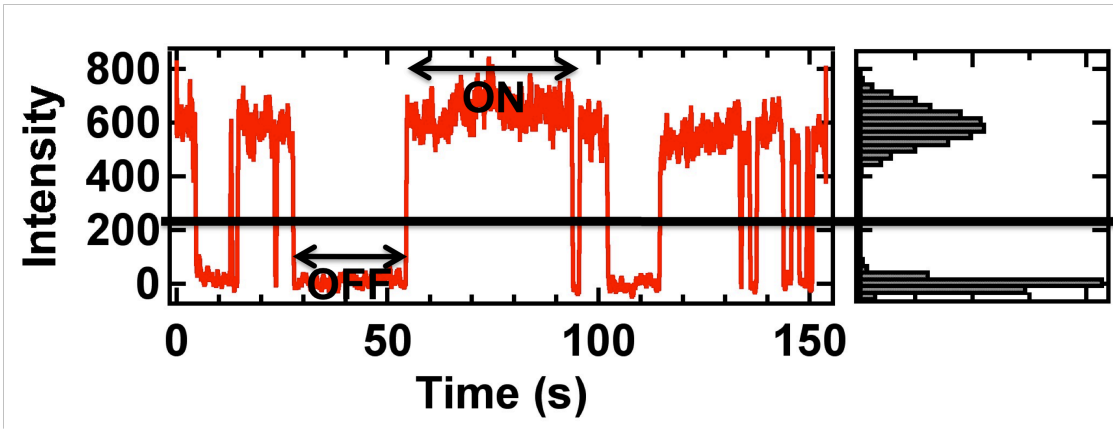

Figure 3.6 Characteristic trace of TAMRA blinking when bound to the SRB2 aptamer. Black line indicates the cutoff to determine on and off events.

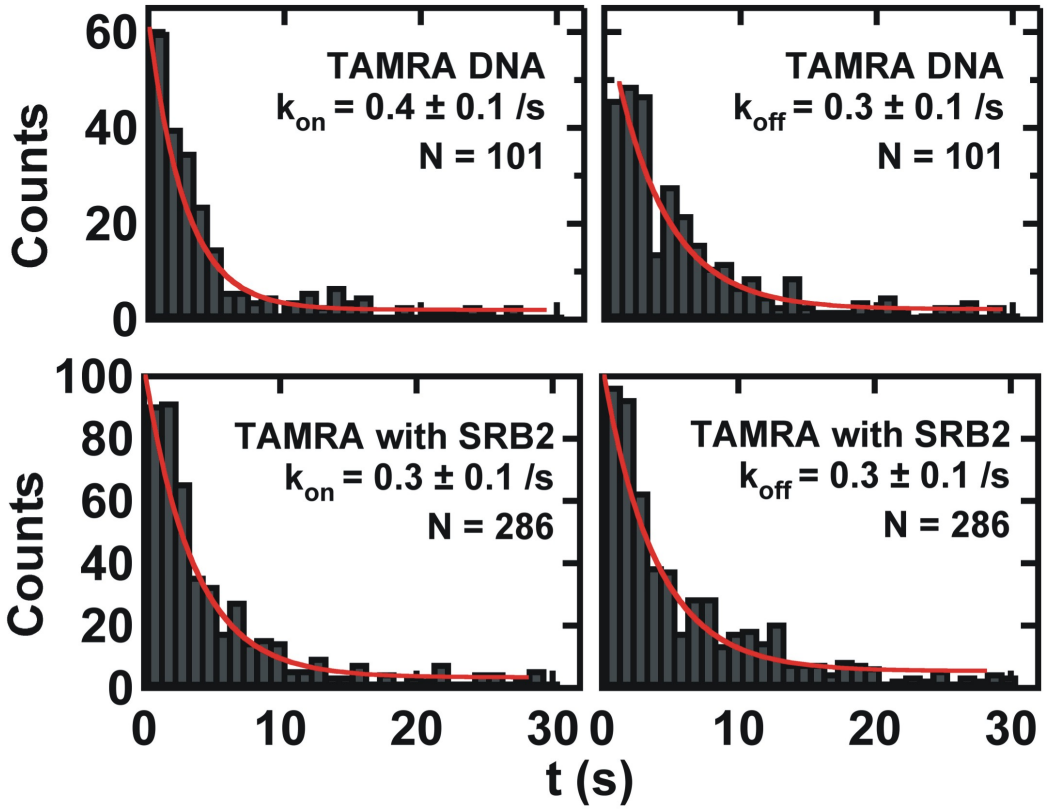

Figure 3.7 Blinking rates for TAMRA-DNA (top) and TAMRA-SRB2 (bottom) where N is the number of molecules used for the analysis.

TAMRA over time. A characteristic trace is shown in Figure 3.6. A DNA with TAMRA linked to the 5'end was used for comparison. The blinking rates of TAMRA did not change upon binding to the aptamer (Figure 3.7).

3.3 Conclusions

Fluorophore-binding aptamers may be a useful tool in studying the localization and trafficking of endogenous mRNAs inside living cells. We sought to characterize how the fluorescence properties of tetramethylrhodamine are affected upon binding to the SRB2 aptamer. Upon binding to the aptamer, the quantum yield and fluorescence lifetime of the fluorophore both increase with a red-shift in absorbance; however the blinking rates of TAMRA are not affected. This change is properties may result from the increase in rigidity of TAMRA upon binding to the aptamer. By itself, TAMRA is a rather flexible molecule but binding to the aptamer restricts its movements. Suppressing these motions in turn suppresses non-radiative decay processes including vibrational and rotational relaxation. This would then make radiative processes, i.e. fluorescence, the principal decay process and increase both quantum yield and lifetime of TAMRA.

3.4 Materials and Methods

3.4.1 RNA purification and labeling

The 54-nt aptamer domain previously described(*21*) was *in vitro* transcribed using T7 DNA polymerase resulting in the sequence of GGA ACC UCG CUU CGG CGA UGA UGG AGA GGC GCA AGG UUA ACC GCC UCA GGU UCC. The RNA was purified by denaturing gel electrophoresis (20% wt/vol polyacrylamide and 8 M urea) and diffusion elution against elution buffer (0.5 M

NH_4OAc and 0.1 mM EDTA) overnight at 4°C, followed by chloroform extraction, ethanol precipitation and C8 reverse-phase HPLC. RNA concentrations were measured by UV-Vis absorbance at 260 nm. The 3' end of the RNA was then biotinylated by 2'-3' oxidation followed by nucleophilic addition of biotin. Briefly, the 2 mmol of RNA was dried and dissolved in 100 µL of oxidation buffer consisting of 10 mM HEPES-KOH pH 7.5 and 1 mM $MgCl_2$. Next, 14 µL of a 50 mM solution of KIO_4 was added to the solution and incubated for 20 min at 0°C then ethanol precipitated. The pellet was then dissolved in 100 µL of 50 mM NaOAc pH 5 followed by the addition of 1 µL of a saturated biotin hydrazide. The reaction was incubated overnight at 4°C and then ethanol precipitated. The biotinylated RNA was purified via C8 reverse-phase HPLC. RNA concentrations were measured by UV-Vis absorbance at 260 nm. Tetramethylrhodamine (TAMRA) was purchased from Invitrogen, and used without further purification. DNA with 5' TAMRA and 3' biotin (CCC ATT GAC CGT TCC CCU CCT ACT CCC was purchased from Keck. The DNA was desalted using a Nap10 column. The DNA was then purified by denaturing gel electrophoresis (20% wt/vol polyacrylamide and 8 M urea) and diffusion elution against elution buffer (0.5 M NH_4OAc and 0.1 mM EDTA) overnight at 4°C, followed by chloroform extraction, ethanol precipitation and C8 reverse-phase HPLC. DNA concentrations were measured by UV-Vis absorbance at 260 nm(*41*).

3.4.2 Anisotropy

Anisotropy measurements of TAMRA both alone and in the presence of aptamer and TAMRA DNA were conducted using a Cary Eclipse (Varian, Inc.)

spectrometer. A 25 nM TAMRA or TAMRA DNA solution in reaction buffer (10 mM Tris-HCl, pH 7.5, 100 mM KCl, 5 mM $MgCl_2$) was heated to 90°C for 2 minutes and slowly cooled to room temperature for 20 minutes. TAMRA was excited at 555 nm (5 nm slit width), and emission was recorded at 585 nm (5 nm slit width). The G factor was measured once and held constant throughout the measurement. During titrations with aptamer, the reaction was equilibrated at each aptamer concentration for five minutes before measurement. To determine the binding affinity (K_D), the anisotropy value (r) which was determined by

$$r = \frac{I_V - I_H}{I_V - 2I_H}$$

where I_v and I_H are the fluorescence intensities in the vertical and horizontal direction was plotted as a function of aptamer concentration and then fitted to a quadratic equation.

3.4.3 Quantum Yield

Quantum yield measurements of TAMRA both alone and in the presence of aptamer and TAMRA DNA were conducted using a Cary Eclipse spectrometer and Varian spectrofluorometer. A solution of TAMRA in reaction buffer (10 mM Tris-HCl, pH 7.5, 100 mM KCl, 5 mM $MgCl_2$) at a concentration to result in an absorbance of 0.1 to 0.15 was scanned to determine the maximum absorbance wavelength. This wavelength was then used to excite the same solution of TAMRA; emission was recorded at the maximum wavelength of emission. The quantum yield of TAMRA in buffer was calculated using the previously measured quantum yield of TAMRA in methanol using the following equation.

$$Q_{unk} = \left(\frac{\eta^2_{unk}}{\eta^2_{k}}\right)\left(\frac{A_k * I_{unk}}{A_{unk} * I_k}\right) * Q_k$$

where Q_{unk} and Q_k are the quantum yields of the unknown and the reference, respectively, n_{unk} and n_k are the refractive indices of the respective solvents, A_{unk} and A_k are the absorbances for the unknown and reference, and I_{unk} and I_k are the fluorescence intensities of the unknown and reference. This value was used as the reference in all further quantum yield calculations. The same procedure was repeated for TAMRA in the presence of a saturating amount of aptamer and for TAMRA DNA. These solutions were heated to 90°C for 2 min and slowly cooled to room temperature for 20 minutes.

3.4.4 Fluorescence lifetime measurements

To determine the fluorescence lifetime of TAMRA in varying conditions, time-correlated single-photon counting (TCSPC) was performed as previously described(*42, 97, 98*) using a home built time resolved FRET setup in combination with an ISS TCSPC module. Solutions of 250 nM TAMRA in the absence and presence of 500 nM aptamer or 250 nM TAMRA DNA in reaction buffer (100 mM KCl, 10 mM Tris-HCl pH 7.5, 5 mM $MgCl_2$) were annealed by heating to 90 °C for two minutes followed by slow cooling at room temperature for 20 minutes. TAMRA was excited at 520 nm (20 nm band-pass dichroic filter) with a class 4 high power Yb-doped fiber laser with 5 ps pulses at 40 MHz. Donor emission was collected at 580 nm (20 nm band-pass dichroic filter). The magic angle of 54.7° was used to detect isotropic emission to a photon count of

at least 40000. Collection of fluorescence decays for TAMRA alone and in the presence of aptamer as well as TAMRA DNA was done in 4816 channels with a time increment of 12.2 ps/channel using a micro-channel photomultiplier tube (Hamamatsu R3890U-52) and a time correlated single photon counting device (SPC-630, Becker & Hickl). The fluorescence intensity of the fluorophore decays exponentially with the following equation

$$I_D(t) = I_0 \exp\left(-\frac{t}{\tau_D}\right)$$

where τ_D is the fluorescence lifetime of the fluorophore and I_0 is the initial intensity dependent upon the concentration of the fluorophore. A dilute solution of non-dairy coffee creamer was used to measure instrument response function. The fluorescence emission decay was fit to a sum of three exponential decays characterized by their lifetimes with fractional contributions. A weighted average was calculated to result in the average lifetime of the fluorophore. The quality of the fit was judged by the χ^2 value.

3.4.5 Single molecule spectroscopy

Single molecule experiments were performed as described(*39, 68*) in order to determine how binding to an aptamer effects the blinking of TAMRA. As surface immobilization is a requirement for our single molecule experiments, a short DNA with a 3' biotin for immobilization and a TAMRA label at the 5' end was used to represent unbound TAMRA. We heated a 10 µL solution of 1 µM TAMRA DNA or aptamer with 0.5 µM TAMRA at 90°C for 45 s before cooling to room temperature over 20 min. We diluted the solutions to 12.5 pM and

immobilized the DNA or RNA aptamer to a streptavidin-coated quartz slide surface via a biotin-streptavidin bridge to generate a surface density of ~0.1 molecules/μm^2. We then excited the TAMRA in a home-built total internal reflection microscope with a laser (532 nm, 3 mW, Spectra-Physics Excelsior). We detected TAMRA emission on a back-illuminated electron-multiplied CCD camera (Andor I-Xon). In order to observe blinking events unhindered, we did not use any oxygen scavenger system. We then constructed histograms and calculated dwell times for each blinking event to determine the blinking rate constants, as described. The dwell time histograms were fit to a single exponential to determine k_{on} and k_{off} for blinking events.

Chapter 4

Analysis of the effects of 2' modifications on molecular beacons

4.1 Introduction

Molecular beacons (MB) are hairpin probes that fluoresce upon hybridization to their target sequence (Figure 4.1). This is accomplished with the use of a fluorophore conjugated to one end of the hairpin and a quencher on the other. The MB consists of a loop sequence, generally 15 to 20 nucleotides, specific for the target of interest, and a self-complementary stem sequence ranging from five to seven base pairs. In the absence of target, the molecular beacon is in the hairpin conformation bringing the fluorophore into close proximity to the quencher, thus quenching the fluorescence. However, when the MB encounters the target sequence, it binds to the target to form a hybrid that is more stable than the stem duplex of the hairpin. Therefore, the hairpin unfolds, thus increasing the distance between the fluorophore and the quencher resulting in a fluorescent signal(*22, 34-36, 99*).

Molecular beacons are advantageous for live cell assays because they only fluoresce in the presence of the target molecule. This negates the need to wash away unbound probes, which is often a problem in other nucleic acid detection methods. An obstacle for their use *ex vivo*, a molecular beacon with an RNA backbone is subject to degradation by nucleases at its 2'OH moiety(*23-25, 100-102*). Nuclease degradation of the molecular beacon would result in non-specific opening of the hairpin probe by breaking the phosphodiester bond and separation of the fluorophore and quencher leading to false-positive signals. To

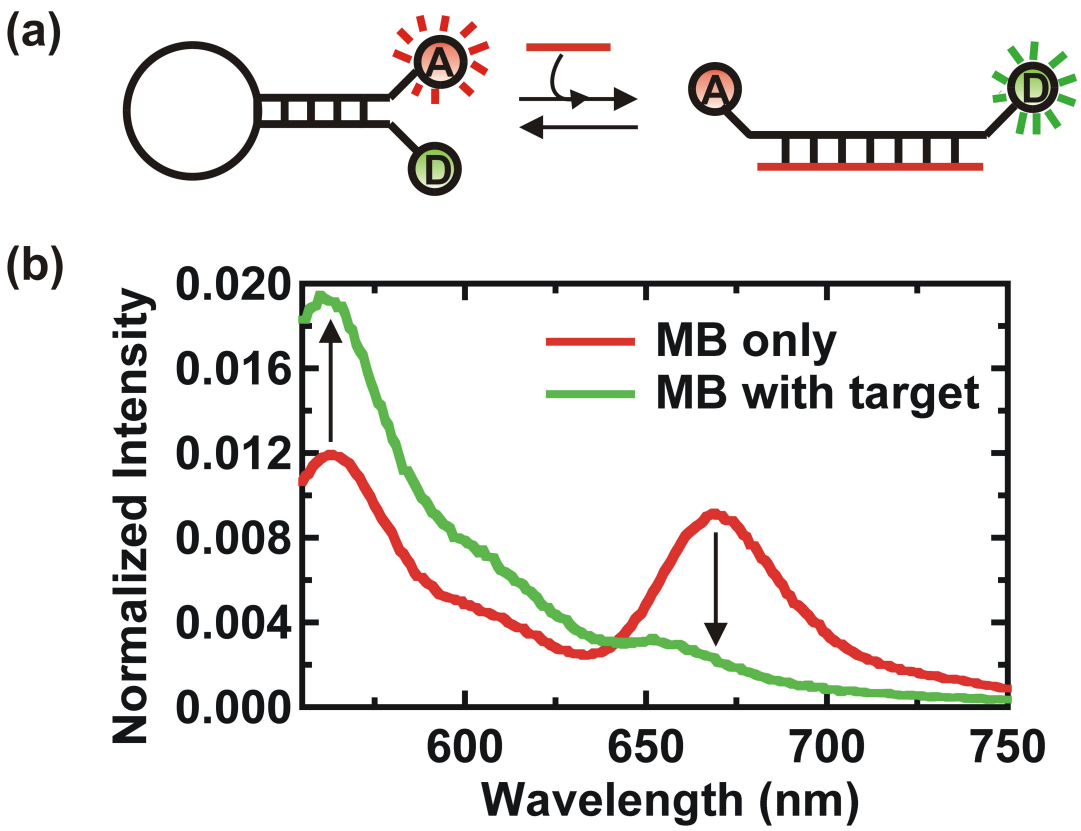

Figure 4.1 **(a)** Molecular beacons are hairpin probes that fluoresce upon hybridization to their target sequence (red). **(b)** In the absence of the target (red trace), the donor fluorophore is in close proximity to the acceptor fluorophore resulting in FRET and acceptor fluorescence. In the presence of the target (green trace), the hairpin opens moving the donor and acceptor from each other resulting in less efficient FRET. Therefore, the donor fluorescence increases as the acceptor fluorescence decreases.

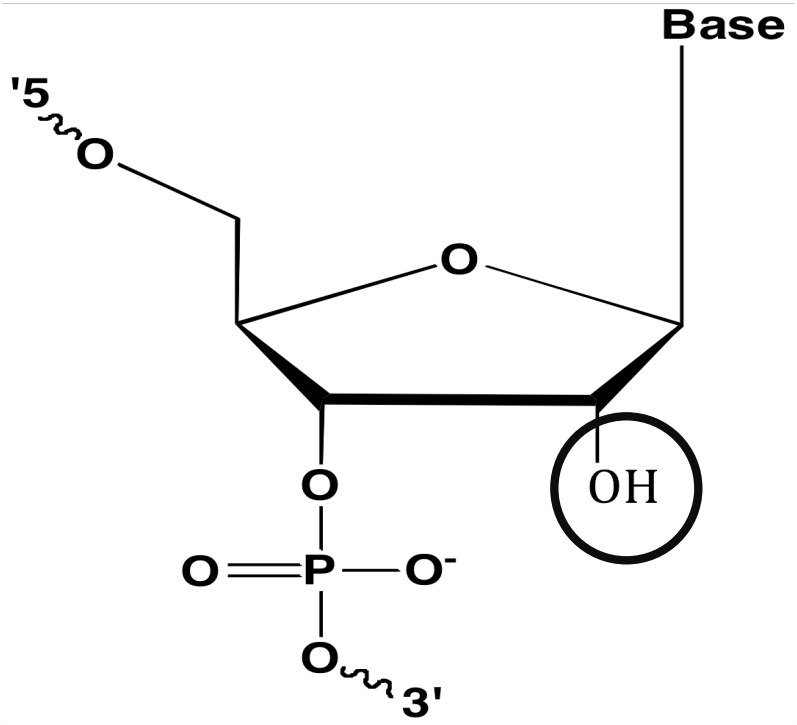

Figure 4.2 Modification of the 2'OH (circled) of the RNA backbone to a 2'F, 2'OMe, and 2'H has been shown to prevent RNase degradation.

prevent enzymatic degradation, several modifications of the oligonucleotide backbone at the 2' position have been used including 2'-fluoro (2'F), 2'-O-methyl (2'OMe), and 2'-deoxy (2'H) (Figure 4.2) (*26-32*). It is not yet fully clear as to the effects that these backbone modifications have on the actions of the molecular beacon, which lends to the need for a comparative study to determine whether or not these modifications hamper and/or alter the behaviors of the probe.

In this study, we have characterized the effects that 2'F, 2'OMe, and 2'H backbone modifications have on the actions of the molecular beacon both in the absence and presence of the target sequence by bulk and single molecule fluorescence techniques. The modified MBs were found to act similarly to the parent 2'OH MB. All of the molecular beacons used in this study bound to the RNA target with similar, tight nanomolar affinity. All of the 2' modified molecular beacons exhibited a large conformational change upon target binding.

4.2 Results and Discussion

4.2.1 The 2' modified molecular beacons bind the complementary RNA target specifically

A native FRET gel assay was performed to evaluate binding of each of the molecular beacons used in this study to the complementary RNA target. Binding to the complementary RNA target results in both a gel shift and a change in FRET. In the closed conformation (unbound to complementary RNA target), the MB appears as a red band. Conversely, in the open conformation (bound to complementary RNA target), the MB appears as a yellow band. A clear red band

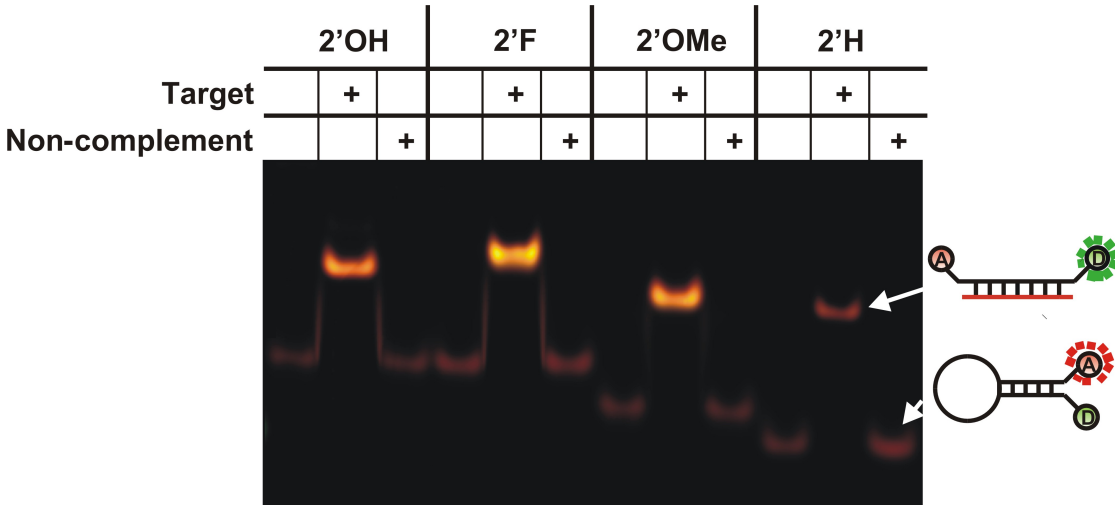

Figure 4.3 Native gel confirms binding and specificity of the molecular beacons. In the absence of target, the MB is in a closed conformation and FRET occurs between fluorescein and rhodamine resulting in the emission of rhodamine and a red band. When the target is present, the MB is in an open conformation resulting in greater emission of fluorescein and a yellow band. A gel shift indicates binding of the MB to the target RNA. Using a non-complementary RNA target, no gel shift was observed indicating that the beacon was specific for its target.

was observed for all MBs with 2' modifications in the absence of complementary RNA target as well as in the presence of the non-complementary target indicating that the MB is in the closed (high FRET), hairpin conformation. (Figure 4.3) However, a yellow band was observed in the presence of the complementary target indicating the open (low FRET) conformation as a result of binding to the complementary RNA target. (Figure 4.3) This change in conformation also results in a gel shift signifying that the MB has bound to the complementary RNA target. However, no gel shift was observed in the presence of the non-complementary RNA target demonstrating specificity of the MB for the complementary RNA target sequence. All four 2' modified molecular beacons used in this study were equally effective in specifically binding the complementary RNA target. Differences in the helical conformations and/or effective charge of the modified MB/RNA duplexes resulted in slight differences in migration.

4.2.2 The 2'OMe modified MB binds the complementary RNA target with the tightest affinity

Steady state fluorescence measurements were used to examine the effects that the 2' modifications exhibited on the binding affinity of each of the MBs for the complementary RNA target. In the absence of complementary RNA target, the molecular beacons exhibited a FRET ratio ranging from 0.5 to 0.6; this range of initial FRET ratios may be a result of differences in the populations of the open conformation or differences in structure; however, the latter is not

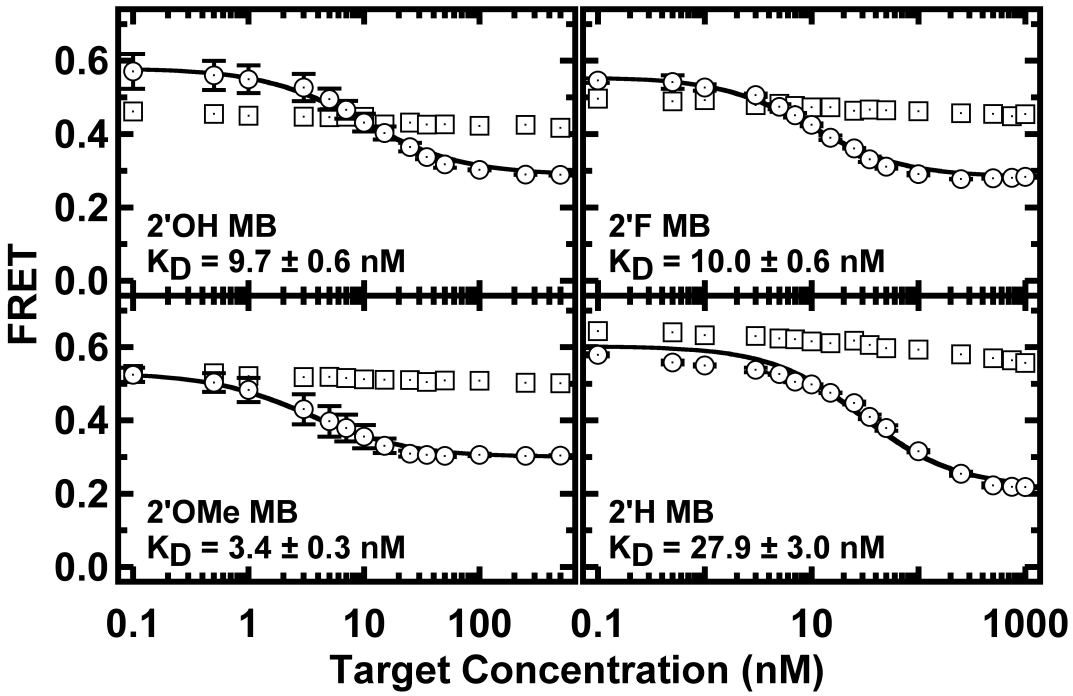

Figure 4.4 The molecular beacons bind with similar affinity to the complementary RNA target. The FRET ratio decreased with increasing target concentration, indicating that the beacon had opened in response to binding the target (circle). The curves were fit to the Hill equation with n fixed to value of 1. Initial and final FRET values did not show much variation indicating that the modifications did not alter the binding of the MB to the RNA target. Apparent K_Ds showed slight variation with the 2'OMe MB binding with slightly better affinity than the 2'OH MB, while the 2'F and 2'H MBs bound with slightly lower affinity. Titration with the non-complement showed no change in FRET values demonstrating that the MB is specific for its target (square).

consistent with gel data (Figure 4.4). As the complementary RNA target concentration increased, the FRET ratio decreased until the MB was saturated with complementary RNA target to give a final FRET ratio of 0.3 for all 2' modified MBs. The decrease in FRET is a result of the MB changing from the closed to the open conformation by binding the complementary RNA target. As expected, the FRET ratios at saturation were similar for all 2' modified MBs. Fitting the resulting titration curves to the Hill equation resulted in an apparent K_D value of 7.0 ± 0.6 nM for the typical 2'OH MB. All MBs bound with tight nM affinity to the complementary RNA target. Apparent K_D values varied slightly among the 2' modified MBs; the 2'OMe MB 3-fold tighter (3.4 ± 0.3 nM) to the complementary RNA target, while the 2'F MB bound with similar affinity (10.0 ± 0.6 nM) and the 2'H MB bound 3-fold weaker (27.9 ± 0.3 nM) (Figure 4.4). This is consistent with prior results(*27, 28, 30*). A ten-fold difference in binding affinity was found between the 2'OMe MB and the 2'H MB. Upon addition of the non-complementary RNA target, no change in FRET efficiency was found, indicating that all 2' modified MBs maintain specificity (Figure 4.4).

4.2.3 The molecular beacon demonstrates a large conformational change upon target binding

Time resolved FRET revealed the distance between the fluorescein and rhodamine fluorophores positioned on the stem of the molecular beacon (Figure 4.5 and Table 4.1). Similar single distance distributions were observed for all of the molecular beacons indicating a single population at an average distance. Distances were similar for the MBs ranging from 18 to 21 Å in the absence of

Sample		Fraction Closed	R_C (Å)	$FWHM_C$ (Å)	Fraction Open	R_O (Å)	$FWHM_O$ (Å)	F	χ^2
2'OH	MB only	0.96 ± 0.02	21 ± 1	18 ± 1	0.04 ± 0.01	56 ± 6	50 ± 6	0.1 ± 0.1	1.2
	MB + target	-	-	-	1.00	79 ± 1	15 ± 1	0.1 ± 0.1	1.2
	Non-comp	0.96 ± 0.01	21 ± 1	18 ± 1	0.04 ± 0.01	51 ± 2	44 ± 1	0.1 ± 0.1	1.3
2'F	MB only	1.00	18 ± 1	16 ± 1	-	-	-	0.2 ± 0.1	1.1
	MB + target	-	-	-	1.00	78 ± 1	18 ± 1	0.1 ± 0.1	1.2
	Non-comp	1.00	16 ± 1	16 ± 1	-	-	-		1.0
2'OMe	MB only	1.00	19 ± 1	12 ± 1	-	-	-	0.3 ± 0.1	1.2
	MB + target	-	-	-	1.00	78 ± 1	19 ± 1	0.1 ± 0.1	1.2
	Non-comp	1.00	15 ± 1	16 ± 1	-	-	-	0.2 ± 0.1	1.2
2'H	MB only	0.97 ± 0.01	18 ± 1	15 ± 1	0.03 ± 0.01	43 ± 1	16 ± 1	0.1 ± 0.1	1.0
	MB + target	-	-	-	1.00	78 ± 1	10 ± 1	0.3 ± 0.1	1.1
	Non-comp	0.97 ± 0.01	17 ± 1	16 ± 1	0.03 ± 0.01	42 ± 1	20 ± 1	0.1 ± 0.1	1.1

Table 4.1 Time resolved FRET results for the molecular beacons in the absence and presence of complementary and non-complementary RNA target. R_C and R_O are the average distance between fluorophores in the closed and open conformation, respectively. $FWHM_C$ and $FWHM_O$ are the full width at half maximum of the distance distributions for the MB in the closed and open conformation, respectively. F is the fraction of molecular beacon that is single-labeled. χ^2 is the chi-squared value that indicates the goodness of the fit.

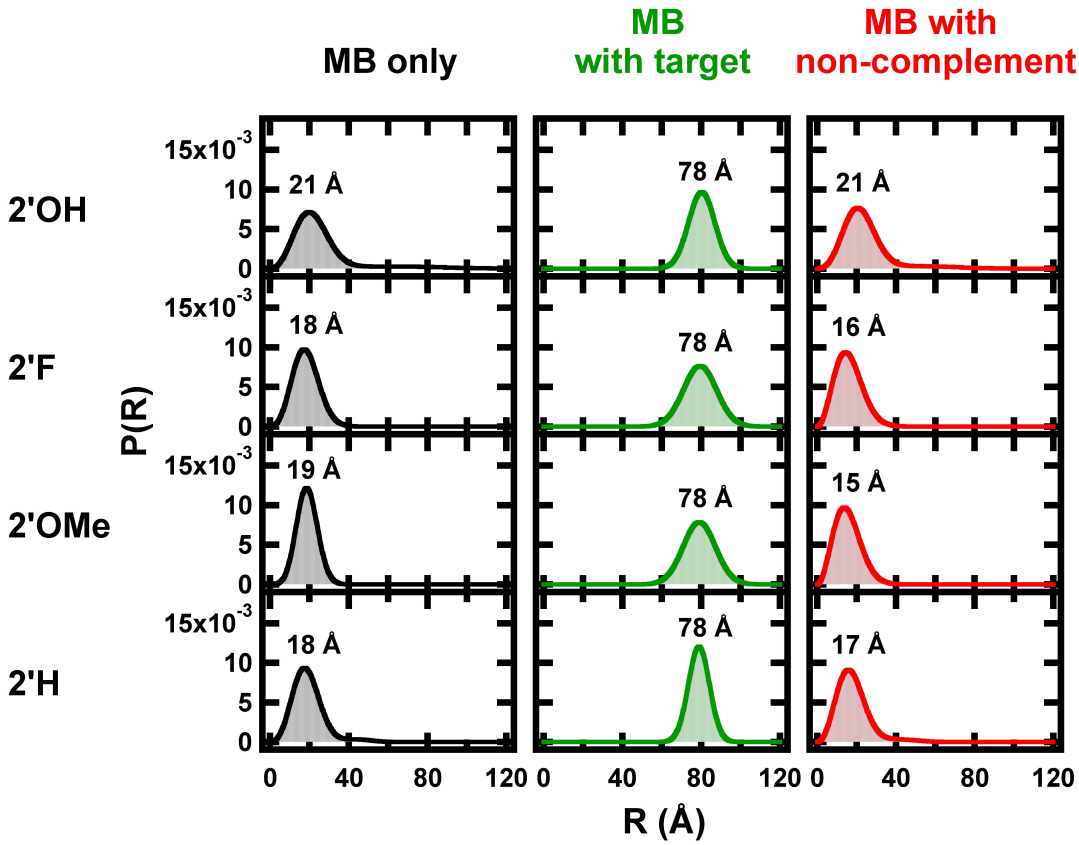

Figure 4.5 The molecular beacon demonstrates a large dynamic range. Time resolved FRET measurements resulted in similar distances between fluorophores for all of the MBs in the absence of target (black), in the presence of target (green) and in the presence of a non-complementary target (red). The distances were also similar for the same beacon in the absence of target and in the presence of the non-complement indicating that the MB is specific for the target sequence.

complementary RNA target, which is expected when taking into account the distance between the complementary nucleotides in the stem as well as the C7 amino linker used to attach the fluorophores, and 78 Å in the presence of complementary RNA target. The distances in the presence of non-complementary RNA target ranged from 15 to 21 Å for all 2' modified MBs and were similar to that of the MB in the absence of complementary RNA target, once again indicating specificity of the MB for its complementary RNA target.

4.2.4 Single molecule FRET reveals an equilibrium between the open and closed MB

Single molecule FRET measurements were used to uncover information, such as possible conformational dynamics, that would otherwise be hidden in ensemble-averaged measurements (Figure 4.6). Time trajectories similar to those in Figure 4.7 were analyzed for 2'OH, 2'F, 2'OMe, and 2'H molecular beacons. The traces were all background subtracted to account for bleed-through of donor fluorescence into the acceptor channel. Time trajectories with a low donor intensity and high acceptor intensity result in a high FRET efficiency (0.9) and are indicative of the MB in the closed, hairpin conformation (Figure 4.7 and 4.8). Alternatively, time trajectories with a high donor intensity and low acceptor intensity result in a low FRET efficiency (0.2) and are indicative of the MB in the open conformation (Figure 4.7 and 4.8). No dynamics were observed in the minute timescale. It is possible that dynamics are present but cannot be resolved either because any conformational changes are faster than the time

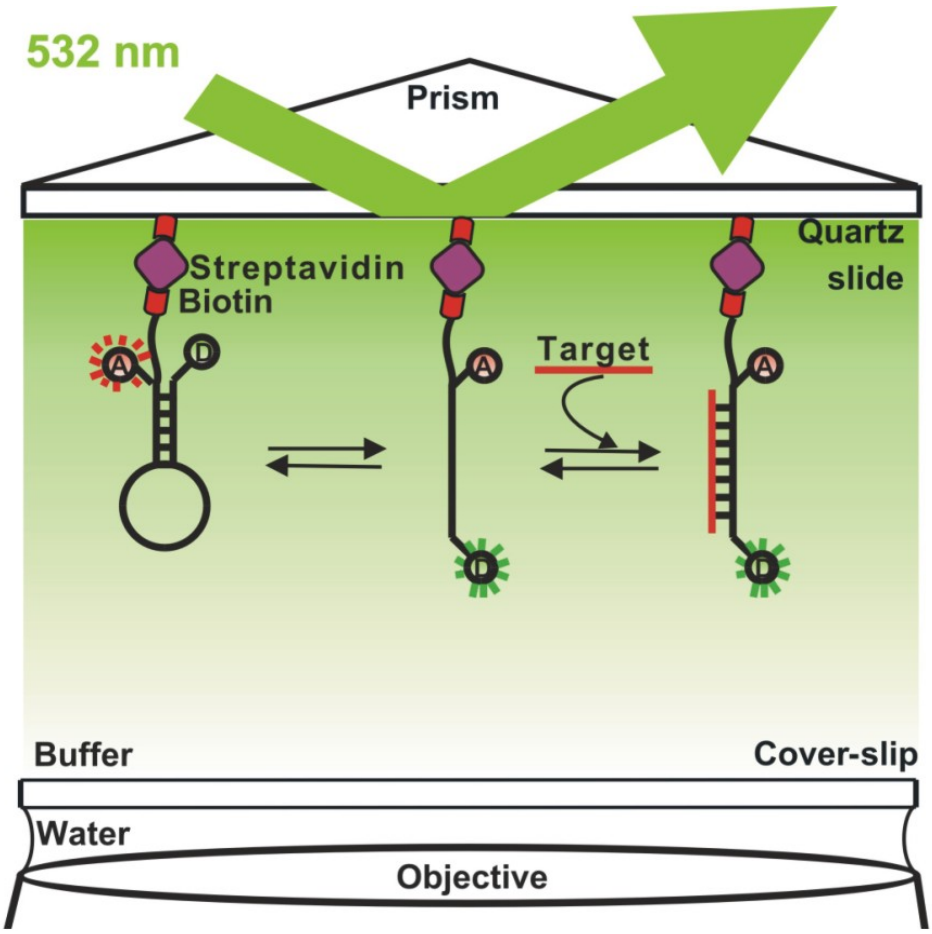

Figure 4.6 Single molecule setup. The molecular beacon is immobilized to a quartz slide via a biotin/streptavidin linkage. The 532 nm laser excites the donor fluorophore (Cy3, D) and the emission of Cy3 and the acceptor fluorophore (Cy5, A) are recorded.

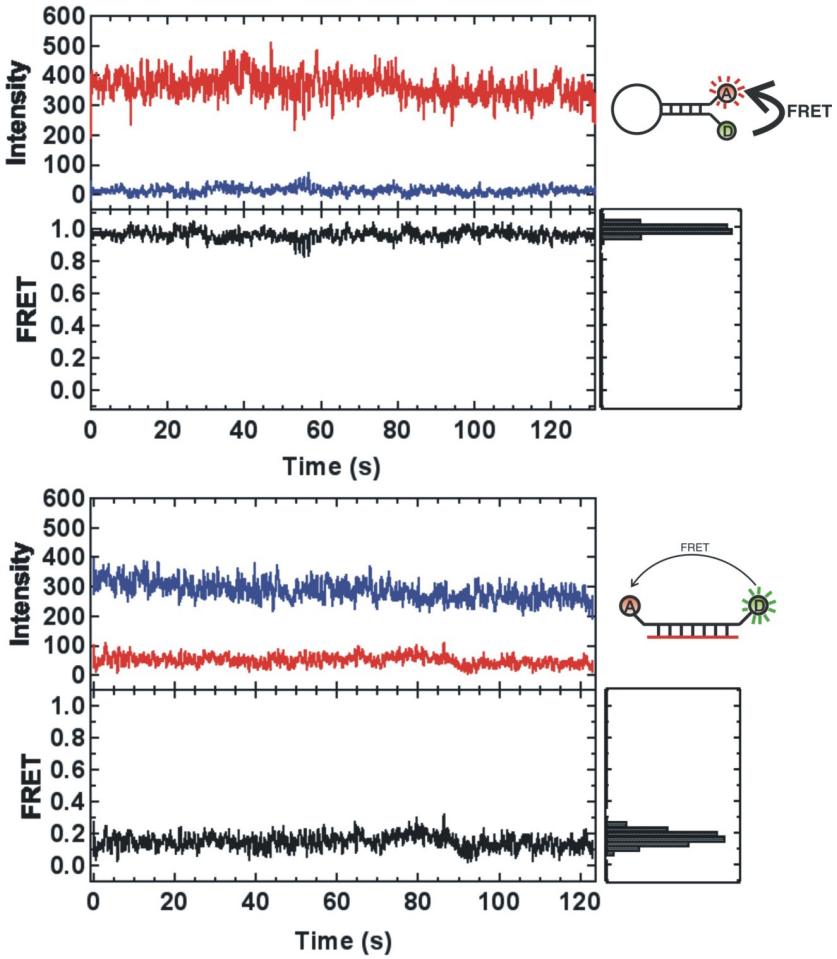

Figure 4.7 Representative single molecule time trajectories of surface-immobilized molecular beacon. A closed MB resulted in a low donor fluorophore intensity (Cy3, blue), high acceptor fluorophore intensity (Cy5, red), and a high FRET ratio of 0.9 (black). An open MB resulted in a high donor fluorophore intensity, a low acceptor fluorophore intensity, and a low FRET ratio of 0.2.

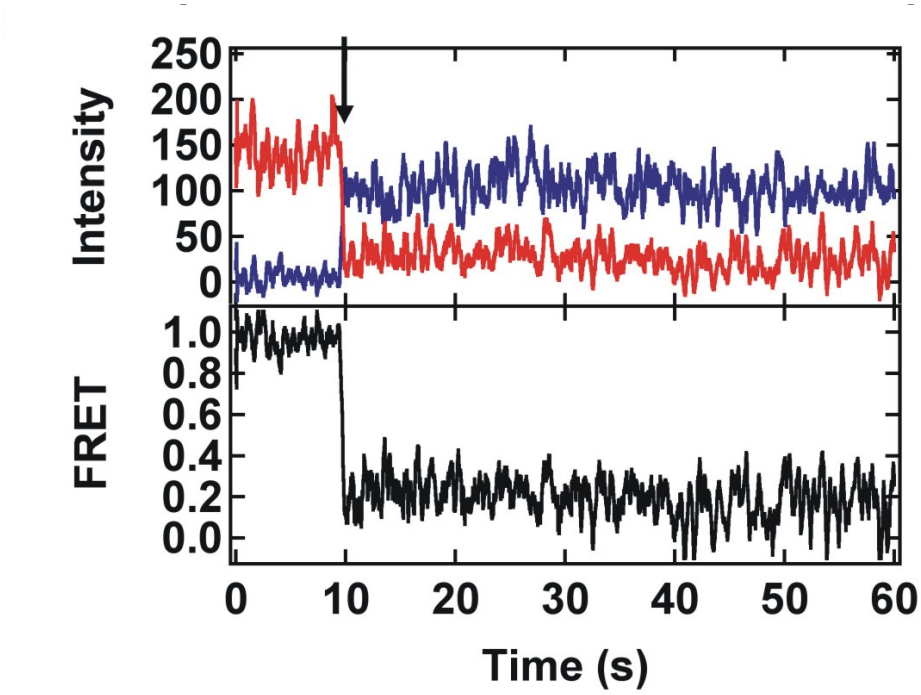

Figure 4.8 The FRET ratio decreases from 0.9 to 0.2 as the MB binds the complementary RNA target as indicated by the arrow.

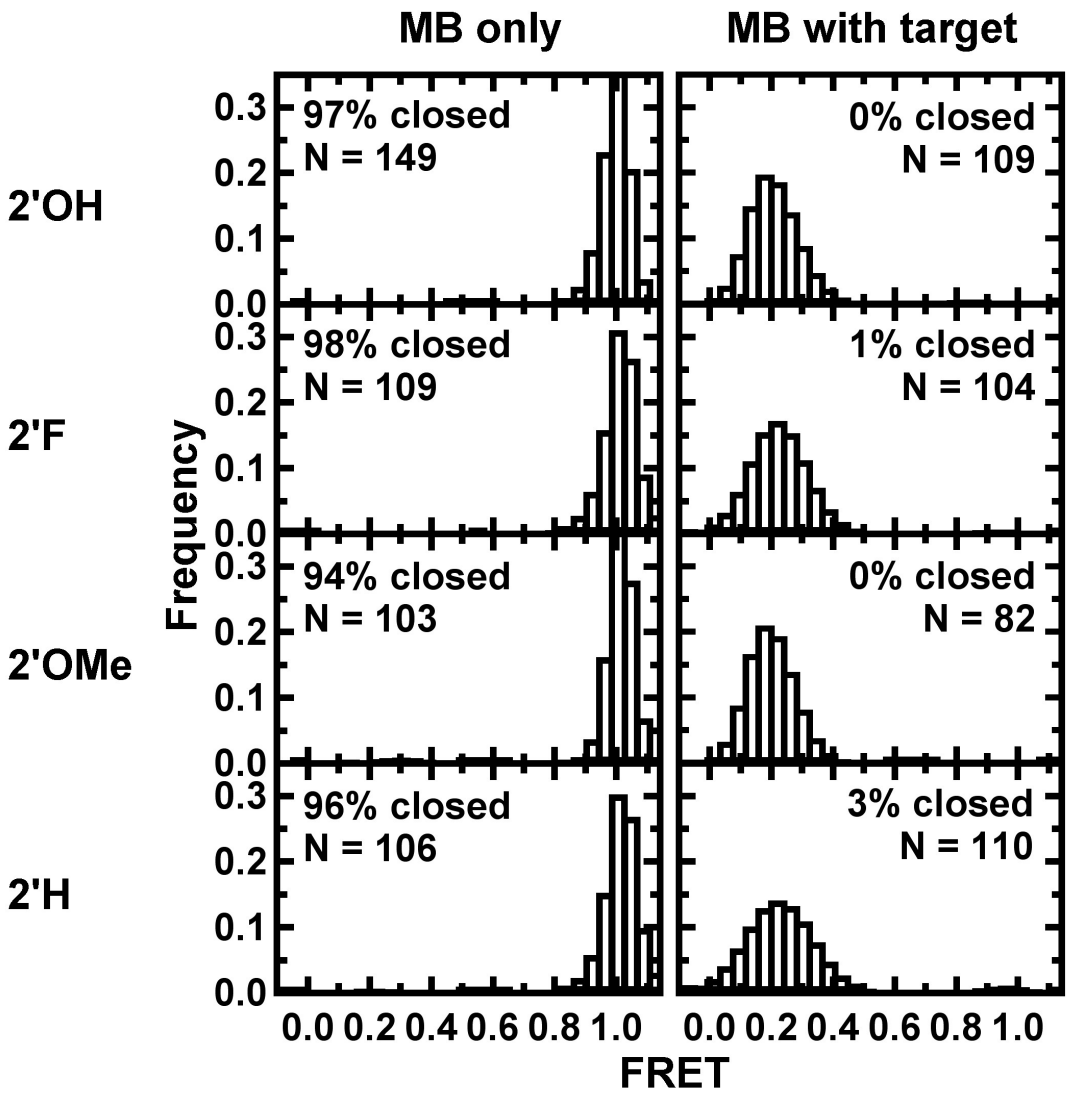

Figure 4.9 Single molecule FRET histograms of both closed and open molecular beacons in the absence and presence of the complementary RNA target. The percentages of closed MBs in the absence of target (MB only) were similar with narrow distributions indicating little conformational variation of the hairpin stem. The presence of the RNA target offered a wider distribution of MBs closed possibly due to the flexibility of the open conformation duplex. A large dynamic range from a FRET ratio of 0.9 to 0.2 was observed for all MBs.

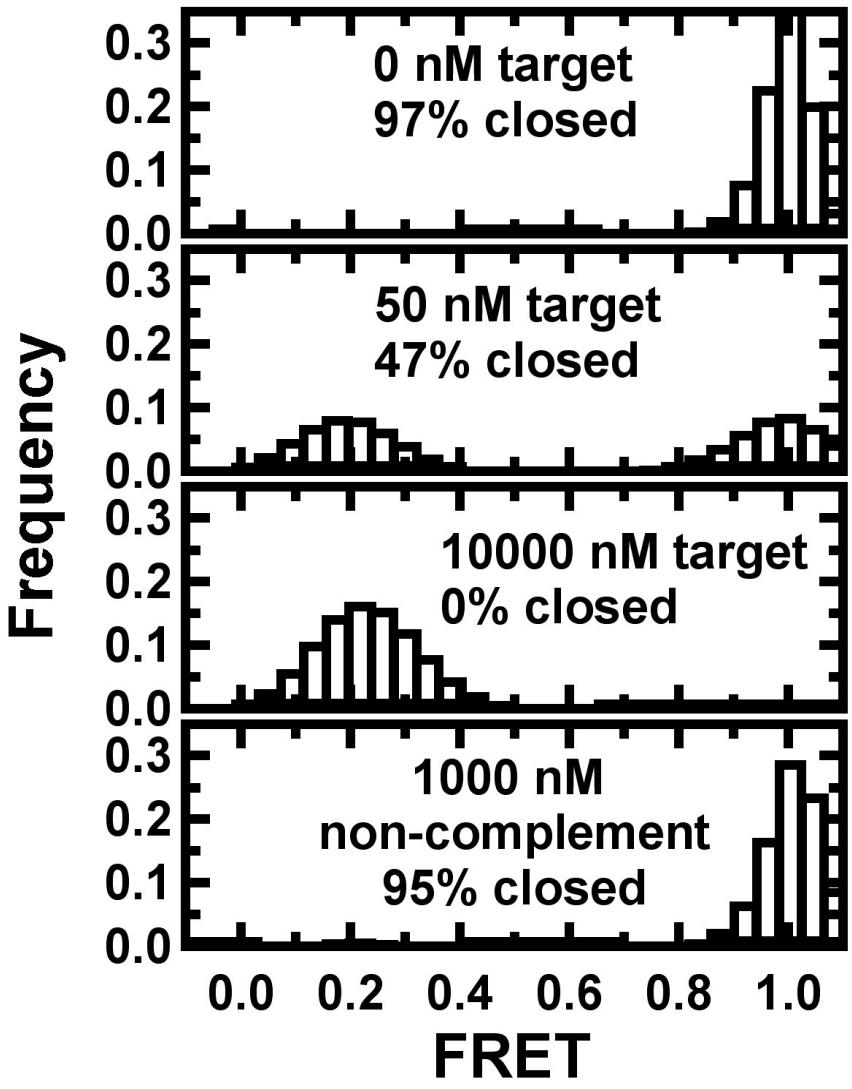

Figure 4.10 Single molecule complementary target titration. As the concentration of complementary target increases (top to bottom), the closed (0.9 FRET) population decreases as the open (0.2 FRET) population increases. The molecular beacon is specific for its complementary RNA target. In the presence of a non-complementary oligonucleotide, the closed conformation (0.9 FRET peak) remains the predominant population.

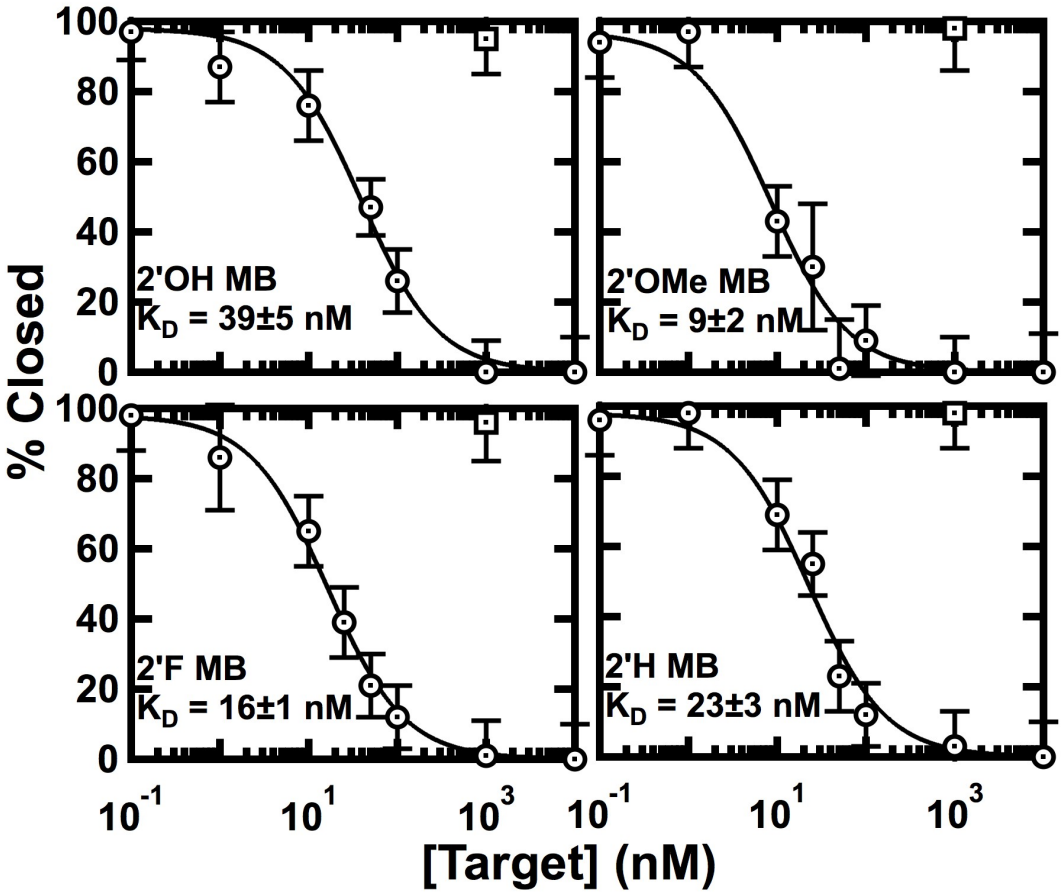

Figure 4.11 Single molecule complementary RNA target titration. For the 2'OH, 2'OMe, 2'F and 2'H molecular beacons, as the concentration of complementary target increased, the percent of molecular beacon in the closed conformation decreased. In the presence of a non-complementary RNA oligonucleotide, the percent of closed molecular beacon remained the same as in the absence of complementary target, illustrating the specificity of the molecular beacon. The line is a fit to a modified Langmuir equation. Error bars are calculated based on the number of molecules.

resolution used or are longer than the life of the fluorophore and the photobleaching of the fluorophore precedes the conformational switch. FRET histograms calculated from greater than 100 single molecule traces for 2'OH, 2'F, 2'OMe, and 2'H MBs in the absence and presence of the complementary RNA target were integrated to yield the percentage of time each molecular beacon spent in the open and closed conformations (Figure 4.9). The percentage of 2'OH, 2'F, 2'OMe, and 2'H MBs in the closed, hairpin conformation (high FRET, 0.9) in the absence of complementary RNA target were 97%, 98%, 94%, and 96%, respectively. Percentages in the closed conformation in the absence of complementary RNA target were similar for the 2'OH, 2'OMe, and 2'H MBs with narrow distributions indicating little conformational variation of the hairpin. The presence of the complementary RNA target resulted in an open conformation upon binding of the loop to the complementary RNA target. The percentage of 2'OH, 2'F, 2'OMe, and 2'H MBs remaining in the closed conformation in the presence of the complementary RNA target were 0%, 1%, 0%, and 3%, respectively. Percentages of MBs remaining in the closed conformation were similar for all MBs in this study. The presence of the complementary RNA target offered wider distributions for the open conformation (low FRET, 0.2) when compared to the closed conformation distribution possibly due to higher flexibility of the longer duplex conformation as opposed to the hairpin. In this experiment, the target oligonucleotide was not preannealed to the molecular beacon, mimicking *ex vivo* experimental conditions in which the molecular beacon could not be preannealed with the target but would have to search for the target

sequence within the cell. Presence of a closed beacon in the presence of an excess of target would result in false negatives when used in a biomedical detection assay suggesting a not fully efficient MB. A large dynamic range from a FRET efficiency of 0.9 (closed conformation) in the absence of target to a FRET efficiency of 0.2 (open conformation) in the presence of target was observed for all MBs used in this study.

An advantage of single molecule FRET over bulk FRET techniques is the ability to distinguish singly-labeled and doubly-labeled constructs. Although HPLC purified, some singly-labeled molecular beacons remained in solution. This mixture of singly- and doubly-labeled molecular beacons is responsible for the lower initial FRET ratios seen in the bulk titrations (Figure 4.4) and may introduce error in the binding affinity calculations. To determine a more accurate binding affinity of the molecular beacons and complementary RNA, a single molecule titration was performed. Increasing amounts of complementary RNA was incubated with the various molecular beacons as in the aforementioned single molecule FRET experiments. The percentage of closed (hairpin) molecular beacons was plotted as a function of target concentration (Figure 4.10 and 4.11). As the concentration of complementary RNA target increased, the percentage of closed hairpin decreased to saturation as more molecular beacons opened upon binding the complementary RNA target. Fitting the resulting titration curves to the Langmuir equation resulted in a K_D value of 39 ± 5 nM for the typical 2'OH MB. All MBs bound with tight nM affinity to the complementary RNA target. As in the bulk titrations, K_D values varied slightly among the 2'

modified MBs; the 2'OMe MB bound with the tightest affinity to the complementary RNA target consistent with the bulk titrations binding 4-fold tighter (9 ± 2 nM), while the 2'F MB bound with a little more that 2-fold tighter affinity (16 ± 1 nM) and the 2'H MB bound almost 2-fold tighter (23 ± 3 nM) (Figure 4.11). Upon addition of the non-complementary RNA target, the percentage of closed molecular beacons was the same as in the absence of a complementary target, indicating that all 2' modified MBs maintain specificity (Figure 4.10 and 4.11).

4.3 Conclusions

FRET and single molecule FRET were used to examine the effects that 2' modifications, including 2'F, 2'OMe, and 2'H, have on the actions of the molecular beacon. The 2' modified MBs were found to act similarly to the 2'OH parent MB. All MBs had similar binding affinity to a complementary RNA target; the 2'OMe MB bound the complementary RNA target with 3-fold tighter affinity than the typical 2'OH MB, while the 2'F MB bound with similar affinity and 2'H MB bound with 3-fold weaker affinity. Time resolved and single molecule FRET both demonstrated a large conformational range upon complementary RNA target binding that was similar for all 2' modified MBs. Similar distances between the 5' and 3' ends of the molecular beacons were found in the absence and presence of the complementary RNA target as well as in the presence of a non-complementary RNA target. Single molecule FRET eluded to an equilibrium, although static, between open and closed conformations. The 2' modifications in

this study do not appear to affect, to any great extent, the actions of the molecular beacon.

4.4 Materials and Methods

4.4.1 Molecular beacon purification and labeling

Molecular beacons were purchased from the Keck Foundation Resource Laboratory at the Yale University School of Medicine (New Haven, CT). Oligonucleotides were purchased with 5'-Cy3 or fluorescein, 3'-biotin, and an internal dT C7 amino linker for fluorophore labeling The MB sequences had 2'-hydroxyl, 2'-fluoro, 2'-O-methyl, or 2'-deoxy backbones. The molecular beacon sequence used in this study was **UUC GUU** AAC UUC AGG GUC AGC UUG **AAC GAA** where the nucleotides indicated in bold formed the stem of the hairpin probe. The complementary RNA target sequence was UUC GUU CAA GCU GAC CCU GAA GUU AAC GAA, and the non-complementary RNA target sequence was AUC UCU UUG CCU UUU GGC UUA GAU CAA GUG UAG UAU. The RNA targets were purchased from Integrated DNA Technologies (IDT) and Keck. The 2'OH MB containing 2'-hydroxyl protection groups was deprotected according to the manufacturer's protocol. The molecular beacons were purified and fluorophore-labeled as previously described(*41*). Briefly, the MBs were purified by denaturing gel electrophoresis (20% polyacrylamide and 8M urea) and diffusion elution against elution buffer (0.4 M NH_4OAc and 0.1 mM EDTA) overnight at 4°C, followed by chloroform extraction and ethanol precipitation. The internal dT C7 amino linker was labeled with Cy5 in labeling buffer (100 mM Na_2CO_3, pH 8.5) or rhodamine in labeling buffer (100 mM sodium

tetraborate, pH 8.5) overnight at room temperature, followed by ethanol precipitation and C8 reverse-phase HPLC purification. A donor and acceptor FRET pair was chosen over the more commonly found fluorophore/quencher pair for ease of single molecule analysis. The doubly-labeled MB concentration was measured by UV-Vis absorbance at 260 nm.

4.4.2 Native gel assay

A native gel assay was performed, as previously described, using 15% non-denaturing polyacrylamide gel electrophoresis using low-fluorescence glass plates with a running buffer consisting of 10 mM Tris-acetic acid, pH 7.3, 20 mM KOAc, 1 mM $Ca(OAc)_2$, and 2 mM $Mg(OAc)_2$.(*103*) Solutions of fluorescein/rhodamine doubly-labeled MB only (10 pmol) with and without 5x complementary RNA target (50 pmol) or non-complementary RNA target (50 pmol) were annealed by heating to 90°C for 45 seconds and slow cooling to room temperature at near-physiological conditions (10 mM Tris-HCl, pH 7.3, 120 mM KCl, 1 mM $CaCl_2$, and 2 mM $MgCl_2$). An equal volume of 40% glycerol was added to each sample after annealing. Solutions were also made of fluorescein only labeled oligonucleotide and a rhodamine only labeled oligonucleotide to be used for color calibration purposes. The acrylamide gel was equilibrated for 15 min before loading. The gel was loaded and run for 8 hours at 4°C at 130 mV and then scanned with a Typhoon 9210 Variable Model Imager (GE Healthcare) and analyzed with ImageQuant software (Amershan Bioscience). Fluorescein and rhodamine were excited at 532 nm and emission was monitored at 526 nm and 580 nm, respectively. Fluorsep software (Amershan Bioscience) was used

to overlay the fluorescein and rhodamine gel images, and the bands were calibrated based on the fluorescein and rhodamine color controls.

4.4.3 Steady state FRET

Steady state FRET measurements of each of the fluorescein/rhodamine doubly-labeled molecular beacons were conducted using a Cary Eclipse (Varian, Inc.) spectrofluorometer as previously described(*41, 98, 104*). A 25 nM MB solution in reaction buffer (10 mM Tris-HCl, pH 7.3, 120 mM KCl, 2 mM $MgCl_2$, and 1 mM $CaCl_2$) was heated at 90°C for 2 minutes to denature any secondary structures and then cooled to room temperature to form the proper hairpin conformation. Fluorescein was excited at 490 nm (10 nm slit width), and the fluorescein and rhodamine emission spectra were measured from 505 to 650 nm (5 nm slit width). Relative FRET efficiency was calculated as

$$FRET = \frac{I_A}{I_D + I_A}$$

where I_D and I_A are the donor (fluorescein) and acceptor (rhodamine) emission intensities, respectively. During titrations with target RNA, the MB was equilibrated at each target RNA concentration for five minutes before scanning. To determine the dissociation constant ($K_{D,app}$), the FRET efficiency was plotted as a function of RNA target concentration and then fitted to a modified Hill equation

$$FRET = FRET_0 + (FRET_{\max} - FRET_0) * \frac{[target]}{K_D + [target]}$$

where $FRET_o$ is the initial FRET efficiency of the MB in the absence of RNA target, $FRET_{max}$ is the FRET efficiency at saturation, and [target] is the concentration of the complementary or non-complementary RNA target.

4.4.4 Time resolved FRET

To determine the distance between the fluorophores on each molecular beacon in the absence and presence of complementary or non-complementary RNA target, time resolved FRET was used, as previously described(*42, 97, 98*). Solutions of 250 nM fluorescein/rhodamine singly or doubly-labeled molecular beacon in the absence and presence of either 750 nM complementary RNA target or 750 nM non-complementary RNA target in reaction buffer were annealed by heating to 90 °C for two minutes slow cooling at room temperature for 20 minutes. The fluorescein was excited at 490 nm and donor emission was collected at 520 nm as previously described. Fluorescence decays were collected for both singly and doubly-labeled MB solutions. These decays were used to determine the donor-acceptor distance distributions as described.

4.4.5 Single molecule FRET

To visualize, at the single molecule level, the conformational changes of the molecular beacons with and without the complementary target RNA, single molecule FRET total internal reflection spectroscopy was used(*68, 98, 102, 104, 105*). A 25 pM molecular beacon solution was injected into a home-built microchannel between a quartz slide and coverslip. The MB was immobilized at the slide/solution interface via a biotin/streptavidin interaction between. The

donor (Cy3) fluorophore was excited at 532 nm laser as previously described (Figure 4.6). The emission from Cy3 and the acceptor (Cy5) was collected through an inverted microscope objective onto a CCD detector (IXon, Andor, South Windsor, CT). Time trajectories of the relative FRET efficiencies were calculated and histograms were generated and integrated to reflect the amount of time a molecule was in each FRET state. An unfolded (open) MB would result in a high I_D and low I_A, resulting in a low FRET efficiency, while a folded (closed) beacon would bring the donor fluorophore into close proximity of the acceptor resulting in low I_D and high I_A and therefore a high FRET efficiency. To analyze the MB in the absence of the RNA target, a solution containing 25 pM MB in reaction buffer was heated to 90°C for two minutes to denature the oligonucleotide and placed directly on ice to anneal. All solutions contained 2 μM BME to prevent photobleaching. In addition, an oxygen scavenger solution consisting of glucose oxidase and catalase was injected onto the slide to inhibit photobleaching of the fluorophores. Once the MB only solution was imaged, a solution containing various concentrations of complementary RNA target/OSS solution was injected onto the same slide and incubated for 10 minutes at room temperature to allow the MB and RNA target to hybridize, then imaged.

4.5 Acknowledgements

We would like to thank Becky Simon and Dr. Karen Myhr for the design of the molecular beacon.

Chapter 5

CONCLUSIONS

We have used FRET, single molecule spectroscopy, and several other biophysical techniques to study how the folding of RNA allows it to perform its various functions by accurately recognizing and binding a target ligand. RNA can fold into structures ranging from the simplest of hairpins to intricate tertiary complexes. These structures are directly linked to how RNA performs its native biological functions as well as its usefulness in analytical methods.

We first investigated how a natural RNA folds in order to recognize a ligand and regulate gene expression. We found the c-di-GMP riboswitch undergoes a large, global conformational change upon binding of its ligand, c-di-GMP. The folding dynamics of the c-di-GMP riboswitch upon Mg^{2+} binding help to pre-organize the aptamer for efficient ligand binding and ultimately efficient gene expression. The riboswitch is capable of transiently folding into a structure similar to its ligand bound form in the absence of ligand, a process that is aided by the presence of Mg^{2+} ions. This pre-organization of the aptamer prepares the riboswitch to quickly and efficiently bind its ligand allowing it to make the decision to turn gene expression on or off in a timely manner. Ligand recognition is also accurate and specific, as the binding pocket is designed to recognize only c-di-GMP and not a structurally similar compound such as c-di-AMP. The aptamer contains a fail-safe measure in that only in the presence of the correct ligand and Mg^{2+} ions can the aptamer stably fold into the final docked conformation, a structure stabilized by tertiary interactions far from the binding site. In sum, the

c-di-GMP riboswitch aptamer domain displays a large-scale pre-organization coupled to ligand binding that increases structural specificity, accelerating ligand binding.

We then investigated two cases in which RNA was used as a tool to detect an analyte. We have demonstrated that binding of the fluorophore, tetramethylrhodamine (TAMRA), to an aptamer enhances the fluorescent properties of the fluorophore. Similar to the c-di-GMP riboswitch, the aptamer is designed to specifically and accurately recognize its ligand. Interestingly, binding to the aptamer resulted in an alteration the photophysical properties of its ligand. Specifically, it increased both the quantum yield and fluorescence lifetime of TAMRA. This is most likely a result of the stabilization and rigidifying of the normally flexible structure of TAMRA. By suppressing these motions, non-radiative decay processes decrease in chance, increasing the likelihood of radiative decay. This side effect of binding can prove useful when utilizing fluorophore-binding aptamers in assays to track the movements of RNA *in vivo.* Multiple copies of this aptamer could be introduced into the RNA in question; fluorescent enhancement of the fluorophore upon binding to the aptamers along the RNA would light up the RNA in the cell allowing for detection and tracking of the RNA.

We also investigated molecular beacons, another example of RNA being used as a tool. Molecular beacons are nucleic acids designed to specifically recognize a target via base pairing. We sought to determine how common modifications to the 2’ position influence the effectiveness of molecular beacons

in recognizing and binding an RNA target. Modification of the 2'OH moiety to 2'H, 2'F, and 2'OMe have all been used to allow the use of molecular beacons in assays in which the medium contains enzymes that would degrade it, including *in vivo* assays. We have shown through several biophysical studies that 2' modifications do not affect the folding and binding of a molecular beacon to its target. Therefore, the common use of these 2' modifications does not hamper their use for *in vivo* studies.

A common thread in all the RNA complexes investigated here is the usefulness of RNA's ability to accurately and specifically recognize a target through various modalities. These structures have been designed, whether by biology or man, to use a diverse array of recognition motifs including sequence and overall shape both at the site of target binding as well as locations distant from the site of target recognition. Target specificity is often a challenge in the development of an analytical method, but biology has been effective in designing complexes that are reliable and specific in the way in which they recognize and bind their respective targets. Studying how naturally found RNA complexes achieve this task can be useful in crafting and improving analytical techniques using biological compounds to detect a variety of analytes.

REFERENCES

1. Kulshina, N., Baird, N. J., and Ferré-D'Amaré, A. R. (2009) Recognition of the bacterial second messenger cyclic diguanylate by its cognate riboswitch, *Nat Struct Mol Biol 16*, 1212-1217.
2. Karunatilaka, K. S., and Rueda, D. (2009) Single-Molecule Fluorescence Studies of RNA: A Decade's Progress, *Chem Phys Lett 476*, 1-10.
3. Butcher, S. E., and Pyle, A. M. The Molecular Interactions That Stabilize RNA Tertiary Structure: RNA Motifs, Patterns, and Networks, *Acc Chem Res*.
4. Blouin, S., Mulhbacher, J., Penedo, J. C., and Lafontaine, D. A. (2009) Riboswitches: ancient and promising genetic regulators, *Chembiochem 10*, 400-416.
5. Edwards, T. E., Klein, D. J., and Ferre-D'Amare, A. R. (2007) Riboswitches: small-molecule recognition by gene regulatory RNAs, *Curr Opin Struct Biol 17*, 273-279.
6. Garst, A. D., and Batey, R. T. (2009) A switch in time: detailing the life of a riboswitch, *Biochim Biophys Acta 1789*, 584-591.
7. Haller, A., Souliere, M. F., and Micura, R. (2011) The Dynamic Nature of RNA as Key to Understanding Riboswitch Mechanisms, *Acc Chem Res*.
8. Montange, R. K., and Batey, R. T. (2008) Riboswitches: emerging themes in RNA structure and function, *Annu Rev Biophys 37*, 117-133.

9. Nahvi, A., Sudarsan, N., Ebert, M. S., Zou, X., Brown, K. L., and Breaker, R. R. (2002) Genetic control by a metabolite binding mRNA, *Chem Biol 9*, 1043.

10. Roth, A., and Breaker, R. R. (2009) The structural and functional diversity of metabolite-binding riboswitches, *Annu Rev Biochem 78*, 305-334.

11. Serganov, A., and Patel, D. J. (2007) Ribozymes, riboswitches and beyond: regulation of gene expression without proteins, *Nat Rev Genet 8*, 776-790.

12. Smith, A. M., Fuchs, R. T., Grundy, F. J., and Henkin, T. M. (2010) Riboswitch RNAs: regulation of gene expression by direct monitoring of a physiological signal, *RNA Biol 7*, 104-110.

13. Zhang, J., Lau, M. W., and Ferré-D'Amaré, A. R. (2010) Ribozymes and riboswitches: modulation of RNA function by small molecules, *Biochemistry 49*, 9123-9131.

14. Sudarsan, N., Lee, E. R., Weinberg, Z., Moy, R. H., Kim, J. N., Link, K. H., and Breaker, R. R. (2008) Riboswitches in eubacteria sense the second messenger cyclic di-GMP, *Science 321*, 411-413.

15. Hengge, R. (2009) Principles of c-di-GMP signalling in bacteria, *Nat Rev Microbiol 7*, 263-273.

16. Jenal, U., and Malone, J. (2006) Mechanisms of cyclic-di-GMP signaling in bacteria, *Annu Rev Genet 40*, 385-407.

17. Tamayo, R., Pratt, J. T., and Camilli, A. (2007) Roles of cyclic diguanylate in the regulation of bacterial pathogenesis, *Annu Rev Microbiol 61*, 131-148.

18. Eydeler, K., Magbanua, E., Werner, A., Ziegelmuller, P., and Hahn, U. (2009) Fluorophore binding aptamers as a tool for RNA visualization, *Biophys J 96*, 3703-3707.

19. Werner, A., Konarev, P. V., Svergun, D. I., and Hahn, U. (2009) Characterization of a fluorophore binding RNA aptamer by fluorescence correlation spectroscopy and small angle X-ray scattering, *Anal Biochem 389*, 52-62.

20. Ellington, A. D., and Szostak, J. W. (1990) In vitro selection of RNA molecules that bind specific ligands, *Nature 346*, 818-822.

21. Holeman, L. A., Robinson, S. L., Szostak, J. W., and Wilson, C. (1998) Isolation and characterization of fluorophore-binding RNA aptamers, *Fold Des 3*, 423-431.

22. Tyagi, S., and Kramer, F. R. (1996) Molecular beacons: probes that fluoresce upon hybridization, *Nat Biotechnol 14*, 303-308.

23. Bratu, D. P., Cha, B. J., Mhlanga, M. M., Kramer, F. R., and Tyagi, S. (2003) Visualizing the distribution and transport of mRNAs in living cells, *Proc Natl Acad Sci U S A 100*, 13308-13313.

24. Santangelo, P. J., Nitin, N., and Bao, G. (2005) Direct visualization of mRNA colocalization with mitochondria in living cells using molecular beacons, *J Biomed Opt 10*, 44025.

25. Santangelo, P. J., Nix, B., Tsourkas, A., and Bao, G. (2004) Dual FRET molecular beacons for mRNA detection in living cells, *Nucleic Acids Res 32*, e57.

26. Birmingham, A., Anderson, E., Sullivan, K., Reynolds, A., Boese, Q., Leake, D., Karpilow, J., and Khvorova, A. (2007) A protocol for designing siRNAs with high functionality and specificity, *Nat Protoc 2*, 2068-2078.

27. Cummins, L. L., Owens, S. R., Risen, L. M., Lesnik, E. A., Freier, S. M., McGee, D., Guinosso, C. J., and Cook, P. D. (1995) Characterization of fully 2'-modified oligoribonucleotide hetero- and homoduplex hybridization and nuclease sensitivity, *Nucleic Acids Res 23*, 2019-2024.

28. Kawasaki, A. M., Casper, M. D., Freier, S. M., Lesnik, E. A., Zounes, M. C., Cummins, L. L., Gonzalez, C., and Cook, P. D. (1993) Uniformly modified 2'-deoxy-2'-fluoro phosphorothioate oligonucleotides as nuclease-resistant antisense compounds with high affinity and specificity for RNA targets, *J Med Chem 36*, 831-841.

29. Rhee, W. J., Santangelo, P. J., Jo, H., and Bao, G. (2008) Target accessibility and signal specificity in live-cell detection of BMP-4 mRNA using molecular beacons, *Nucleic Acids Res 36*, e30.

30. Tsourkas, A., Behlke, M. A., and Bao, G. (2002) Hybridization of 2'-O-methyl and 2'-deoxy molecular beacons to RNA and DNA targets, *Nucleic Acids Res 30*, 5168-5174.

31. Yazbeck, D. R., Min, K. L., and Damha, M. J. (2002) Molecular requirements for degradation of a modified sense RNA strand by Escherichia coli ribonuclease H1, *Nucleic Acids Res 30*, 3015-3025.

32. Zamaratski, E., Pradeepkumar, P. I., and Chattopadhyaya, J. (2001) A critical survey of the structure-function of the antisense oligo/RNA heteroduplex as substrate for RNase H, *J Biochem Biophys Methods 48*, 189-208.

33. Dirks, R. W., Molenaar, C., and Tanke, H. J. (2001) Methods for visualizing RNA processing and transport pathways in living cells, *Histochem Cell Biol 115*, 3-11.

34. Santangelo, P., Nitin, N., and Bao, G. (2006) Nanostructured probes for RNA detection in living cells, *Ann Biomed Eng 34*, 39-50.

35. Bonnet, G., Tyagi, S., Libchaber, A., and Kramer, F. R. (1999) Thermodynamic basis of the enhanced specificity of structured DNA probes, *Proc Natl Acad Sci U S A 96*, 6171-6176.

36. Tsourkas, A., and Bao, G. (2003) Shedding light on health and disease using molecular beacons, *Brief Funct Genomic Proteomic 1*, 372-384.

37. Kettunen, P., Demas, J., Lohmann, C., Kasthuri, N., Gong, Y., Wong, R. O., and Gan, W. B. (2002) Imaging calcium dynamics in the nervous system by means of ballistic delivery of indicators, *Journal of neuroscience methods 119*, 37-43.

38. Albarran, B., To, R., and Stayton, P. S. (2005) A TAT-streptavidin fusion protein directs uptake of biotinylated cargo into mammalian cells, *Protein engineering, design & selection : PEDS 18*, 147-152.

39. Zhao, R., and Rueda, D. (2009) RNA folding dynamics by single-molecule fluorescence resonance energy transfer, *Methods 49*, 112-117.

40. Walter, N. G. (2003) Probing RNA structural dynamics and function by fluorescence resonance energy transfer (FRET), *Curr Protoc Nucleic Acid Chem Chapter 11*, Unit 11 10.

41. Rueda, D., and Walter, N. G. (2006) Fluorescent energy transfer readout of an aptazyme-based biosensor, *Methods Mol Biol 335*, 289-310.

42. Rueda, D., Hsieh, J., Day-Storms, J. J., Fierke, C. A., and Walter, N. G. (2005) The 5' leader of precursor tRNAAsp bound to the Bacillus subtilis RNase P holoenzyme has an extended conformation, *Biochemistry 44*, 16130-16139.

43. Steiner, M., Karunatilaka, K. S., Sigel, R. K., and Rueda, D. (2008) Single-molecule studies of group II intron ribozymes, *Proc Natl Acad Sci U S A 105*, 13853-13858.

44. Dorywalska, M., Blanchard, S. C., Gonzalez, R. L., Kim, H. D., Chu, S., and Puglisi, J. D. (2005) Site-specific labeling of the ribosome for single-molecule spectroscopy, *Nucleic Acids Res 33*, 182-189.

45. Smith, G. J., Sosnick, T. R., Scherer, N. F., and Pan, T. (2005) Efficient fluorescence labeling of a large RNA through oligonucleotide hybridization, *RNA 11*, 234-239.

46. Crawford, D. J., Hoskins, A. A., Friedman, L. J., Gelles, J., and Moore, M. J. (2008) Visualizing the splicing of single pre-mRNA molecules in whole cell extract, *RNA 14*, 170-179.

47. Wood, S., Ferre-D'Amare, A. R., and Rueda, D. (2012) Allosteric Tertiary Interactions Preorganize the c-di-GMP Riboswitch and Accelerate Ligand Binding, *ACS chemical biology 7*, 920-927.

48. Edwards, T. E., Klein, D. J., and Ferré-D'Amaré, A. R. (2007) Riboswitches: small-molecule recognition by gene regulatory RNAs, *Curr Opin Struct Biol 17*, 273-279.

49. Haller, A., Souliere, M. F., and Micura, R. (2011) The dynamic nature of RNA as key to understanding riboswitch mechanisms, *Acc Chem Res 44*, 1339-1348.

50. Winkler, W. C., Nahvi, A., Roth, A., Collins, J. A., and Breaker, R. R. (2004) Control of gene expression by a natural metabolite-responsive ribozyme, *Nature 428*, 281-286.

51. Ferré-D'Amaré, A. R. (2010) The *glmS* ribozyme: use of a small molecule coenzyme by a gene-regulatory RNA, *Q Rev Biophys 43*, 423-447.

52. Baird, N. J., and Ferré-D'Amaré, A. R. (2010) Idiosyncratically tuned switching behavior of riboswitch aptamer domains revealed by comparative small-angle X-ray scattering analysis, *RNA 16*, 598-609.

53. Baird, N. J., Kulshina, N., and Ferré-D'Amaré, A. R. (2010) Riboswitch function: flipping the switch or tuning the dimmer?, *RNA Biol 7*, 328-332.

54. Schirmer, T., and Jenal, U. (2009) Structural and mechanistic determinants of c-di-GMP signalling, *Nat Rev Microbiol 7*, 724-735.

55. Christen, M., Kulasekara, H. D., Christen, B., Kulasekara, B. R., Hoffman, L. R., and Miller, S. I. (2010) Asymmetrical distribution of the second messenger c-di-GMP upon bacterial cell division, *Science 328*, 1295-1297.

56. Lee, E. R., Baker, J. L., Weinberg, Z., Sudarsan, N., and Breaker, R. R. (2010) An allosteric self-splicing ribozyme triggered by a bacterial second messenger, *Science 329*, 845-848.

57. Weinberg, Z., Barrick, J. E., Yao, Z., Roth, A., Kim, J. N., Gore, J., Wang, J. X., Lee, E. R., Block, K. F., Sudarsan, N., Neph, S., Tompa, M., Ruzzo, W. L., and Breaker, R. R. (2007) Identification of 22 candidate structured RNAs in bacteria using the CMfinder comparative genomics pipeline, *Nucleic Acids Res 35*, 4809-4819.

58. Smith, K. D., Lipchock, S. V., Ames, T. D., Wang, J., Breaker, R. R., and Strobel, S. A. (2009) Structural basis of ligand binding by a c-di-GMP riboswitch, *Nat Struct Mol Biol 16*, 1218-1223.

59. Fujita, Y., Tanaka, T., Furuta, H., and Ikawa, Y. (2011) Functional roles of a tetraloop/receptor interacting module in a cyclic di-GMP riboswitch, *Journal of bioscience and bioengineering*.

60. Woodson, S. A. (2010) Compact intermediates in RNA folding, *Annu Rev Biophys 39*, 61-77.

61. Chauhan, S., and Woodson, S. A. (2008) Tertiary interactions determine the accuracy of RNA folding, *J Am Chem Soc 130*, 1296-1303.

62. Aleman, E. A., Lamichhane, R., and Rueda, D. (2008) Exploring RNA folding one molecule at a time, *Curr Opin Chem Biol 12*, 647-654.

63. Brenner, M. D., Scanlan, M. S., Nahas, M. K., Ha, T., and Silverman, S. K. (2010) Multivector fluorescence analysis of the xpt guanine riboswitch aptamer domain and the conformational role of guanine, *Biochemistry 49*, 1596-1605.

64. Greenleaf, W. J., Frieda, K. L., Foster, D. A., Woodside, M. T., and Block, S. M. (2008) Direct observation of hierarchical folding in single riboswitch aptamers, *Science 319*, 630-633.

65. Haller, A., Rieder, U., Aigner, M., Blanchard, S. C., and Micura, R. (2011) Conformational capture of the SAM-II riboswitch, *Nat Chem Biol 7*, 393-400.

66. Heppell, B., Blouin, S., Dussault, A. M., Mulhbacher, J., Ennifar, E., Penedo, J. C., and Lafontaine, D. A. (2011) Molecular insights into the ligand-controlled organization of the SAM-I riboswitch, *Nat Chem Biol 7*, 384-392.

67. Lemay, J. F., Penedo, J. C., Tremblay, R., Lilley, D. M., and Lafontaine, D. A. (2006) Folding of the adenine riboswitch, *Chem Biol 13*, 857-868.

68. Roy, R., Hohng, S., and Ha, T. (2008) A practical guide to single-molecule FRET, *Nat Methods 5*, 507-516.

69. Witte, G., Hartung, S., Buttner, K., and Hopfner, K. P. (2008) Structural biochemistry of a bacterial checkpoint protein reveals diadenylate cyclase activity regulated by DNA recombination intermediates, *Mol Cell 30*, 167-178.

70. Fang, X., Littrell, K., Yang, X. J., Henderson, S. J., Siefert, S., Thiyagarajan, P., Pan, T., and Sosnick, T. R. (2000) Mg^{2+}-dependent compaction and folding of yeast tRNAPhe and the catalytic domain of the B. subtilis RNase P RNA determined by small-angle X-ray scattering, *Biochemistry 39*, 11107-11113.

71. Russell, R., Millett, I. S., Doniach, S., and Herschlag, D. (2000) Small angle X-ray scattering reveals a compact intermediate in RNA folding, *Nat Struct Biol 7*, 367-370.

72. Moghaddam, S., Caliskan, G., Chauhan, S., Hyeon, C., Briber, R. M., Thirumalai, D., and Woodson, S. A. (2009) Metal ion dependence of cooperative collapse transitions in RNA, *J Mol Biol 393*, 753-764.

73. Fang, X. W., Pan, T., and Sosnick, T. R. (1999) Mg^{2+}-dependent folding of a large ribozyme without kinetic traps, *Nat Struct Biol 6*, 1091-1095.

74. Rangan, P., Masquida, B., Westhof, E., and Woodson, S. A. (2003) Assembly of core helices and rapid tertiary folding of a small bacterial group I ribozyme, *Proc Natl Acad Sci USA 100*, 1574-1579.

75. Draper, D. E. (2004) A guide to ions and RNA structure, *RNA 10*, 335-343.

76. Ebel, H., and Gunther, T. (1980) Magnesium metabolism: a review, *J Clin Chem Clin Biochem 18*.

77. Smith, K. D., Lipchock, S. V., Livingston, A. L., Shanahan, C. A., and Strobel, S. A. (2010) Structural and biochemical determinants of ligand binding by the c-di-GMP riboswitch, *Biochemistry 49*, 7351-7359.

78. Batey, R. T., Gilbert, S. D., and Montange, R. K. (2004) Structure of a natural guanine-responsive riboswitch complexed with the metabolite hypoxanthine, *Nature 432*, 411-415.

79. Serganov, A., Yuan, Y. R., Pikovskaya, O., Polonskaia, A., Malinina, L., Phan, A. T., Hobartner, C., Micura, R., Breaker, R. R., and Patel, D. J. (2004) Structural basis for discriminative regulation of gene expression by adenine- and guanine-sensing mRNAs, *Chem Biol 11*, 1729-1741.

80. Neupane, K., Yu, H., Foster, D. A. N., Wang, F., and Woodside, M. T. (2011) Single-molecule force spectroscopy of the add adenine riboswitch relates folding to regulatory mechanism, *Nucleic Acids Res 39*, 7677-7687.

81. Tremblay, R., Lemay, J. F., Blouin, S., Mulhbacher, J., Bonneau, E., Legault, P., Dupont, P., Penedo, J. C., and Lafontaine, D. A. (2011) Constitutive regulatory activity of an evolutionarily excluded riboswitch variant, *J Biol Chem 286*, 27406-27415.

82. Pan, J., Thirumalai, D., and Woodson, S. A. (1997) Folding of RNA involves parallel pathways, *J Mol Biol 273*, 7-13.

83. Zhuang, X., Bartley, L. E., Babcock, H. P., Russell, R., Ha, T., Herschlag, D., and Chu, S. (2000) A single-molecule study of RNA catalysis and folding, *Science 288*, 2048-2051.

84. Bokinsky, G., and Zhuang, X. (2005) Single-molecule RNA folding, *Acc Chem Res 38*, 566-573.

85. Ditzler, M. A., Rueda, D., Mo, J., Håkansson, K., and Walter, N. G. (2008) A rugged free energy landscape separates multiple functional RNA folds throughout denaturation, *Nucleic Acids Res 36*, 7088-7099.

86. Okumus, B., Wilson, T. J., Lilley, D. M. J., and Ha, T. (2004) Vesicle encapsulation studies reveal that single molecule ribozyme heterogeneities are intrinsic, *Biophysical Journal 87*, 2798-2806.

87. Lipfert, J., Das, R., Chu, V. B., Kudaravalli, M., Boyd, N., Herschlag, D., and Doniach, S. (2007) Structural transitions and thermodynamics of a glycine-dependent riboswitch from Vibrio cholerae, *J Mol Biol 365*, 1393-1406.

88. Ali, M., Lipfert, J., Seifert, S., Herschlag, D., and Doniach, S. (2010) The ligand-free state of the TPP riboswitch: a partially folded RNA structure, *J Mol Biol 396*, 153-165.

89. Lang, K., Rieder, R., and Micura, R. (2007) Ligand-induced folding of the thiM TPP riboswitch investigated by a structure-based fluorescence spectroscopic approach, *Nucleic Acids Res 35*, 5370-5378.

90. Kulshina, N., Edwards, T. E., and Ferré-D'Amaré, A. R. (2010) Thermodynamic analysis of ligand binding and ligand binding-induced tertiary structure formation by the thiamine pyrophosphate riboswitch, *RNA 16*, 186-196.

91. Smith, K. D., and Strobel, S. A. (2011) Interactions of the c-di-GMP riboswitch with its second messenger ligand, *Biochem Soc Trans 39*, 647-651.

92. Ditzler, M. A., Aleman, E. A., Rueda, D., and Walter, N. G. (2007) Focus on function: single molecule RNA enzymology, *Biopolymers 87*, 302-316.

93. Walter, N. G., Harris, D. A., Pereira, M. J., and Rueda, D. (2001) In the fluorescent spotlight: global and local conformational changes of small catalytic RNAs, *Biopolymers 61*, 224-242.

94. Souliere, M. F., Haller, A., Rieder, R., and Micura, R. (2011) A powerful approach for the selection of 2-aminopurine substitution sites to investigate RNA folding, *J Am Chem Soc 133*, 16161-16167.

95. Noeske, J., Buck, J., Furtig, B., Nasiri, H. R., Schwalbe, H., and Wohnert, J. (2007) Interplay of 'induced fit' and preorganization in the ligand induced folding of the aptamer domain of the guanine binding riboswitch, *Nucleic Acids Res 35*, 572-583.

96. Wilson, R. C., Smith, A. M., Fuchs, R. T., Kleckner, I. R., Henkin, T. M., and Foster, M. P. (2011) Tuning riboswitch regulation through conformational selection, *J Mol Biol 405*, 926-938.

97. Klostermeier, D., and Millar, D. P. (2001) Time-resolved fluorescence resonance energy transfer: a versatile tool for the analysis of nucleic acids, *Biopolymers 61*, 159-179.

98. Rueda, D., Wick, K., McDowell, S. E., and Walter, N. G. (2003) Diffusely bound Mg2+ ions slightly reorient stems I and II of the hammerhead

ribozyme to increase the probability of formation of the catalytic core, *Biochemistry 42*, 9924-9936.

99. Tsourkas, A., Behlke, M. A., Rose, S. D., and Bao, G. (2003) Hybridization kinetics and thermodynamics of molecular beacons, *Nucleic Acids Res 31*, 1319-1330.

100. Bokinsky, G., Rueda, D., Misra, V. K., Rhodes, M. M., Gordus, A., Babcock, H. P., Walter, N. G., and Zhuang, X. (2003) Single-molecule transition-state analysis of RNA folding, *Proc Natl Acad Sci U S A 100*, 9302-9307.

101. Rueda, D., Bokinsky, G., Rhodes, M. M., Rust, M. J., Zhuang, X., and Walter, N. G. (2004) Single-molecule enzymology of RNA: essential functional groups impact catalysis from a distance, *Proc Natl Acad Sci U S A 101*, 10066-10071.

102. Rueda, D., and Walter, N. G. (2005) Single molecule fluorescence control for nanotechnology, *J Nanosci Nanotechnol 5*, 1990-2000.

103. Pereira, M. J., Harris, D. A., Rueda, D., and Walter, N. G. (2002) Reaction pathway of the trans-acting hepatitis delta virus ribozyme: a conformational change accompanies catalysis, *Biochemistry 41*, 730-740.

104. Harris, D. A., Rueda, D., and Walter, N. G. (2002) Local conformational changes in the catalytic core of the trans-acting hepatitis delta virus ribozyme accompany catalysis, *Biochemistry 41*, 12051-12061.

105. Zhao, R., and Rueda, D. (2009) RNA folding dynamics by single-molecule fluorescence resonance energy transfer, *Methods*.

ABSTRACT

SINGLE MOLECULE STUDIES OF RNA-TARGET INTERACTIONS

by

SHARLA WOOD

August 2012

Advisor: Dr. David Rueda

Major: Chemistry (Analytical)

Degree: Doctor of Philosophy

We have used FRET, single molecule spectroscopy, and several other biophysical techniques to study how the folding of RNA allows it to perform its various functions by recognizing and binding a target ligand. We have shown that the c-di-GMP riboswitch undergoes a large, global conformational change upon binding of the ligand. The folding dynamics of the c-di-GMP riboswitch upon Mg^{2+} binding help to pre-organize the aptamer for efficient ligand binding and ultimately efficient gene expression. We have also investigated two instances, a fluorophore-binding aptamer and molecular beacon, where the folding of RNA can be used to detect an analyte. We have demonstrated that binding of the fluorophore, TAMRA, to an aptamer enhances the fluorescent properties of the fluorophore. Specifically, it increases both its quantum yield and fluorescent lifetime. This will provide an added advantage to the use of these aptamers in labeling an mRNA *in vivo.* We have shown that 2' modifications do not affect the folding and binding of a molecular beacon to its target. The common use of these 2' modifications does not hamper their use for *in vivo* studies. Whether

natural or artificial, the folding of RNA to specifically recognize a target can be employed by both cells and scientists to perform a wide array of functions.

AUTOBIOGRAPHICAL STATEMENT

SHARLA WOOD

I was born and raised in Tawas City, Michigan, a small tourist town in northern Michigan. I graduated from Tawas Area High School in 2002 and headed to Sault Sainte Marie, Michigan where I received a Bachelor's of Science in Chemistry from Lake Superior State University after dabbling for two years in biology. While at Lake State, I developed a strong interest in environmental issues and studies. I then went to the big city to continue my educational pursuits at Wayne State University in 2006 where I received a Ph.D. in analytical chemistry in June of 2012.

Education

Ph.D.	Chemistry (Analytical), Wayne State University	2012
B.S.	Chemistry, Lake Superior State University	2006

Publications

1. **Wood S.**, Ferre-d'Amare A., and Rueda D. Allosteric Tertiary Interactions Preorganize the c-di-GMP Riboswitch and Accelerate Ligand Binding. *ACS Chemical Biology,* **2012**, 7(5): 920-927.

2. Wood S. and Rueda D. Fluorescence Labeling of Nucleic Acids. *Encyclopedia of Biophysics*, **2011**, in press.